MULTIPHOTON IONISATION OF RARE GAS ATOMS

Heather Dawn Symons

October, 1990

a thesis submitted for the degree of Master of Science at the Australian National University

Laser Physics Centre
Research School of Physical Sciences
Australian National University
Canberra ACT

STATEMENT

The theoretical and computational investigations presented in this thesis are the original work of the author, except where otherwise acknowledged. No part of this thesis has been submitted towards a degree or diploma in any other university or tertiary institution.

Heather Dawn Symons

October, 1990

ABSTRACT

A model describing the ponderomotive acceleration of electrons produced by multiphoton ionisation (MPI) of rare gas atoms is developed. Electron energy spectra are calculated for this process and are examined in detail. Simulations of MPI in argon and helium are performed and the results are compared with those from the experiments of Baldwin (1979) and Boreham (1979). The results indicate that due to the spread in electron energies caused by the ponderomotive acceleration, structure due to above threshold ionisation processes could not have been observed in these experiments.

ACKNOWLEDGEMENTS

I would like to acknowledge my principal superviser, Ken Baldwin, for his assistance during the development of the work reported here and for his extremely thorough checking of this thesis. Barry Luther-Davies supervised my work during Ken's absences and advised on preliminary experimental work associated with the investigations in this thesis: I would like to thank him for his help. I would also like to acknowledge very useful discussions on the more theoretical aspects of this work with my adviser, the late Ranko Dragila.

Theoretical work associated with this thesis (but not included here) was developed under the guidance of Peter Knight, head of the Laser Optics Theory Group at Imperial College, London. I would like to extend my sincere thanks to Peter and to Bernard Piraux and Keith Burnett for their help and advice with the work done while I was at Imperial College. I would also like to thank Peter and others in the Laser Optics Group for making my stay at Imperial a pleasant one.

Financial support during my full-time study from the Commonwealth Department of Employment, Education and Training is gratefully acknowledged as is the funding I received from Caltex Australia and the Australian Federation of University Women (South Australia) which enabled me to study in London.

Finally, special thanks must go to my partner-in-crime, Bob McKay, for his support during the long hours spent at the computer terminal and especially during the writing of this thesis.

CONTENTS

LIST OF FIGURES

CHAPTER ONE
INTRODUCTION

Experiments on the multiphoton ionisation (MPI) of argon and helium performed at the Australian National University by Boreham and Luther-Davies (1979), Baldwin (1979), Baldwin and Boreham (1981) and Boreham and Hughes (1981), resulted in some of the first experimental observations of ponderomotive and tunnelling effects in MPI. The analysis of the electron energy spectra at that time was limited by an incomplete knowledge of the processes involved in multiphoton ionisation. The purpose of this thesis is to use the knowledge accumulated in the years since 1979 to simulate the multiphoton ionisation and ponderomotive acceleration processes and compare the results obtained with the experiments of Baldwin and others. The major effect under investigation will be the ponderomotive acceleration of the liberated electrons along the electric field gradient formed by the laser pulse.

Theoretical work on the use of electromagnetic radiation in the ionisation of atoms began almost sixty years ago. Göppert-Mayer published the first theoretical paper on multiphoton ionisation in 1931. Dirac and Harding (1932) also discussed the problem at length and sought to give a rigorous mathematical treatment by calculating the matrix elements involved in the expression for the probability of transition of an atom from an unperturbed ground state to a continuum of free states.

Volkov (1935) examined the problem of a free electron in an electromagnetic field and found solutions to the Dirac equation (the relativistic version of the Schrödinger equation) for an electron in both a sinusoidal field and a field

consisting of the superposition of a number of electromagnetic waves of varying phase and frequency. The solutions became known as Volkov states and have been widely used to describe the final state of an electron after ionisation (see, for example, Reiss (1980 and 1987) and Becker et al (1986 and 1987)).

The next major contribution to the theory of atomic ionisation occurred in 1965 when Keldysh derived expressions for the ionisation probability of both multiphoton ionisation and tunnel auto-ionisation and showed that they were merely two limits of the same process. Keldysh showed that multiphoton ionisation occurred for incident radiation of frequency $\omega >> \omega_t$ and that tunnel auto-ionisation occurred for $\omega << \omega_t$ where

$$\omega_t = \frac{eE}{\sqrt{2mE_{ion}}} \qquad \ldots 1.1$$

with

e and m ≡ charge and mass of an electron (respectively)

E ≡ electric field strength

and

E_{ion} ≡ ionisation potential.

Kibble (1966) discussed the refraction of electron beams from intense electromagnetic waves and noted two aspects of electron-light interactions pertinent to the present work. The first was that an electron in an electromagnetic field had an energy associated with its motion in the field and that the conservative force under which it was moving served to "push the electron away from regions of high intensity". Kibble found the oscillation energy (as it was called) to be proportional to the square of the field strength, such that

$$E_{OSC} = \frac{e^2E^2}{4m\omega^2}$$

. . . 1.2

Secondly, Kibble (and Eberly(1965)) noted that electrons near the focus of a laser beam could be "overtaken" by an electromagnetic wave and accelerated, thereby gaining a velocity in the direction of propagation of the laser pulse.

However, it was not until later that the above two properties were used when Hora (1969) was attempting to analyse the appearance of high energy ions during the production of laser induced plasmas. Hora suggested that since electrons (or ions) were charged particles, they had a force exerted on them by an electromagnetic field and that the force (and consequently, the acceleration) experienced by the electrons was proportional to the gradient of the field intensity

$$\mathbf{f} = \frac{-e^2}{4m\omega^2}\nabla E^2$$

. . . 1.3

In this manner, under certain conditions, the plasma (and hence, electrons) could have a momentum (or energy) gain which was much greater than the vacuum photon momentum (energy). This force was simply the ponderomotive force as described by Landau and Lifshitz (1960).

It was also during the 1960s that the laser became useful as a laboratory tool and experiments on the multiphoton ionisation of atoms using intense fields were possible. Early experiments (Voronov and Delone, 1966 and Agostini et al, 1968) concentrated on determining the ionisation cross-section (i.e., the probability of ionisation) and the intensity scaling law for multiphoton ionisation was proposed at this time. Basically, the scaling law stated that the N-photon ionisation rate, R_I, was proportional to the Nth power of the photon flux (Φ) produced by the laser, where the constant of proportionality was the ionisation

cross-section, σ (Bebb and Gold, 1966); that is

$$R_I = \sigma_N \Phi^N \qquad \ldots 1.4$$

Experimental work continued into the mid seventies. Papers by Martin and Mandel (1976) and later, Hollis (1978), reported high energy electrons arising from laser-electron interactions and resulted in the first experimental evidence of the ponderomotive acceleration of electrons. This work led to the electron energy measurements by Boreham and Luther-Davies (1979), Baldwin and Boreham (1981) and Agostini et al (1979). The last group studied electron energy spectra arising from the six-photon ionisation of xenon, rather than use the energy spectra from ions (as had previously been the practice). Using an instrumental resolution of ~0.5 eV and a photon energy of 2.34 eV, Agostini et al observed an electron energy spectrum consisting of two peaks separated by the photon energy. In other words, some of the atoms were absorbing more energy than they required for ionisation. The newly observed phenomenon became known as above-threshold ionisation or ATI. Agostini et al argued that laser intensities lower than those used by Martin and Mandel and Hollis were required to observe individual photoelectron peaks since considerable amounts of energy could be gained by the electron from ponderomotive acceleration and thus mask the individual photoelectron peaks that would be expected from the absorption of more photons than the minimum number required for ionisation.

Around the same time, Baldwin studied the photoionisation of argon, but did not see any individual photoelectron peaks. Instead, broad peaks for successively higher ionisation states of argon were observed. It was later thought that one possible reason for this was that the resolution of the detector (a few eV) was not fine enough to distinguish between adjacent peaks, thereby resulting in merged

peaks in the electron energy spectra. It will be shown in this thesis that the reason for the lack of individual peaks was not necessarily due to poor detector resolution, but rather, due to ponderomotive acceleration of the electrons, causing energy gains and a subsequent spread in energies greater than the widths between the individual peaks.

Various groups (such as those at Saclay and Amsterdam) began investigating the ATI process by systematically altering parameters such as the laser intensity. In 1983, Kruit et al published electron energy spectra where some photoelectron peaks were significantly reduced in size, even to the point where they were barely distinguishable from the background signal. The group had been performing experiments using xenon and observed that if the laser intensity was increased from $2x10^{13}W/cm^2$ to $6x10^{13}W/cm^2$, the first photoelectron peak was gradually suppressed and the higher energy peaks were enhanced. This behaviour became known as peak suppression and similar results were later noted by other groups (see, for example, Lompré et al (1985)).

However, Kruit et al could not explain the suppression of the first photoelectron peaks. The widths of the individual peaks were attributed to energy gains due to the ponderomotive potential, although it was noted that the energy shift was not as great as would have been expected from this mechanism. Debate on the suppression of the lower order peaks ensued for some time, (see, for example, Muller et al (1983), Lompré et al (1985), Szöke (1985), Crance (1986) and Yergeau et al (1986)). Becker et al (1986 and 1987) developed a model for ATI processes involving final-state interactions between the laser field and the ejected electron which also exhibited peak suppression, but did not explain the physical mechanism behind the phenomenon. Then, in 1987, Kupersztych explained that the suppression of the lower peaks occurred because the electron had to exist in the electromagnetic field after ionisation and that to do so, it would require an

energy E_{osc}. Simultaneously, experiments carried out by the AT&T Bell Lab group (McIlrath et al, 1987) confirmed this suggestion. Under this model, before an electron could escape from the atom, a total energy of E_{osc} plus that normally required for ionisation must be absorbed by the atom from the irradiating field, thereby effectively raising the ionisation energy threshold (see Figure 1.1).

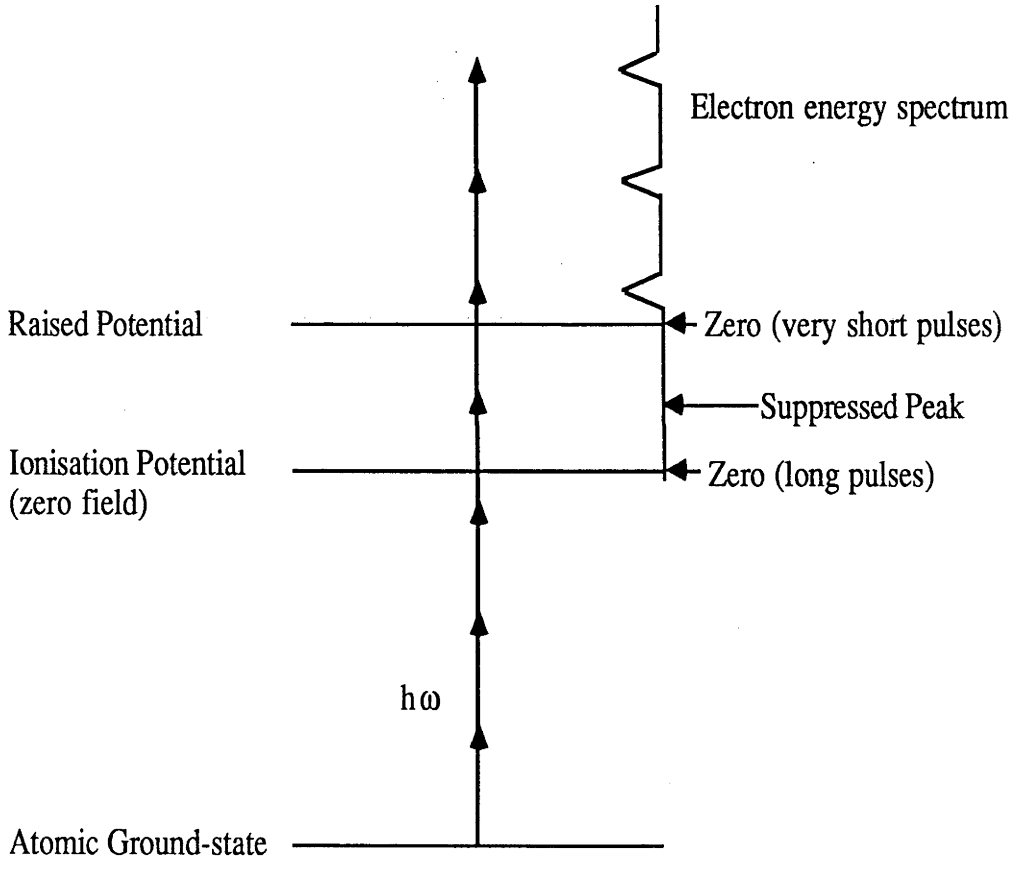

Figure 1.1: Schematic of above-threshold ionisation processes

Since then, many workers have studied various aspects of multiphoton and above-threshold ionisation. A brief synopsis of the more pertinent papers (in the context of the present work) follows, although very good reviews on MPI and ATI can be found in Agostini and Petite (1988), Eberly and Javanainen (1988) and Mainfray and Manus (1991).

Groups at Saclay and Amsterdam performed numerous experiments on various aspects of above-threshold and multiphoton ionisation using lasers of varying intensity (10^{12} to 10^{15}W/cm^2) and pulse duration (picosecond and subpicosecond) - see, for example, Lompré et al (1987), Agostini et al (1987), Muller et al (1988) and Petite et al (1988).

Similar experiments were performed by the group at the AT&T Bell Laboratories using subpicosecond and picosecond laser pulses and included the effect of ponderomotive acceleration on photoelectron angular distributions (Freeman et al, 1986) which will be examined in more detail in Chapter Three. Other experiments explored ATI processes in xenon, krypton and helium (McIlrath et al (1987), Freeman et al (1987) and Bashkansky et al (1988)). A general review of their work during this period can be found in Freeman et al (1988).

Experiments using resonant multiphoton ionisation were performed by Landen et al (1987) and Gontier et al (1988), among others. Basically, it was found that by tuning the laser frequency so that the atom was raised to an excited state prior to ionisation, the electron yield at ionisation was enhanced. Recent experiments by McIlrath et al (1989) concerning the high-intensity multiphoton ionisation of xenon show that atomic levels may also shift into resonance due to the strong fields involved in the ionisation process.

Further experiments on MPI of noble gases were performed by Perry et al (1988a and 1988b) who also developed a technique for determining the intensity at the focus of a laser by analysing the energy shifts observed in MPI of krypton (Perry et al, 1989).

Experimental work on long-wavelength (10μm) ATI of xenon has recently been done by Corkum et al, 1989 and tunnelling ionisation of rare gases (similar to Baldwin and Boreham) has been examined by Augst et al (1989).

There has also been a great number of contributions to the theoretical aspects of multiphoton ionisation, above-threshold ionisation and the subsequent ponderomotive acceleration of electrons in recent years.

A number of authors have developed theoretical models for ATI using a variety of techniques. However, they can, in general, be placed into two classes, depending on which types of final states have been used - perturbed Coulomb or Volkov states (Agostini and Petite).

Models for ATI transition probabilities using perturbation theory have been examined by Gontier and Trahin (1980), Aymar and Crance (1981), Deng and Eberly (1985) and Roso-Franco and Eberly (1990). Qualitatively, the simulated results compare well with experimental results for fields less than about 10^{11}W/cm^2, but the models break down for field intensities of the order of 10^{12}W/cm^2 or more (Agostini and Petite). Another difficulty with perturbation theory is that for a strong laser field, all of the continuum states are coupled together and must therefore be evaluated simultaneously. Since perturbation theory only allows continuum-continuum coupling to occur via the initial (bound) state, the calculations are extremely computer intensive, even for a simple atom such as hydrogen (Eberly and Javanainen).

Faisal (1973) and Reiss (1980) developed a theory for ATI using Volkov final states, based on the work of Keldysh which became known as the Keldysh-Faisal-Reiss (KFR) theory. Using these techniques, Reiss (1987) published simulation results which gave good qualitative agreement with the experimental observations of the groups at Saclay and Amsterdam. A similar method was also used by Chen et al (1987) who calculated ATI electron energy spectra by using plane-wave solutions of the unperturbed Schrödinger equation and subsequently showed that the spectra depended on the angular momentum of the atomic ground state and the intensity and polarisation of the laser beam. The KFR technique and related methods have also been used by Becker et al (1986 and 1987), Basile et al (1988), Perry et al (1988b) and Collins and Merts (1990). A comparison of Keldysh type models with other models of ATI can be found in Javanainen and Eberly (1989).

Theories for multiphoton ionisation and above-threshold ionisation have also tended to concentrate on intense field and/or short-pulse regimes. Models calculating ionisation rates for MPI in intense fields have been developed, for example, by Shakeshaft and Potvliege (1987) and Basile et al. Short-pulse MPI was examined by Bardsley et al (1988) who numerically solved a 1-D time-dependent Schrödinger equation to give electron energy spectra as a function of laser intensity, frequency and pulse duration.

Recent work includes nonlinear light scattering accompanying MPI such as in Eberly, Su and Javanainen (1989) and work on ATI for negative ions, which can be found in Roso-Franco and Eberly (1990). Models based on the hydrogen atom have also been recently developed in order to help isolate particular ATI mechanisms. See, for example, Basile et al and Sundaram and Armstrong (1990).

The electron energy gain due to acceleration by the ponderomotive potential was examined by Jönsson (1987) who proposed three regimes, characterised by pulse size and duration. Similar results were also presented by Symons et al (1988).

Within the past decade or so, both experimentalists and theoreticians have discovered that electron energy spectra can vary (under different conditions of light intensity, polarisation and focussing) from a single peak to a couple of peaks separated by the photon energy to a series of peaks in which the lowest order peaks are either partially or totally suppressed. In addition to this, researchers have found that the spectra are further enhanced by the resonant absorption of photons, due to either the selection of laser light of an appropriate wavelength or from a strong-field induced shift into resonance of the atomic levels. As a consequence of these observations, workers in the areas of MPI and ATI have gained new understanding of the processes involved in matter-light interactions.

This thesis will examine ponderomotive effects which occur during the multiphoton ionisation of rare gas atoms. Primarily, the aim is to determine whether individual ATI peaks would be expected to be observed under the experimental conditions of Baldwin and Boreham using the pulsed Nd laser system at ANU. Secondly, this study may allow the determination of regimes where ATI peaks may be observed in future experiments.

The ponderomotive acceleration of electrons down the electromagnetic field gradient formed by a laser pulse will be examined in detail in Chapter Two. In Chapter Three, the results from the ponderomotive acceleration calculations will be combined with postulated ATI spectra to simulate electron energy spectra for argon and helium and compare the results to those obtained by Baldwin and Boreham (1979), respectively. A summary of the results and suggestions for further work will be given in Chapter Four.

CHAPTER TWO
PONDEROMOTIVE ACCELERATION

2.1 INTRODUCTION

Experiments on the multiphoton ionisation of atoms in intense laser fields have shown that the width and position of the photoelectron peaks in the electron energy spectrum can vary greatly depending on the laser intensity, pulse duration and focal parameters. More specifically, Freeman et al (1988) have shown that most of these effects can be explained in terms of the ponderomotive potential created by the intense laser fields used to ionise the atoms under investigation.

In this chapter, the role of ponderomotive effects in multiphoton ionisation will be examined and the results of computer simulations of ponderomotive electron acceleration from high intensity, picosecond laser pulses will be presented. It will be demonstrated that the final electron energy spectrum is a strong function of the focal, beam and energy parameters and detection geometry, all of which serve to considerably complicate the interpretation of experimental results.

2.2 THEORY AND DESCRIPTION OF LASER BEAM

Suppose we have a volume of atoms, which, upon interaction with laser radiation of a particular wavelength and intensity, ionise to produce electrons. Once the electrons have been ejected from the atoms, they experience a force from the oscillating electromagnetic field, which gives the electrons an additional energy of

$$E_{OSC} = \frac{e^2E^2}{4m\omega^2} \qquad \ldots 2.2.1$$

For radiation of wavelength $\lambda = 1.064\mu m$, equation 2.2.1 becomes

$$E_{OSC} \sim 10^{-13}\, I\ (W/cm^2)$$

The force exerted on the electrons by the oscillating electromagnetic field is given by Landau and Lifshitz as

$$\mathbf{f} = \frac{-e^2}{4m\omega^2}\nabla E^2 \qquad \ldots 2.2.2$$

From Lorrain and Corson, the laser intensity, I, is related to the field strength, E, by

$$I = \frac{|E|^2}{8\pi c} \qquad \ldots 2.2.3$$

Hence

$$\mathbf{f} = \frac{-e^2.2\pi c}{m\omega^2}\nabla I \qquad \ldots 2.2.4$$

or

$$\mathbf{f} = \frac{-e^2\lambda^2}{2\pi cm} \nabla I$$

. . . 2.2.5

Thus, for radiation of wavelength λ, the ponderomotive force exerted on an electron by an electromagnetic field is directly proportional to the gradient of the field intensity. The electron will therefore be initially accelerated out of the laser beam with an acceleration proportional to the gradient of the field intensity at the point of its ejection from the atom.

If it is assumed that the focal region of a laser beam is approximately Gaussian both in space and time, the intensity at any point is given by (Freeman et al, 1987)

$$I(r,z,t) = I_p\,(R_o/R(z))^2 \exp(-(r/R(z))^2)\exp(-((t-z/c)/\tau)^2)$$

. . . 2.2.6

where

I_p is the peak intensity,

R_o is the (spatial) 1/e radius of the laser beam at z=0,

τ is the (temporal) 1/e halfwidth of the laser pulse and

$R(z)^2 = R_o^2(1 + (\lambda z/\pi R_o^2)^2)$ is the square of the radius of the beam at z.

Figures 2.1(a) and 2.1(b) show iso-intensity contours for an intensity $^1/_{10}$ of the peak intensity as the laser pulse propagates through the focal region. The 1/e focal spot radius used was 6.5μm and the pulse lengths used are 1000ps and 1ps, respectively. A 1eV electron moving through such a laser beam in a transverse direction (i.e., perpendicular to the direction of propagation of the light) will take ~21ps to traverse the 13μm focal region. From Figure 2.1(a), it can be seen that for a pulse much longer in duration, the intensity profile varies very little. That is, at any given point in the focal volume, the local laser beam intensity will not change significantly during the time it takes the electron to move through that region and hence, the acceleration will occur in a conservative, steady state potential. However, as the pulse length becomes shorter (as in Figure 2.1(b)), the electron can experience large temporal changes in the local laser intensity. In this case, the potential formed by the light field can no longer be regarded as stationary. Finally, it should also be noted that the scale in the z-direction in Figures 2.1(a) and 2.1(b) is much greater than the scale used for the transverse direction. Consequently, the gradients in the transverse direction are much greater than those in the axial direction.

(a)

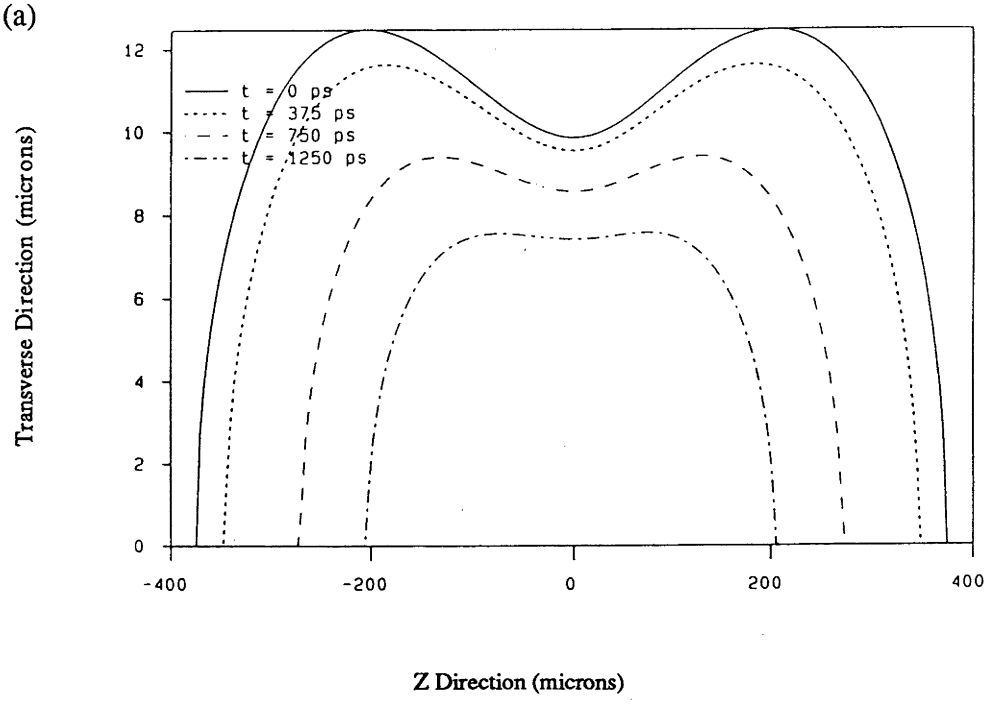

(b)

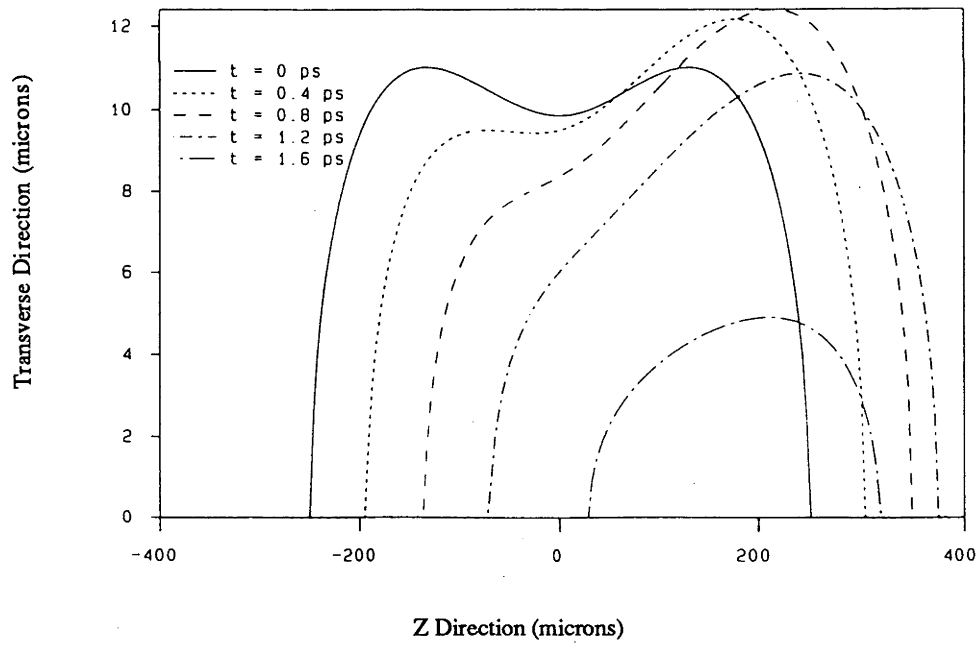

Figure 2.1: Laser pulse iso-intensity contours for an intensity of $I_p/10$

(a) τ = 1000ps; (b) τ = 1ps.

2.3 COMPUTER SIMULATIONS

The energy with which the ejected electrons reach the detector depends upon three factors. The first contribution comes from the initial (excess) energy of the electron arising from the difference between the energy from the absorbed photons and the raised ionisation potential - see Figure 1.1. The electron is ejected with this energy in a direction determined by its final angular momentum state. The second source is the energy the electron gains from (ponderomotive) acceleration down the potential gradient created by the light pulse used to irradiate the atoms. This is merely the conversion of the oscillation energy the electron has in the field to the directed kinetic energy it possesses once the electron is free of the field. The third effect is the energy lost or gained through the presence of a net coulombic force generated by the ions and other electrons. However, in the following cases, the gas pressure will be assumed to be low enough ($\leq 10^{-6}$torr) that coulombic type forces may be ignored (Lompré et al, 1985).

It will be further assumed that the laser pulse ($\geq$50fs) is much longer than the period of one oscillation (~3.5fs) of the field, so that the pulse can be seen as a smooth envelope and field oscillations do not have to be accounted for when calculating the macroscopic motion of an electron along the electromagnetic field gradient.

The simulation is performed in the following way. The focal region is assumed to be cylindrically symmetric about the direction of propagation of the laser pulse and is divided into slices in the axial (z), radial (r) and polar (θ) directions - see Figure 2.2. Because of the cylindrical symmetry used here, the radial direction is taken to be purely in the x-y plane, i.e., there is no z component in the radial direction. Electrons are generated instantaneously once the laser pulse intensity

has reached a specified threshold at the location the electron is to be liberated. They are then assigned a "weighting" corresponding to the volume element ($dz.dr.d\theta$) in which they are generated. The electrons are accelerated down the slope of the laser intensity profile and are stepped out in time using either an Euler or a Runge-Kutta technique to solve the Newtonian equations of motion. Each electron is assumed to be independent of all the others, i.e., there are no collective effects. This is a valid assumption because experimental conditions generally use gas pressures low enough ($\approx 10^{-6}$torr) that any coulombic forces exerted on an electron by the ions and other electrons are negligible compared to the force felt from the laser pulse. When they have reached their terminal velocity, i.e., they are no longer accelerated and therefore gain no further energy, the positions, velocities and energies of the electrons are recorded.

The simulations were successively performed in one, two and three dimensions and are described individually in Sections 2.4 to 2.6. The one- and two-dimensional cases were simulated using a VAX 8700 mainframe computer, while the three-dimensional simulations were performed on the Fujitsu VP-100 supercomputer at the Australian National University, due to the extensive computational time involved.

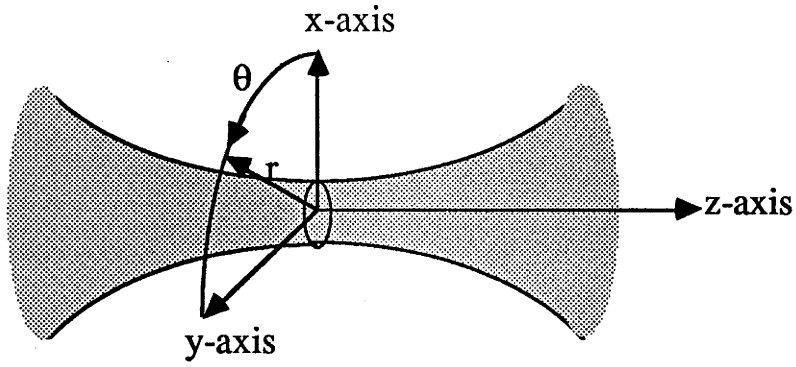

Figure 2.2: Schematic of laser focus, showing cylindrical symmetry.

2.4 1-D STUDIES

Initially, a simple one-dimensional case is examined in order to determine the dependence of the final electron energy on factors such as laser pulse width and focal spot size and subsequently, to use these results to guide the 2-D and 3-D simulations. The ponderomotive acceleration of the electron is assumed to be purely transverse and the z-dependence of the beam intensity is ignored, so that

$$a_r(t) = \frac{e^2\lambda^2 r}{\pi c m^2 R(z)^2} I(r,z,t) \qquad \ldots 2.4.1$$

It is assumed that one atom is singly ionised, i.e., only one electron is accelerated from the centre of the focal volume (r=0) in a transverse direction. This is in order to study the effects of varying focal, beam and energy parameters, so that the acceleration history of an individual electron can be clearly seen. In the following tests, the final energy of the electron depends on its initial excess energy and the conversion of its oscillation energy to directed kinetic energy. These two sources of electron energy are varied by altering the excess energy directly and indirectly, by changing the pulse length, the threshold ionisation potential, the peak field intensity and the focal spot size.

Preliminary tests for a peak intensity of $2\text{x}10^{14}\text{W/cm}^2$, a threshold intensity of $1\text{x}10^{14}\text{W/cm}^2$ and a range of pulse widths (0.2ps to 20ns) show that by the time an electron with 2eV excess energy has travelled a distance two to three times the spot radius of 5 microns from where it was ionised, it had over 99.9% of its final energy. Low excess energy electrons (0.02eV) experiencing the same intensities and pulses ≥2ns, however, have to travel roughly 5-6 spot radii before gaining their final energy. This suggests that for an electron sufficiently low in initial

energy, the pulse may catch up with it, i.e., the electron is not accelerated instantly from the beam. Hence, the electron may ride along on the front of the pulse, or "surf", for a while before being accelerated down the potential hill and gaining energy (see, for example, the asymmetric angular distributions of Xenon, Krypton and Helium in Bashkanksy et al).

Tests on very short pulses (≤0.4ps) showed that the final energy of the electron is approximately equal to its excess energy. This is because the pulse disappears immediately following ionisation, before the electron has a chance to be accelerated down the potential hill. That is, the pulse is so short that the electron does not have time to convert its oscillation energy to directed kinetic energy.

Finally, convergence testing using the Euler routine showed that for the intensities, spot size and range of pulse lengths used above, time steps of 0.001ps were sufficiently small to ensure that errors in the final energy were less than 0.01%. It should be noted that no physical significance should be placed on the use of time steps less than one optical cycle. They were simply used here to test the convergence of the solution and were valid under the assumption that the pulse was a broad envelope.

The first set of parametric tests (like the preliminary tests) were performed using a wavelength of 1.064μm and a spot size of 5 microns, with the ionisation occurring at the origin. The peak intensity was $2x10^{14}W/cm^2$ with an ionisation threshold intensity of $1x10^{14}W/cm^2$. The pulse width (as the independent variable) ran from 0.1ps to 20ns, although the main changes occurred for pulses less than about 80ps. Several curves, for differing excess energies, were plotted with the dependent variable being the ratio of the final energy of the electron to the sum of its initial (excess) energy plus that it was expected to gain from the

conversion of its oscillation energy to kinetic energy - see Figure 2.3. It was found that as the excess energy increased, the pulse width that was required for the final energy to approach the $E_{osc} + E_{excess}$ asymptote decreased as did the deviation from the asymptote for short pulses. This indicated that an electron with a lower initial energy would not be accelerated out of the beam as fast as one with higher initial energy and would therefore gain relatively more energy from surfing.

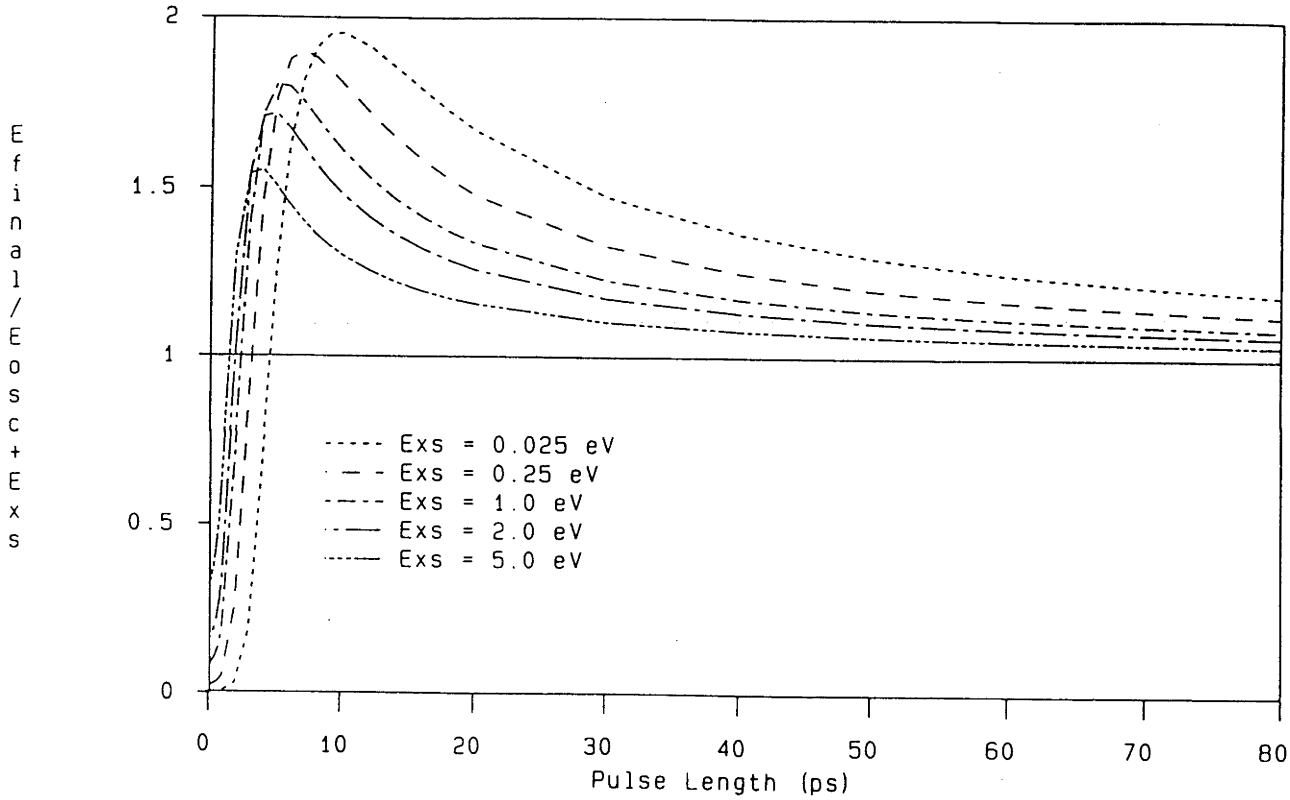

Figure 2.3: Final electron energy plots for 1-D simulations using various excess energies

$I_p = 2x10^{14} W/cm^2$; $I_t = 10^{14} W/cm^2$; $R_o = 5\mu m$

The second set of curves were obtained using the same wavelength, spot size and ionisation position, with an excess energy of 1eV. The peak intensity was varied between $2x10^{12}W/cm^2$ and $2x10^{15}W/cm^2$, while the ratio of the peak intensity to the threshold intensity was kept at a constant value of 2.

From Figure 2.4, it can be seen that the greater the peak intensity, the greater the deviation from the asymptote and the shorter the pulse length required to gain the maximum energy. At first glance, it appears that the relative energy gains for electrons in the higher intensity fields are greater than those for lower intensity fields. However, this is misleading. The relative energy gains are approximately the same. An electron accelerated from near the peak of a low intensity pulse will gain substantially less energy than one accelerated from the same position in a high intensity pulse. Consequently, the excess energy is a larger component of the asymptotic value for low intensities than for high intensity pulses. Hence, the ratio of the final energy to the asymptotic value will be lower for an electron accelerated from a low intensity pulse than for one accelerated from a high intensity pulse.

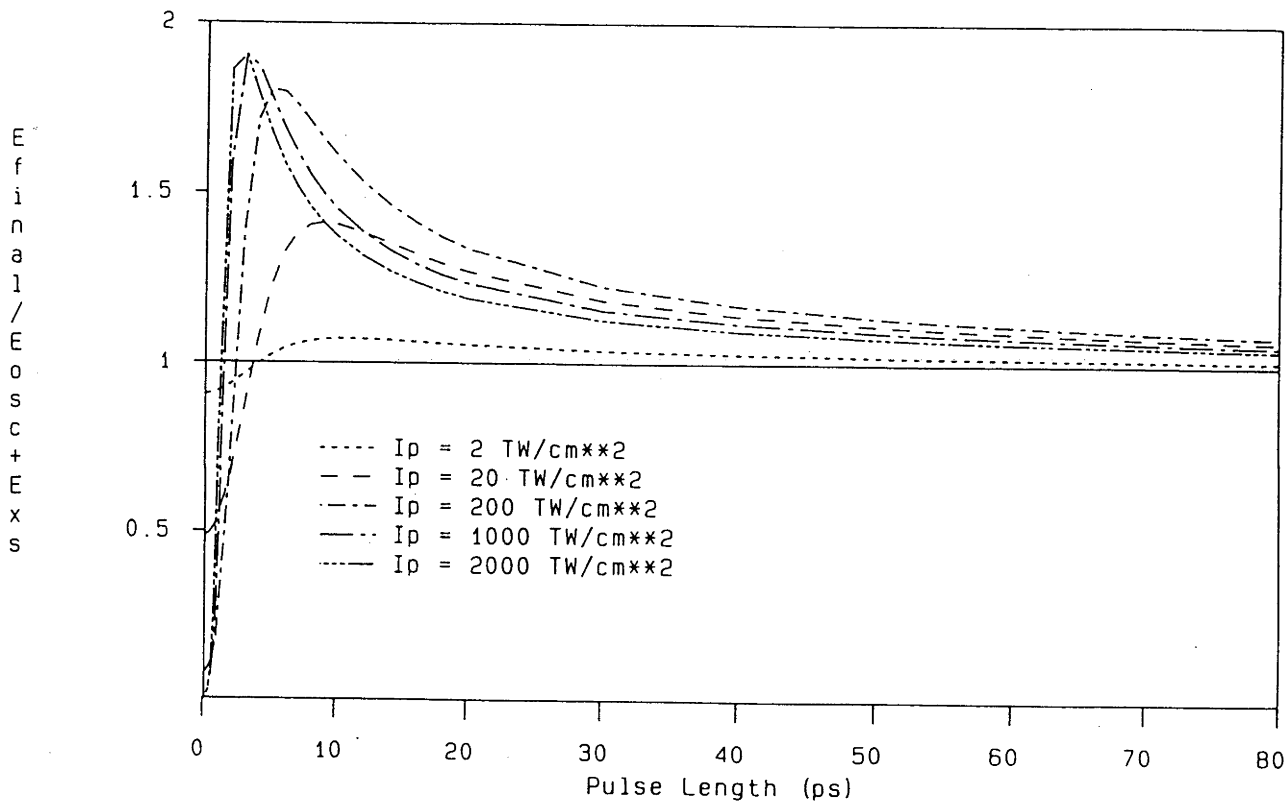

Figure 2.4: Final electron energy plots for 1-D simulations using various peak field intensities

$I_p/I_t = 2$; $E_{excess} = 1eV$; $R_o = 5\mu m$

The next five sets of curves were obtained under the much the same conditions, but differed by keeping the peak intensity constant while varying the threshold intensity (see Figure 2.5(a)-(e)). For peak intensities of $2x10^{14}W/cm^2$ or greater, as the threshold intensity decreased, the deviation from the asymptote for short pulses increased. The deviation also grew with increasing peak intensity. Basically, for high peak intensities and high peak to threshold intensity ratios, an electron can gain a large amount of energy (compared to its initial energy) from the laser beam by converting its oscillation energy in the field to directed kinetic energy. However, for peak intensities $\leq 2x10^{13}$ W/cm^2, the above observations do not, in general, apply. At these intensities, the excess energy of the electron is comparable to, or even greater than, the energy it gains from ponderomotive acceleration. Consequently, the energy gained from the conversion of oscillation energy to directed kinetic energy does not influence the final energy of the electron as much as it does for high intensity cases and the final energy does not, therefore, deviate as much from the asymptotic value.

(a)

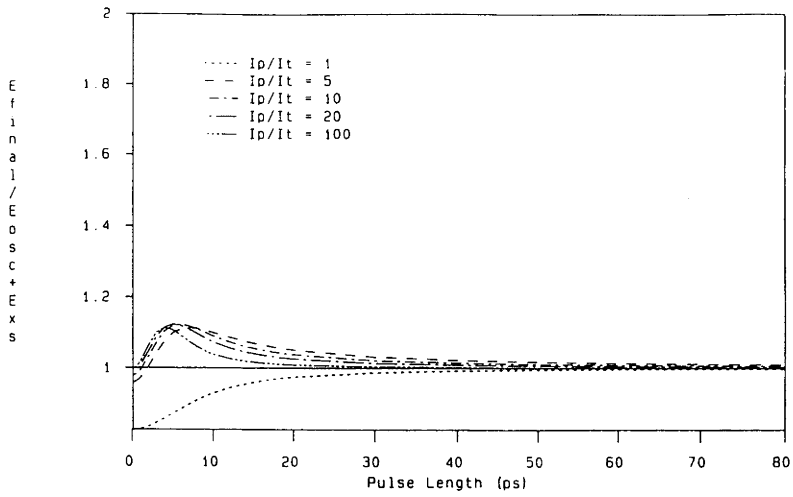
Efinal/Eosc+Exs
Ip/It = 1
Ip/It = 5
Ip/It = 10
Ip/It = 20
Ip/It = 100
2
1.8
1.6
1.4
1.2
1
0
10
20
30
40
50
60
70
80
Pulse Length (ps)

(b)

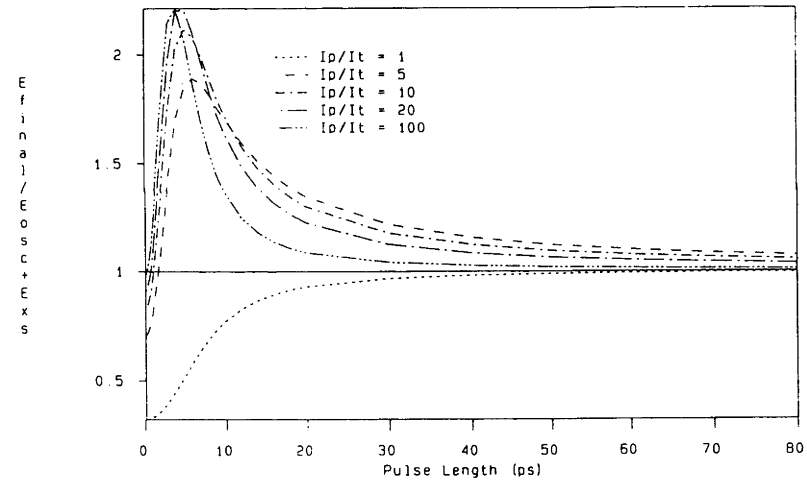
Efinal/Eosc+Exs
Ip/It = 1
Ip/It = 5
Ip/It = 10
Ip/It = 20
Ip/It = 100
2
1.5
1
0.5
0
10
20
30
40
50
60
70
80
Pulse Length (ps)

(c)

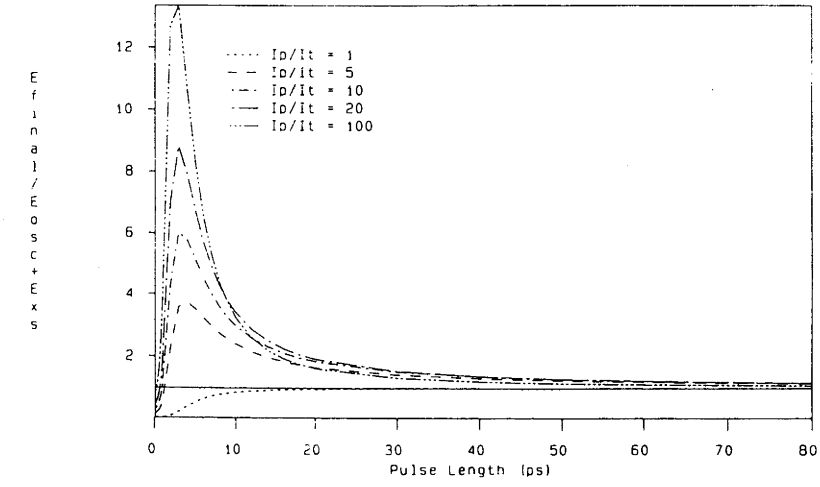
Efinal/Eosc+Exs
Ip/It = 1
Ip/It = 5
Ip/It = 10
Ip/It = 20
Ip/It = 100
12
10
8
6
4
2
0
10
20
30
40
50
60
70
80
Pulse Length (ps)

(d)

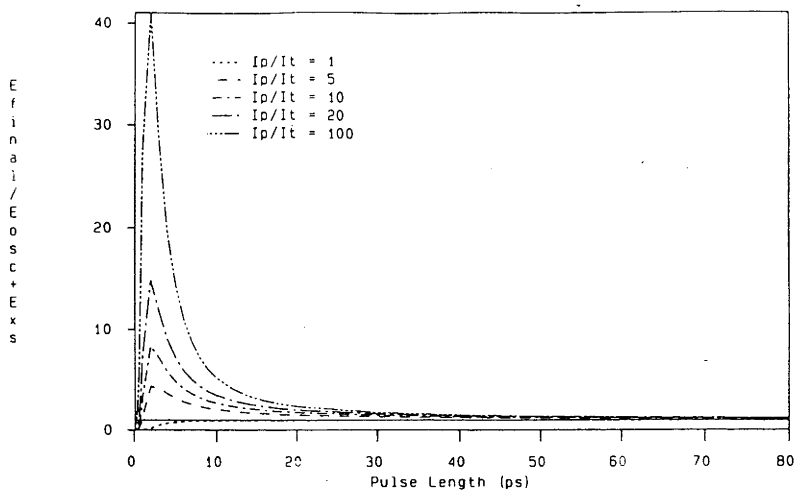

(e)

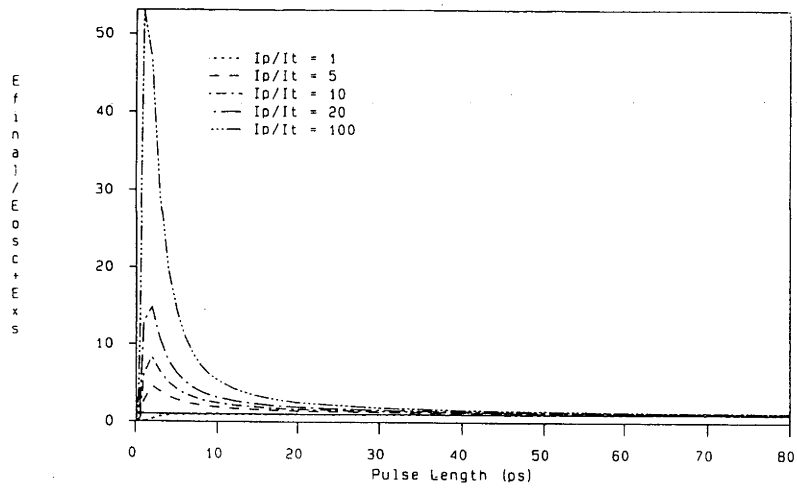

Figure 2.5: Final electron energy plots for 1-D simulations using various peak to threshold intensity ratios

E_{excess} = 1eV; R_o = 5μm

(a) $I_p = 2x10^{12}W/cm^2$; (b) $I_p = 2x10^{13}W/cm^2$;

(c) $I_p = 2x10^{14}W/cm^2$; (d) $I_p = 10^{15}W/cm^2$;

(e) $I_p = 2x10^{15}W/cm^2$

The final sets of plots generated with the pulse length as the independent variable were performed for an electron starting at the origin with an excess energy of 1eV, experiencing a pulse with a peak intensity of $2x10^{14}W/cm^2$ with varying threshold intensities and different spot sizes (see Figure 2.6(a)-(c)). The curves showed the same trends as before and converged to the asymptotic value at pulse lengths proportional to their spots sizes, i.e., the plots with a 1/e spot radius of 2μm converged for a pulse width about five times shorter than those with a 1/e spot radius of 10μm.

For cases where the peak intensity exceeded the threshold intensity, four regimes were identified:

(i) For a pulse width to spot size ratio <0.1 ps/μm, the electron emerged from the laser beam with $E_{final} = E_{excess}$.

(ii) For a pulse width to spot size ratio >0.1 ps/μm but <0.2 ps/μm, the electron emerged with $E_{excess} < E_{final} < E_{osc} + E_{excess}$.

(iii) For a pulse width to spot size ratio >0.2 ps/μm but <10 ps/μm, the electron emerged with $E_{final} > E_{osc} + E_{excess}$.

(iv) For a pulse width to spot size ratio >10 ps/μm, the electron emerged with $E_{final} = E_{osc} + E_{excess}$, i.e., the asymptotic value.

The third regime supports the idea of "surfing" as it shows that if an electron is caught by a pulse which is long enough for the electron to ride, but sufficiently short so that the electron sees a substantial change in intensity before or while accelerating down the potential gradient, the electron may gain energy in non-quantal amounts. Similarly, if a pulse is sufficiently short, it may disappear before the electron has time to convert its oscillation energy in the field into directed kinetic energy. Hence, the electron emerges from the beam with a final energy lower than $E_{osc} + E_{excess}$. It should be noted that the values of the

pulse width to spot size ratio are only estimates as these regimes tend to vary slightly with peak to threshold intensity ratios. These regimes have also been independently identified by Jönsson.

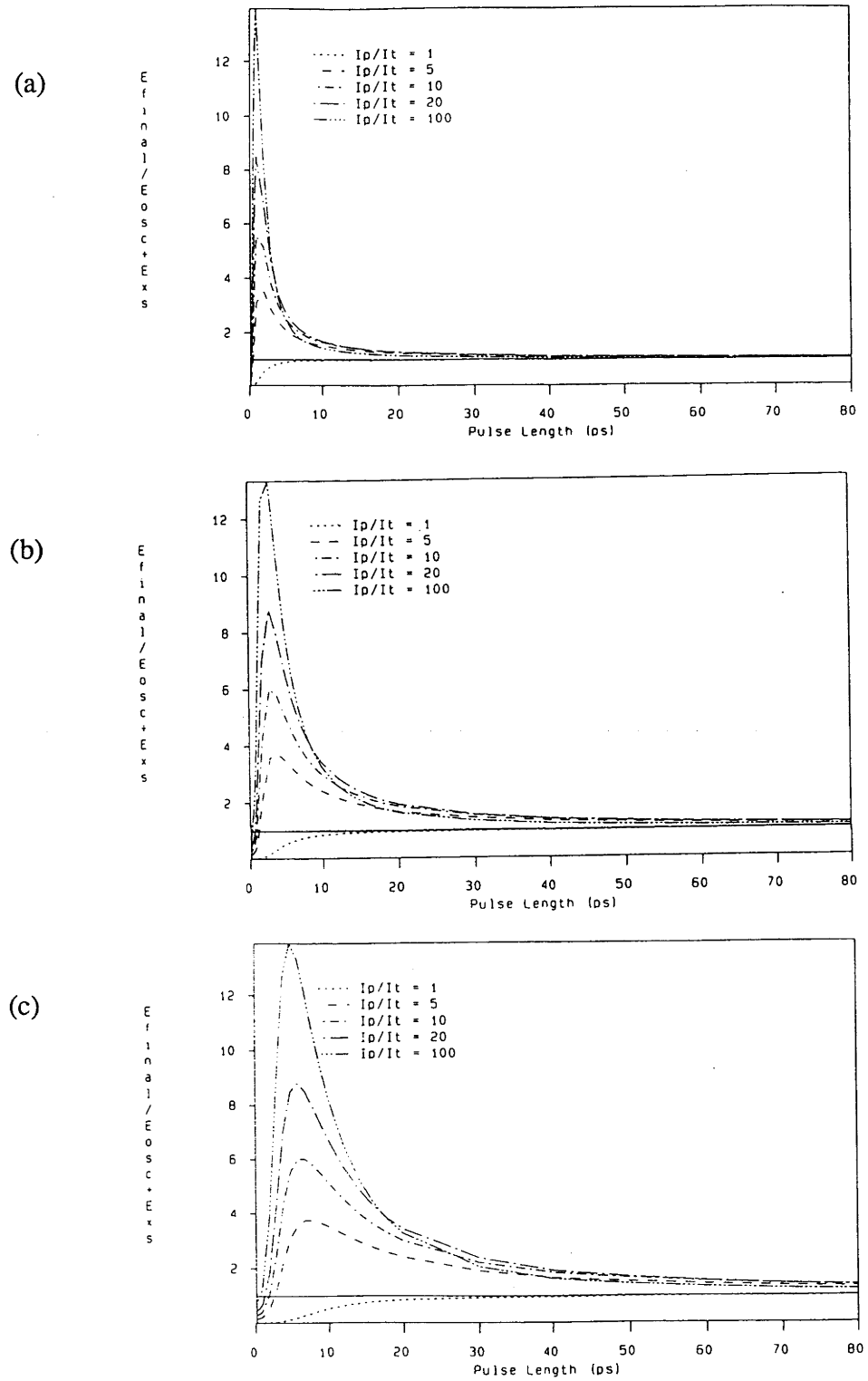

Figure 2.6: Final electron energy plots for 1-D simulations using various focal spot sizes

$I_p = 2x10^{14} W/cm^2$; $E_{excess} = 1eV$

(a) $R_o = 2\mu m$; (b) $R_o = 5\mu m$; (c) $R_o = 10\mu m$

Finally, in order to validate the above observations, more sets of curves were generated by holding the peak intensity to threshold intensity ratio at a constant value of 5 and by varying the peak intensity. The spot size was also varied linearly with the pulse width. The resulting plots were straight lines (see Figure 2.7), thus showing that varying the spot size would have much the same effect as varying the pulse width and hence, it was unnecessary to plot curves with the spot size as the independent variable. There was a slight deviation of the final energy curves from the asymptote for small pulse lengths, but this was thought to arise from a numerical instability due to the step size. The ratios of E_{final} to $(E_{osc}+E_{excess})$ differ due to varying peak intensities. It is interesting to note that the ratio is the lowest (~1.02) for the lowest peak intensity ($2x10^{12}W/cm^2$) and increases to ~1.3 for peak intensities up to $2x10^{14}W/cm^2$, (as would be expected), but then decreases again for intensities of $1x10^{15}W/cm^2$ and $2x10^{15}W/cm^2$. However, these values are all close to 1 and so, the energy differences merely highlight the slightly different rates of convergence to the $E_{osc}+E_{excess}$ asymptote.

The final energy of the electron, therefore, was found to be determined by the pulse width to spot size ratio, the peak to threshold intensity ratio and the relative value of the field intensity compared to the excess energy.

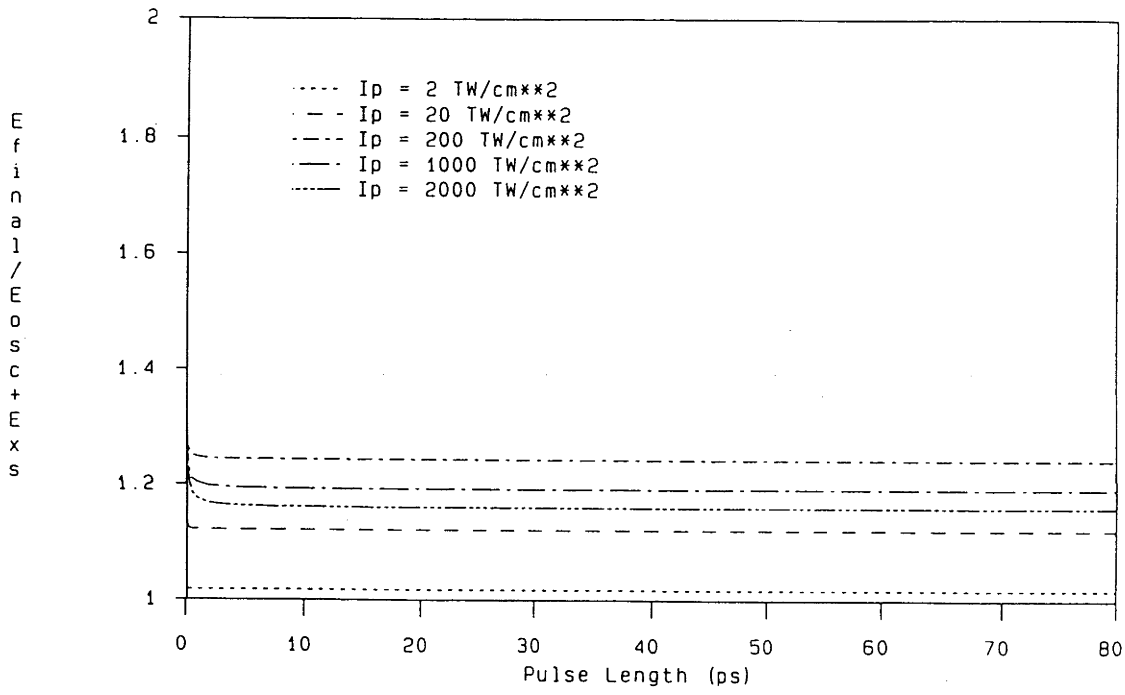

Figure 2.7: Final electron energy plots for 1-D simulations using various peak intensities

$I_p/I_t = 5$; $E_{excess} = 1eV$; $\tau/R_o = 10ps/\mu m$

2.5 2-D STUDIES

In the following cases, both r- and z-dependences of the intensity profile are taken into account. The acceleration is along the r-z potential gradient (i.e, there is no θ dependence). The excess energy (i.e., the initial velocity of each electron) is assumed to be directed purely transversely to the direction of light propagation, i.e., in the r direction (Figure 2.2). Although each electron is generated at a different radius in the focal region, the results from this study can be understood in terms of the four regimes as identified in the 1-D case.

To demonstrate the effect of ponderomotive acceleration on ATI, the first five unsuppressed peaks (i.e., those states resulting from the absorption of 10 to 14 photons above that required for zero-field ionisation) of ArI were calculated for 1.064μm radiation in the following simulations. The ionisation threshold intensity was taken as 10^{14}W/cm^2 (from the theoretical data of Baldwin) and the excess energy for ATI peak 10 was 0.471eV. Higher order ATI peaks were successively generated by adding the photon energy (1.165eV) to the excess energy of the peak before.

The effect of changing the pulse width and the peak intensity can be seen in Figure 2.8. The 1/e radius of the focal spot was 1μm. Figure 2.8(a) was generated using a 1/e pulse width of 22ps and a peak intensity of 2x10^{14}W/cm^2. Figure 2.8(b) used the same peak field intensity, with a 1/e pulse width of 13ps. Finally, Figure 2.8(c) used a pulse width of 13ps and a peak intensity of 10^{15}W/cm^2. Comparing Figures 2.8(a) and 2.8(b) shows that decreasing the pulse width from 22ps to 13ps for a 1μm spot results in a broadening of the spectral peaks due to an increased amount of "surfing". This is similar to the four regimes identified in the one-dimensional studies. Similarly, by comparing

Figures 2.8(b) and 2.8(c), the effect of increasing the peak intensity from $2x10^{14}W/cm^2$ to $10^{15}W/cm^2$ is to also broaden the spectral peaks due to an increased amount of surfing.

(a)

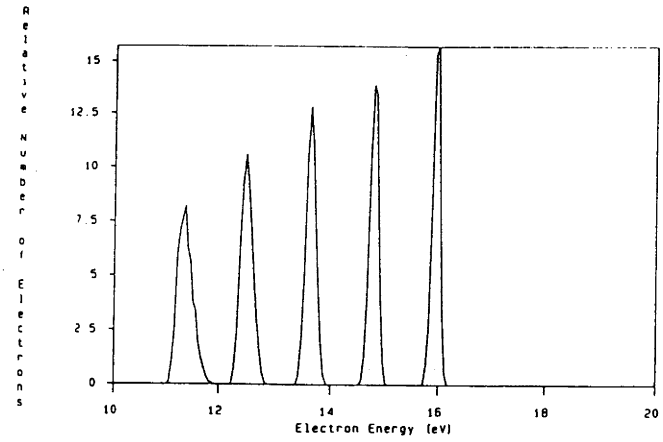

(b)

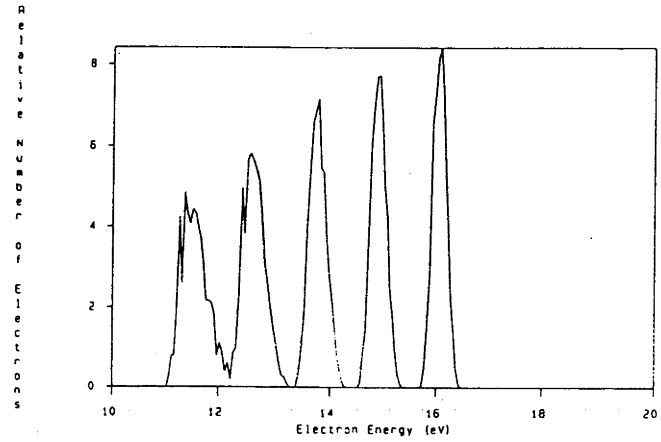

(c)

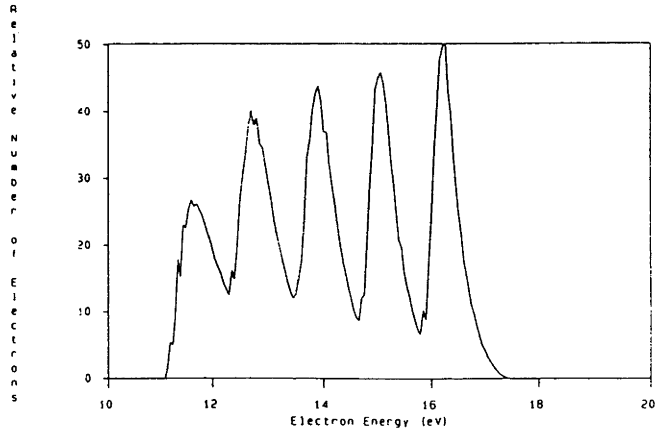

Figure 2.8: ATI peaks 10-14 for ArI - the effects of varying pulse width and peak intensity. $I_t = 10^{14}W/cm^2$; $R_0 = 1\mu m$

(a) $I_p = 2x10^{14}W/cm^2$; $\tau = 22ps$

(b) $I_p = 2x10^{14}W/cm^2$; $\tau = 13ps$

(c) $I_p = 10^{15}W/cm^2$; $\tau = 13ps$

The effects of altering the focal geometry on the resultant electron energy spectrum can be seen from Figures 2.9(a) to 2.9(c). The peak intensity used was $10^{15}W/cm^2$, the threshold intensity was $10^{14}W/cm^2$ and the 1/e pulse width was 13ps. Figure 2.9(a) used a 1μm spot size with a divergence in accordance with its Gaussian beam shape. Figure 2.9(b) was generated using a 6.5μm spot size, with a divergence similar to that of a 1μm Gaussian beam, i.e., the geometry of the beam was that resulting from broadening a 1μm spot by 5.5μm. This is a situation where the beam was not diffraction limited, being roughly equivalent to an aberrated beam. The situation was included to test the effects of beam divergence, as opposed to beam diameter, on the calculations. Figure 2.9(c) used a Gaussian beam with a 6.5μm 1/e spot size and a corresponding divergence.

As can be seen from Figure 2.9, increasing the focal spot size leads to the individual ATI peaks merging to form one broad peak with a greater range of electron energies. Examining Figures 2.9(b) and 2.9(c) shows that this is due to the increase in the focal spot size and is not due to altering the apparent beam divergence. The effects observed in Figure 2.9 can be explained in the following way. The higher energy electrons arise because the pulse width to spot size ratio decreases from 13 to 2 ps/μm and is now small enough to allow them to "surf" on the laser pulse and gain energy. The appearance of electrons lower in energy than expected (Figure 2.9(b)) can also be explained when one considers that these electrons are generated further out in the focal region and therefore see the pulse disappearing before they have the opportunity to totally convert their oscillation energy in the field to directed kinetic energy.

The conditions used to generate Figure 2.9(c) were similar to those governing an experiment on argon performed by Baldwin in 1979, using a Nd:YAG glass laser which emitted light with a wavelength of 1.064μm. The laser beam was focussed to a 1/e waist size of 13±2μm. The pulse length was 22±2ps and the peak laser intensity for the first argon experiment was $3x10^{15}W/cm^2$, while for the second one it was $2x10^{16}W/cm^2$.

Figure 2.10 shows the experimental results. It can be seen by comparison with Figure 2.9(c) that the absence of individual spectral peaks in these results is not necessarily due to limits in instrumental resolution, but may be characteristic of the ponderomotive acceleration under these conditions. A full comparison with the experimental work will be left until discussion of the full 3-D calculations in Section 3.6.

(a)

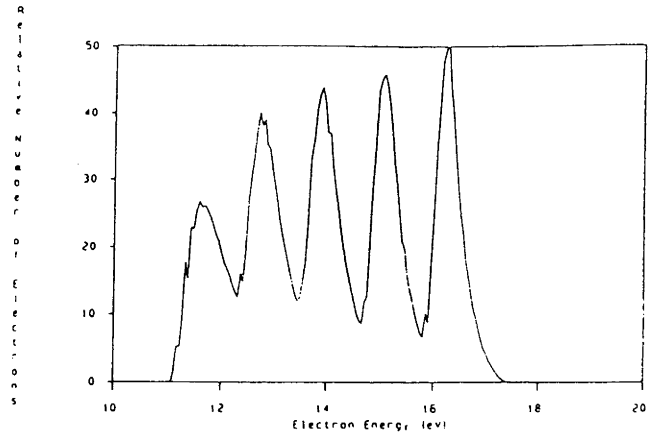

(b)

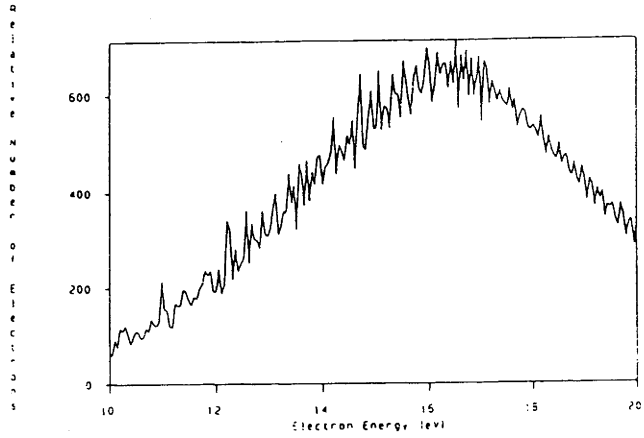

(c)

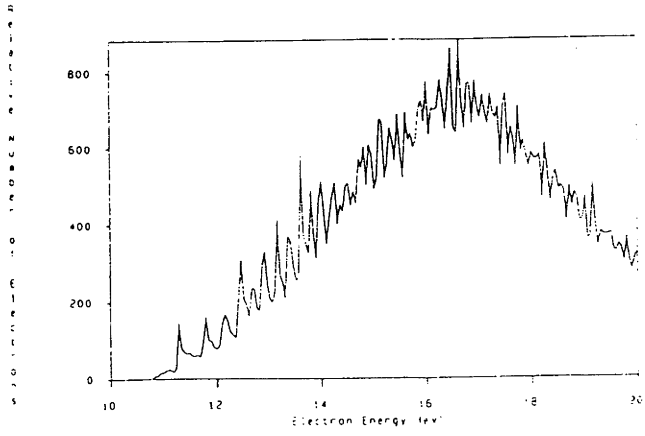

Figure 2.9: ATI peaks 10-14 for ArI - the effects of varying focal and beam parameters. $I_p = 10^{15}$ W/cm^2; $I_t = 10^{14}$ W/cm^2; τ = 13 ps

(a) R_o = 1 μm (divergence = 1 μm beam)

(b) R_o = 6.5 μm (divergence = 1 μm beam)

(c) R_o = 6.5 μm (divergence = 6.5 μm beam)

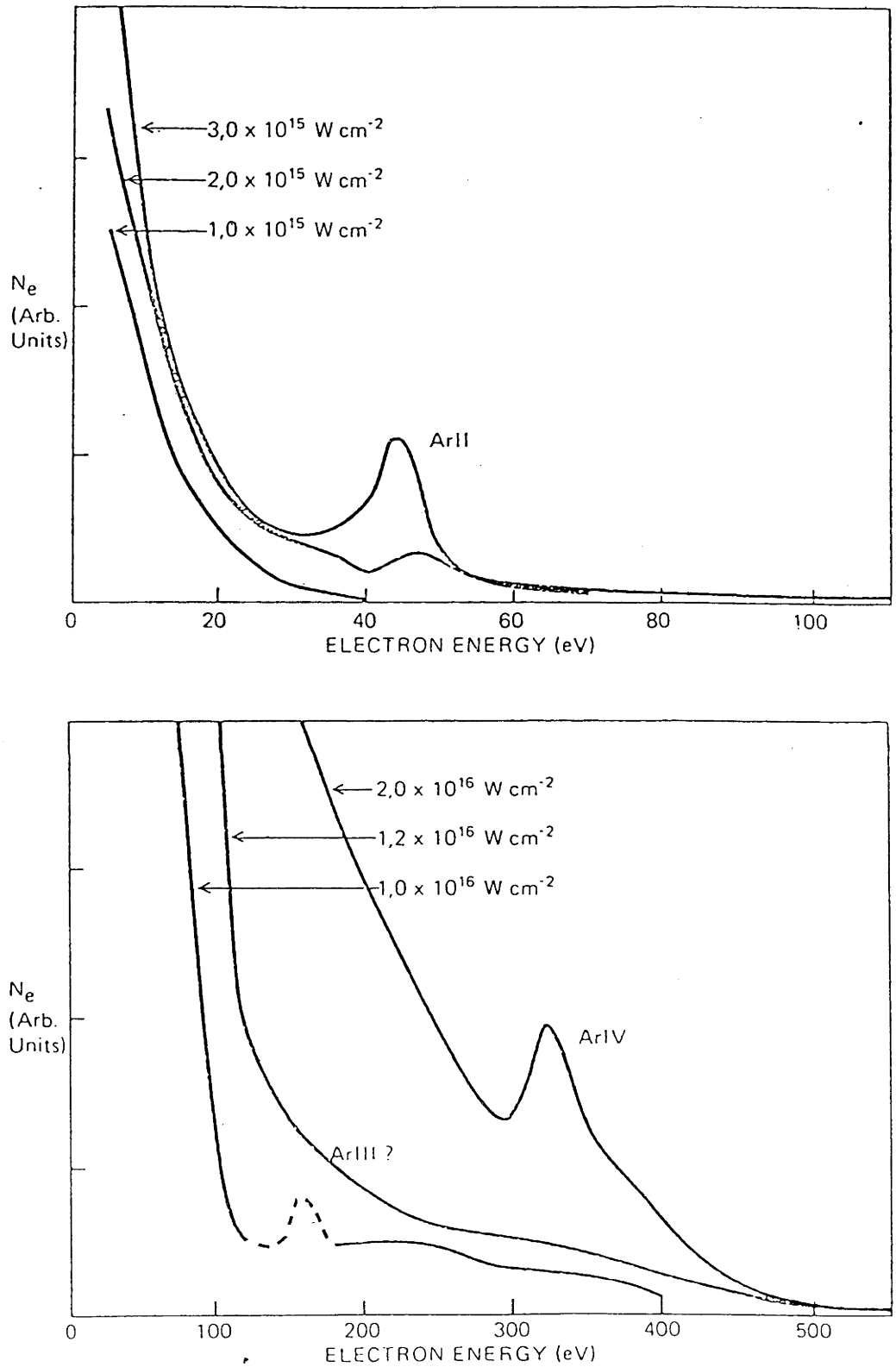

Figure 2.10: Experimental Results (Baldwin)

2.6 3-D STUDIES

Electrons were generated in the focal region of a Gaussian laser beam and were accelerated out of the laser beam in three dimensions. The electrons were generated at various r, z locations in the focal volume and were ejected from the atoms with initial energies in directions ranging from $\theta = 0$ to $\theta = 2\pi$ radians (see Figure 2.2). The electrons therefore had accelerations in the x, y and z directions, defined by

$$a_x(t) = \frac{e^2\lambda^2 x}{\pi c m^2 R(z)^2} I(x,y,z,t)$$

$$a_y(t) = \frac{e^2\lambda^2 y}{\pi c m^2 R(z)^2} I(x,y,z,t)$$

$$a_z(t) = \frac{e^2\lambda^2}{\pi c m^2} \left\{ \frac{z}{R(z)^2} \left(\frac{\lambda}{\pi R_0}\right)^2 \left(1 - \frac{r^2}{R(z)^2}\right) - \left(\frac{t - z/c}{c\tau^2}\right) \right\} I(x,y,z,t) \quad \ldots 2.6.1$$

where

$$x = r\cos\theta$$

and

$$y = r\sin\theta.$$

The 3-D simulations were performed using the program ELECTRON, which was written in consultation with Dr L Brewin of the Australian National University Supercomputer Facility and run on the Fujitsu VP-100 supercomputer. A listing of the program can be found in Appendix A. The 1-D and 2-D results were reproduced using this code by omitting the relevant components from the calculations.

Bucksbaum et al showed experimentally that the electrons are ejected from the atoms in a non-isotropic distribution that depends on the angular momentum of the final state of the electron and on the polarisation of the laser field. Figure 2.11 shows a typical distribution of measured electron energies taken for short pulses where no ponderomotive effects are present. The results indicate that electrons are more likely to be ejected in the $\pm y$ (polarisation) direction than in the $\pm x$ direction in a linearly polarised laser beam. The model calculations used the initial excess energy distribution and were found to correlate closely with the initial distribution in the short pulse regime.

This data enables the final electron energy spectra to be calculated by weighting the different electron ejection directions according to the shape of the electron ejection distribution obtained from experimental or theoretical results. These spectra can also be weighted (as before) in proportion to the volume of the ionised segment where they originate. The final spectrum arising from acceleration in three dimensions can then be created by adding together the accelerated contributions from each volume.

Figure 2.12 shows the electron ejection distributions used in the 3-D simulations described in this section. The distributions shown in Figures 2.12 (b) and (c) were chosen primarily for their similarity to linearly polarised electron ejection distributions for helium (Bucksbaum et al) and krypton (Bashkansky et al). Figures 2.12 (a) and (d) were also included to test the effects of changing from a completely isotropic (circular) distribution to a highly directional (linear) one. For each polar plot, the peak value in the polarisation ($\pm$y) direction has a value of 1 and the other probabilities are scaled accordingly. The initial velocity of the electrons is directed in the x-y plane as indicated in Figure 2.12, with no component in the z-direction.

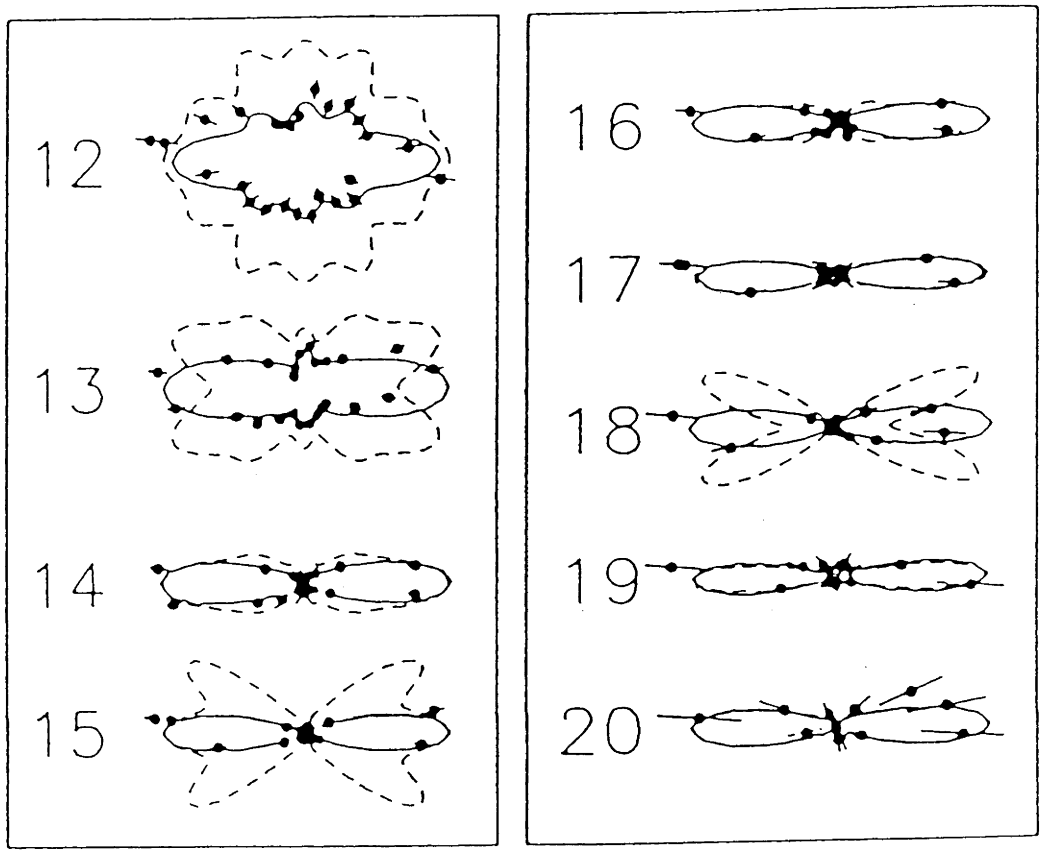

Figure 2.11: Photoelectron distributions in the azimuthal plane (perpendicular to the laser direction) for helium ATI peaks corresponding to 12 to 20 photons absorbed. The laser polarisation is horizontal in these diagrams. The peak laser intensity is $2 \times 10^{14} W/cm^2$. Points are data. The error bars are statistical. The solid lines are empirical fits. Dashed lines are predictions of the KFR theory. (Bucksbaum et al)

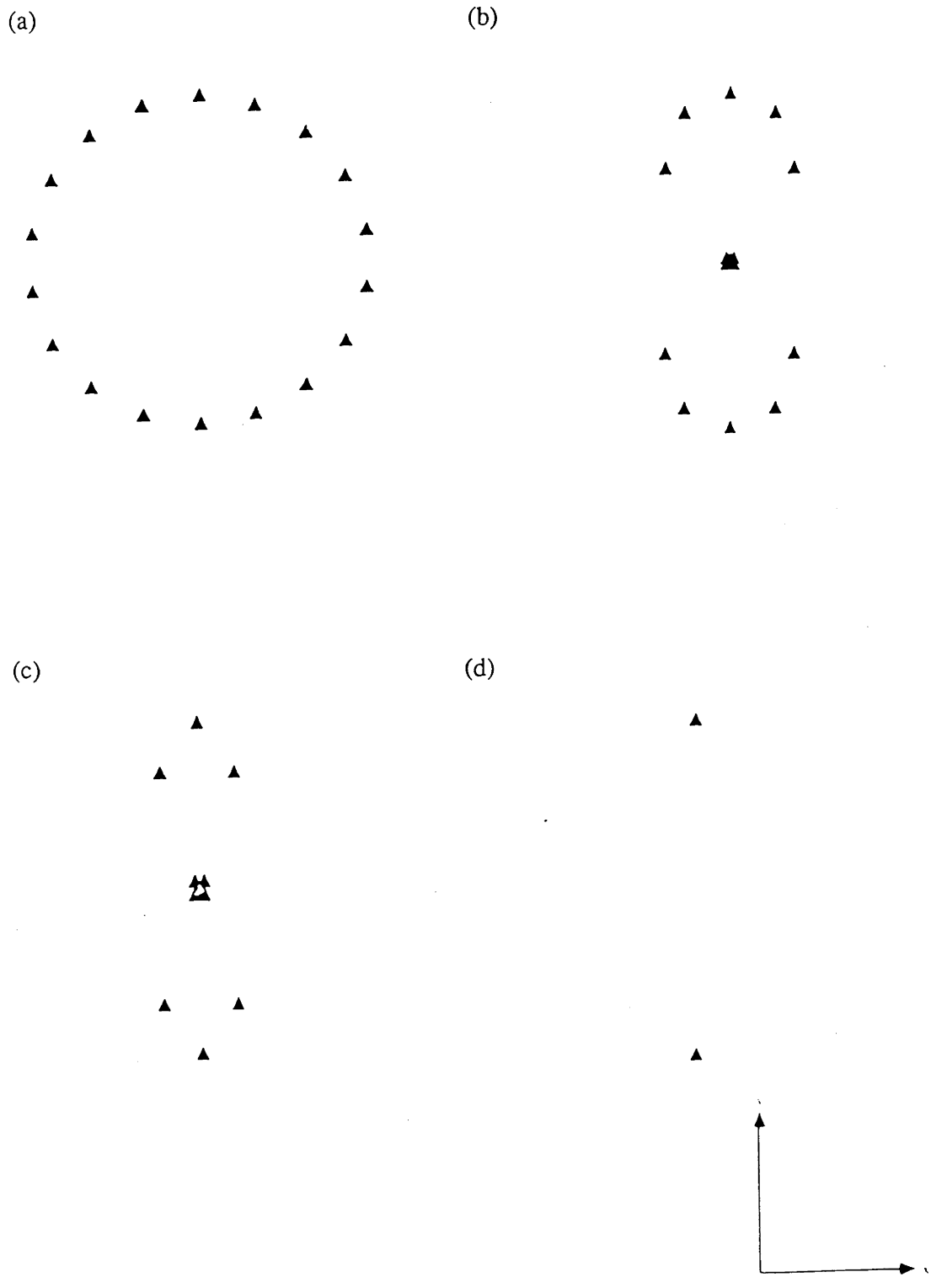

Figure 2.12 Electron ejection distributions used in 3-D simulations

(a) Circular; (b) Fat dumb-bell; (c) Thin dumb-bell; (d) ±y directions

Simulations of the first unsuppressed ATI peak for ArI calculated by this method are shown in Figure 2.13 ((a) - (e)). The parameters used are $I_p = 10^{15}W/cm^2$, $I_t = 10^{14}W/cm^2$, $R_0 = 1\mu m$, $E_{excess} = 0.471eV$, with 1/e pulse widths of 0.05ps, 0.25ps, 1ps, 10ps and 1000ps.

As can be seen, the only difference the various electron ejection distributions cause in each spectrum is the overall intensity or peak height. The different heights are simply due to the fact that fewer spectra are being added together for the more directional cases than for the isotropic case and so, the total number of electrons in the final spectrum is lower.

Comparing the spectra resulting from different pulse lengths, however, shows peaks at different energies and with different widths, corresponding to the regimes found in the 1-D simulations. Consequently, there are no low energy electrons for long pulses (10ps, 1000ps). For these cases, the beam can be regarded as stationary (or almost stationary) and all of the electrons have time to convert their oscillation energy to directed kinetic energy. As the width of the peaks increase, so does the signal noise - compare, for example Figure 2.13(a) and Figure 2.13(c). However, this is simply an artifact of the calculations. Because the electrons in the simulation are being spread over different energy ranges and since there are a fixed number of electrons for any ejection distribution used in the simulation, the final spectrum becomes less smooth as the width of the peaks increases. For example, the relative number of electrons in the peak of Figure 2.13(c) is about 5500, whereas for Figure 2.13(e), it is about 580000. The difference is a factor of about 100 and since the signal noise is roughly proportional to the square root of the signal, the spectrum in Figure 2.13(c) is approximately 10 times noiser than the spectrum in Figure 2.13(e).

Of particular interest is the spectrum in Figure 2.13(c). The pulse width to spot size ratio is 1 and the spectrum consequently shows a number of high energy electrons being generated from "surfing" on the laser pulse. The main peak occurs at 12-15eV, a little above the E_{osc} (~10.6eV) plus E_{excess} (~0.5eV) value of approximately 11.1eV. However, there is also a smaller peak at around 3-4eV. The lower energy peak could arise from electrons which fell off the back of the laser pulse and which subsequently find the pulse has disappeared before they can convert their oscillation energy into directed kinetic energy. In fact, a small number of electrons are ejected from the laser pulse with only the excess energy they had at ionisation. A 1ps pulse, therefore, is long enough for some electrons to gain substantial amounts of energy - five times (E_{osc}+E_{excess}) - from surfing, but also short enough that some electrons come out of the laser beam with an energy close to E_{excess}.

(a)

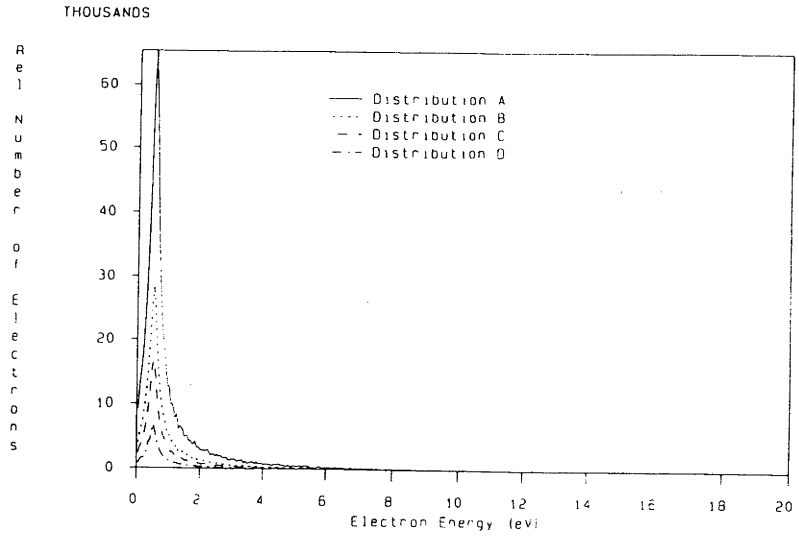
THOUSANDS
Rel Number of Electrons
Distribution A
Distribution B
Distribution C
Distribution D
0
10
20
30
40
50
60
0
2
4
6
8
10
12
14
16
18
20
Electron Energy (eV)

(b)

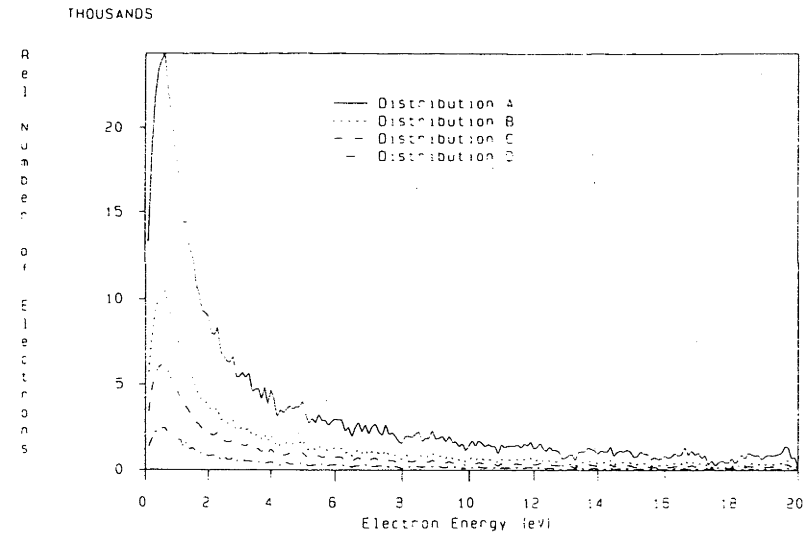
THOUSANDS
Rel Number of Electrons
Distribution A
Distribution B
Distribution C
Distribution D
0
5
10
15
20
0
2
4
6
8
10
12
14
16
18
20
Electron Energy (eV)

(c)

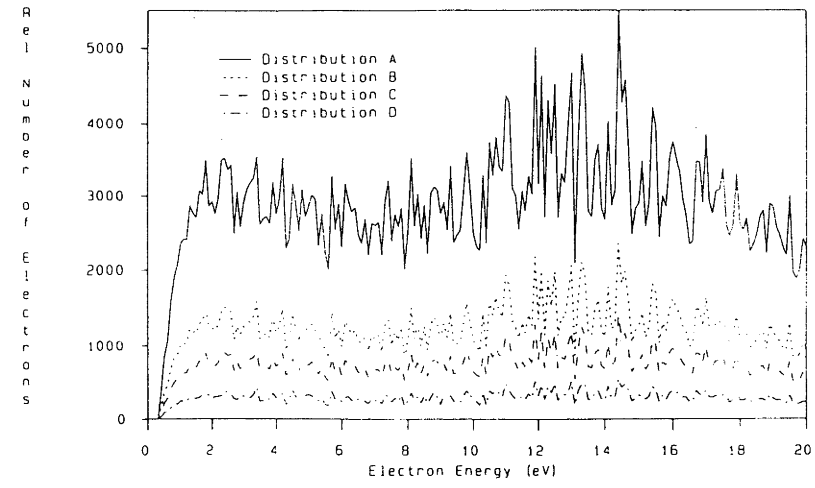
Rel Number of Electrons
Distribution A
Distribution B
Distribution C
Distribution D
0
1000
2000
3000
4000
5000
0
2
4
6
8
10
12
14
16
18
20
Electron Energy (eV)

(d)

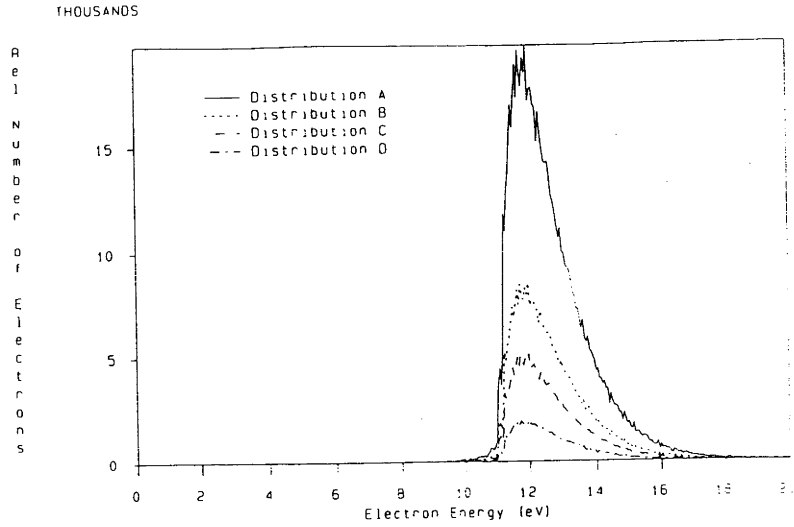

(e)

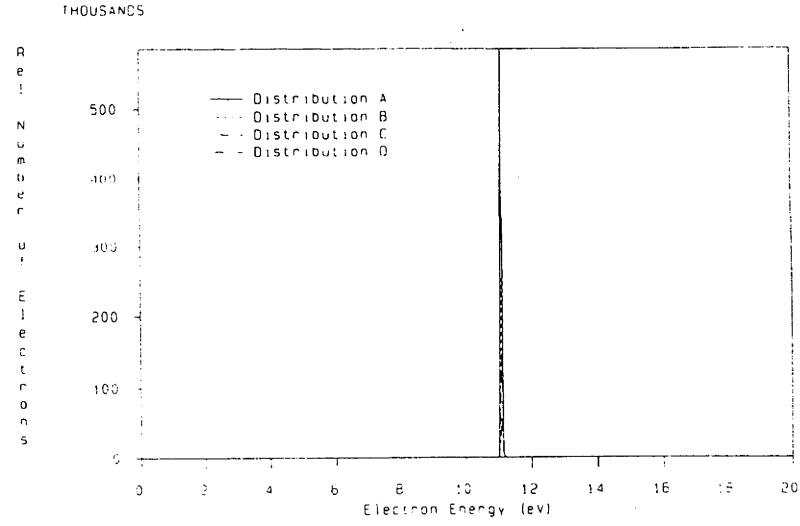

Figure 2.13 Electron energy spectra for ArI ATI peak 10

$I_p = 10^{15}W/cm^2$; $I_t = 10^{14}W/cm^2$; $R_0 = 1\mu m$; $E_{excess} = 0.471eV$

(a) $\tau = 0.05ps$; (b) $\tau = 0.25ps$; (c) $\tau = 1ps$;

(d) $\tau = 10ps$; (e) $\tau = 1000ps$

2.7 DETECTION OF ELECTRONS

The previous electron energy spectra were the result of detecting all of the electrons emitted from the focal region of the laser beam. However, experiments do not always detect all of the electrons and so, the detection geometry of the experiment must be taken into account when performing simulations of experimental conditions.

When an electron has reached its final energy, its position is at some point (x,y,z) on the surface of a sphere, radius r, centred on the focal region of the laser. It is assumed that the distance between the point of ionisation (a few microns) and zero is small compared to the distance to the point where the final energy is reached (tens to hundreds of microns from the origin). (Note: this distance is greater than that found for the 1-D case, due to electrons arising from the outer regions of the focal volume and not solely from the origin.) Detectors are typically a few centimetres away from the focal region. Hence, when simulating the detection of electrons, negligible error arises from using the origin as the place where the electrons are generated.

After it has stopped accelerating, the electron will travel with constant velocity

$$|v^2| = v_x^2 + v_y^2 + v_z^2 \qquad \ldots 2.7.1$$

to a point (X,Y,Z) on the surface of a sphere, radius R, on which the detector is located (see Figure 2.14).

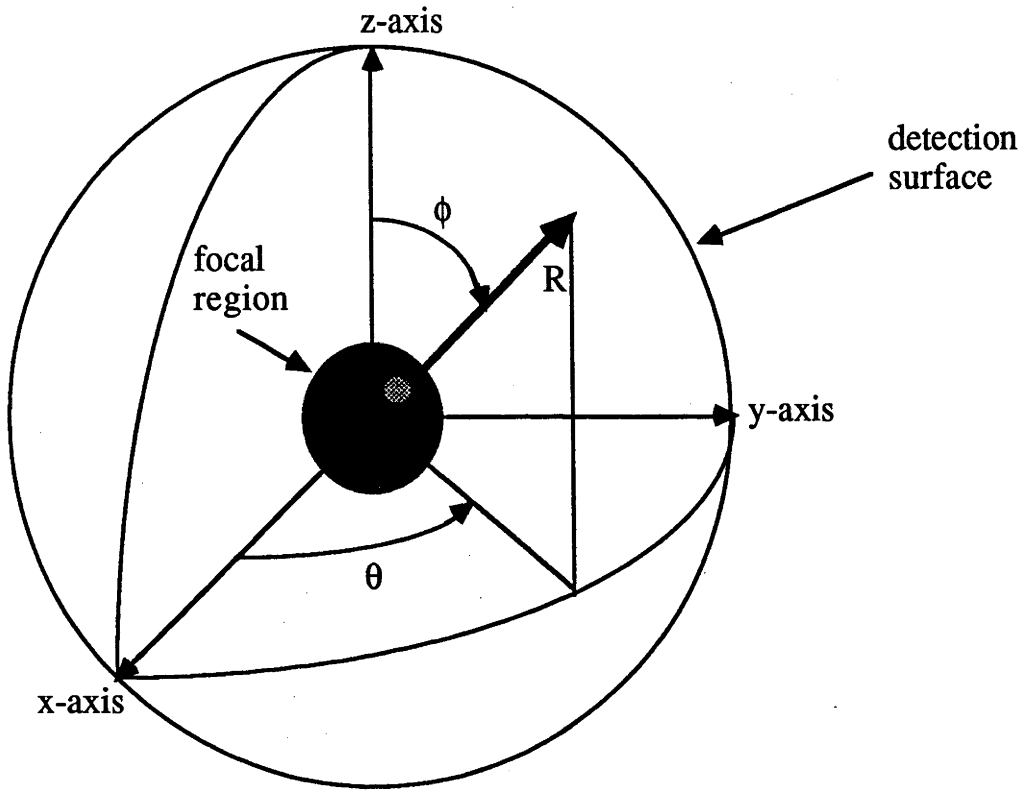

Figure 2.14: Spherical surface defining placement of detectors around the focal region. The direction of propagation of the laser beam is along the z-axis.

From geometry,

$$X^2 + Y^2 + Z^2 = R^2$$

. . . 2.7.2

Squaring equations for X, Y and Z (from Newtonian mechanics) and substituting into Equation 2.7.2 gives a quadratic in t

$$t^2 + \frac{2\,(xv_x + yv_y + zv_z)\,t}{|v|^2} + \frac{(r^2 + R^2)}{|v|^2} = 0$$

. . . 2.7.3

where t is the time of flight from the point at which the electron reaches its final energy to the point at which it is detected.

Using the solution for a quadratic, where

$$a = 1$$

$$b = \frac{2\,(xv_x + yv_y + zv_z)}{|v|^2}$$

$$c = \frac{r^2 + R^2}{|v|^2}$$

. . . 2.7.4

the time of flight can be calculated and the final position of the electron can be determined.

The final position of the electron can be converted into spherical polar co-ordinates (r,θ,ϕ) from the relationships specified by

$$x = r \sin\phi \cos\theta$$
$$y = r \sin\phi \sin\theta$$
$$z = r \cos\phi$$

and

$$\theta = \arctan(y/x)$$
$$\phi = \arctan((x^2 + y^2) / z)$$

...2.7.8

Detection of the electron will then occur if the electron lies within the $\theta \pm \Delta\theta$ and $\phi \pm \Delta\phi$ limits set for the detector.

The above equations have been implemented numerically in the program DETECT (see Appendix B). The use of the detector program enables two aspects of the electron energy spectra to be examined. The first is the distribution of electrons, i.e., in which directions most/least electrons are accelerated. Secondly, it is possible to calculate electron energy spectra for different detector positions and so determine where electrons of different energies will be detected in experiments.

The following results come from data generated using the methodology described in Section 2.6. The laser parameters used were the same as those used for Figure 2.13 (i.e., $I_p = 10^{15}W/cm^2$; $I_t = 10^{14}W/cm^2$; $R_0 = 1\mu m$; $E_{excess} = 0.471eV$) and the electron ejection distribution used is shown in Figure 2.12(b). This distribution was chosen as it is typical of the electron ejection distributions for linearly polarised light given in Bucksbaum et al and Baskansky et al.

Figure 2.15 shows the number of electrons detected in the ϕ plane for pulse lengths of 0.05ps, 0.25ps, 1ps, 10ps and 1000ps, while Figure 2.16 shows the relative number of electrons detected in the θ plane. The number of electrons is equal to the vector distance from the origin and have been normalised to one. Examination of Figure 2.15 shows that, for all pulse lengths, the electrons are ejected most strongly in the x-y plane. Figure 2.16 shows that for short pulses ($\leq$0.25ps), electron ejection is most strong in the $\pm$y direction (along the polarisation vector of the laser pulse), while for pulses 1ps or longer, there is only a slight preference for electron ejection in the $\pm$y direction over the $\pm$x direction.

A comparison of Figure 2.16(a) with Figure 2.12(b) shows that the distribution of electrons in the x-y plane after the electrons have been emitted from the laser field is very nearly the same as the distribution of electrons at the instant they were ejected from the atom. This result is not surprising, since, for the short pulse to spot size ratio used here (0.05ps/μm), the laser pulse will have disappeared before the electron could convert its oscillation energy to directed kinetic energy. Consequently, the electrons would not have experienced much ponderomotive acceleration and would not have been able to change their direction to any great extent. Once the pulse length to spot size ratio has increased to 0.25ps/μm, however, the number of electrons emerging from the laser beam in the $\pm$x directions has increased by about a factor of three and at higher pulse length to spot size ratios, the electron distributions are almost circularly symmetric in the x-y plane. Thus, the ponderomotive acceleration process can serve to considerably change the direction of the electrons before they emerge from the laser beam with their final energy, making the distribution almost cylindrically symmetric for $E_{excess} << E_{osc}$ (Bucksbaum et al).

Electron energy spectra resulting from a 0.25ps pulse, (where electron velocity distributions are expected to be important), are shown in Figures 2.17 and 2.18 as a function of detector angles. The electrons are collected from a 20° solid angle about $\theta = 0$ and $\phi = \pi/2$. From Figure 2.17, it can be seen that as the detection angle is changed from $\theta = 0$, $\phi = 0$ to $\theta = 0$, $\phi = \pi/2$, higher energy electrons appear. Thus, there is a higher proportion of high energy electrons being emitted from the laser beam in the x-y plane than along the z-axis. If the detector is then kept at $\phi = \pi/2$ and successively moved from $\theta = 0$ to $\theta = \pi/2$, (as in Figure 2.18), the spectra stay relatively the same, although there are more electrons (particularly around 3eV) for angles between $\theta = \pi/3$ and $\theta = \pi/2$. This corresponds to a slightly larger number of electrons being accelerated from the focal region along the y-axis than along the x-axis, reflecting the electron ejection distribution. From the scales given on the plots in Figures 2.17 and 2.18, it is evident that most of the electrons go in the $\phi = \pi/2$ direction (x-y plane), confirming that there is a preference (for a pulse length to spot size ratio of 0.25ps/μm) for electrons to be emitted from the irradiating field in the direction of polarisation of the laser beam.

There are a couple of minor features in Figures 2.17 and 2.18 that need explanation. The apparent discontinuity in Figure 2.17(a) is due to the last point in the data file not being zero when the graph was plotted. Noise present in Figures 2.17 and 2.18 and the reproducible structure in the noise in Figure 2.18 for small ϕ may be due to the finite mesh size ($dz.dr.d\theta$) used in the simulation. However, due to computer time and memory constraints, a smaller mesh size could not be used.

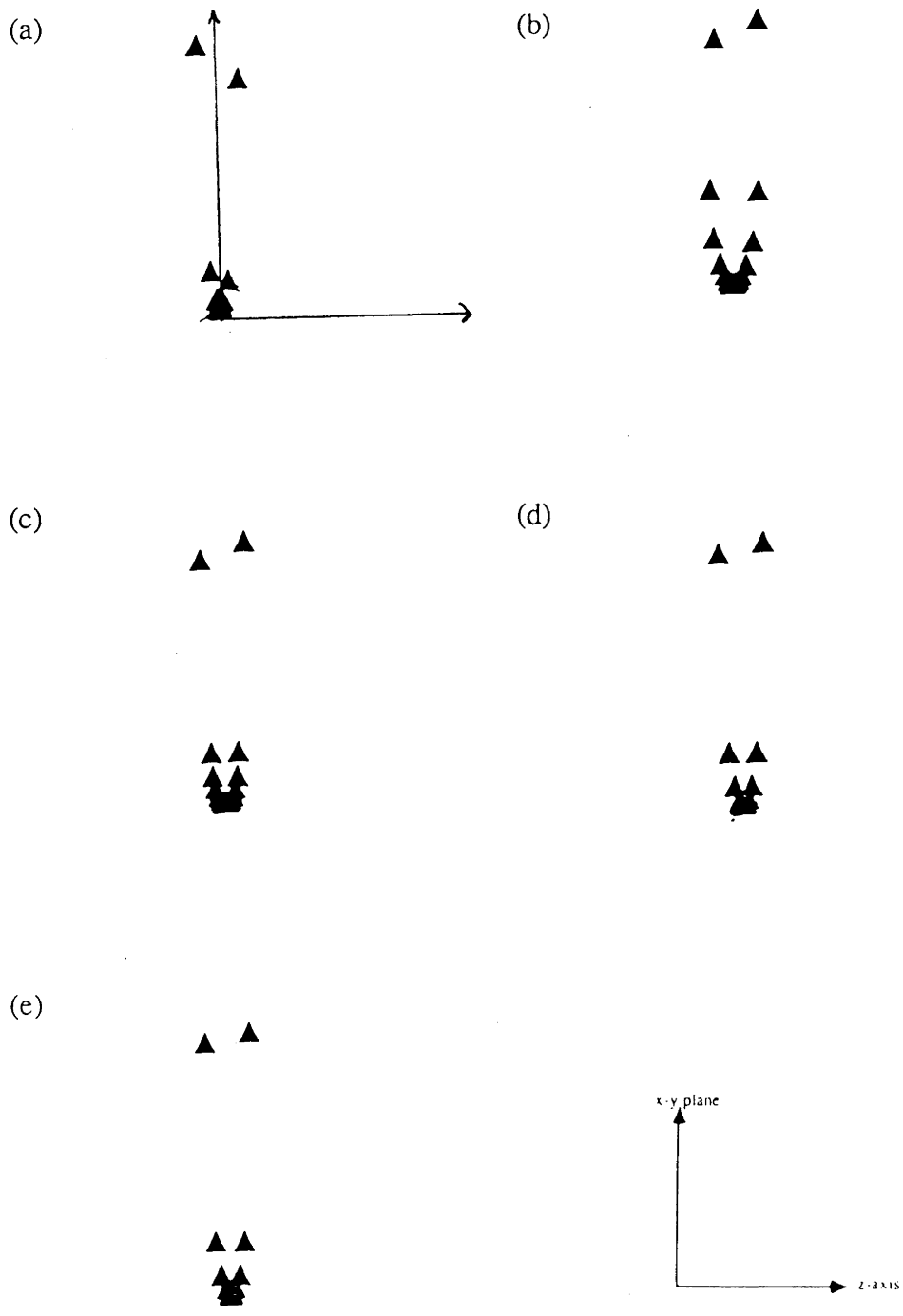

Figure 2.15: Detection of electrons in the ϕ plane

(a) τ = 0.05ps; (b) τ = 0.25ps; (c) τ = 1ps;

(d) τ = 10ps; (e) τ = 1000ps.

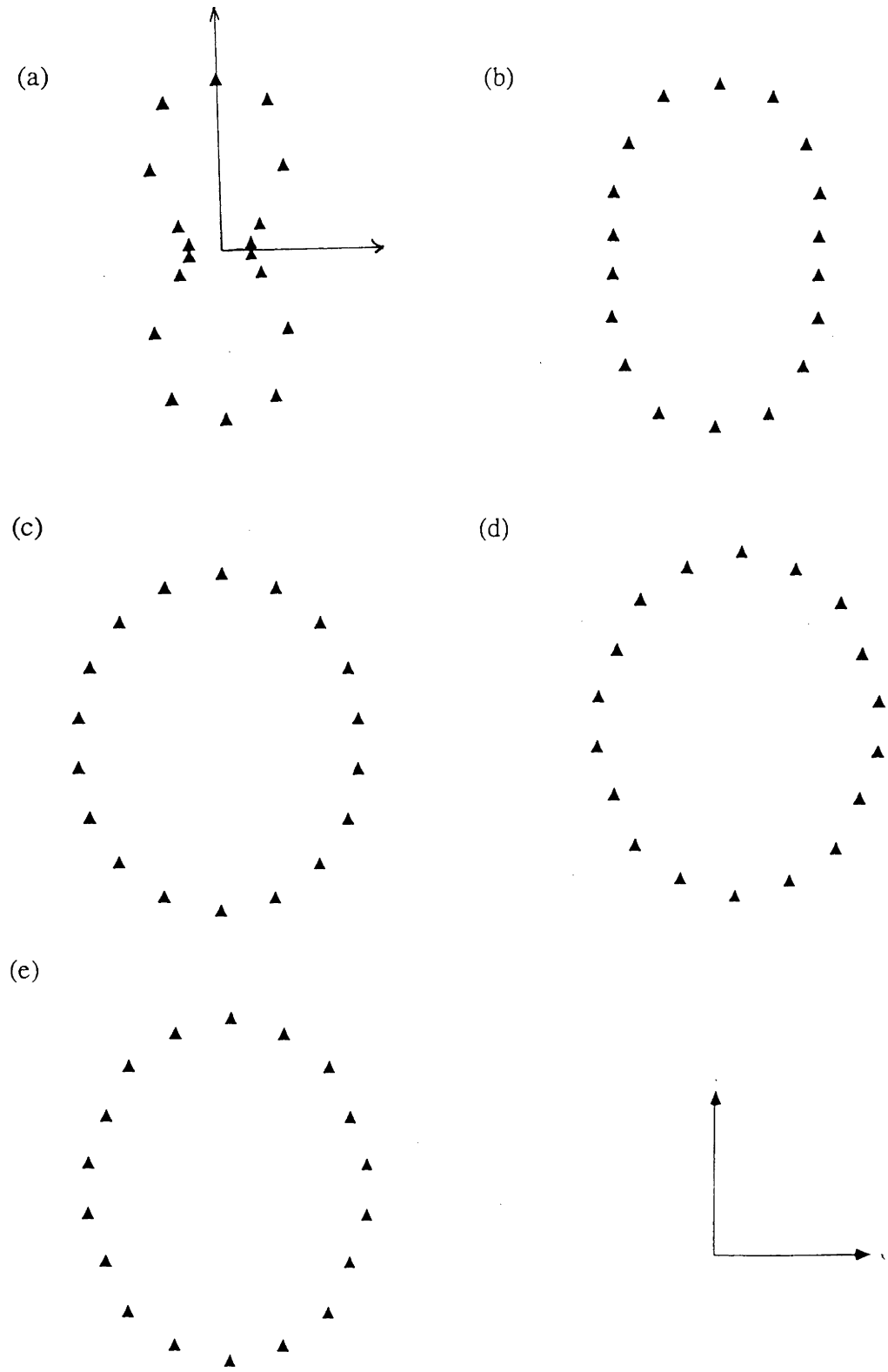

Figure 2.16: Detection of electrons in the θ plane

(a) τ = 0.05ps; (b) τ = 0.25ps; (c) τ = 1ps;

(d) τ = 10ps; (e) τ = 1000ps.

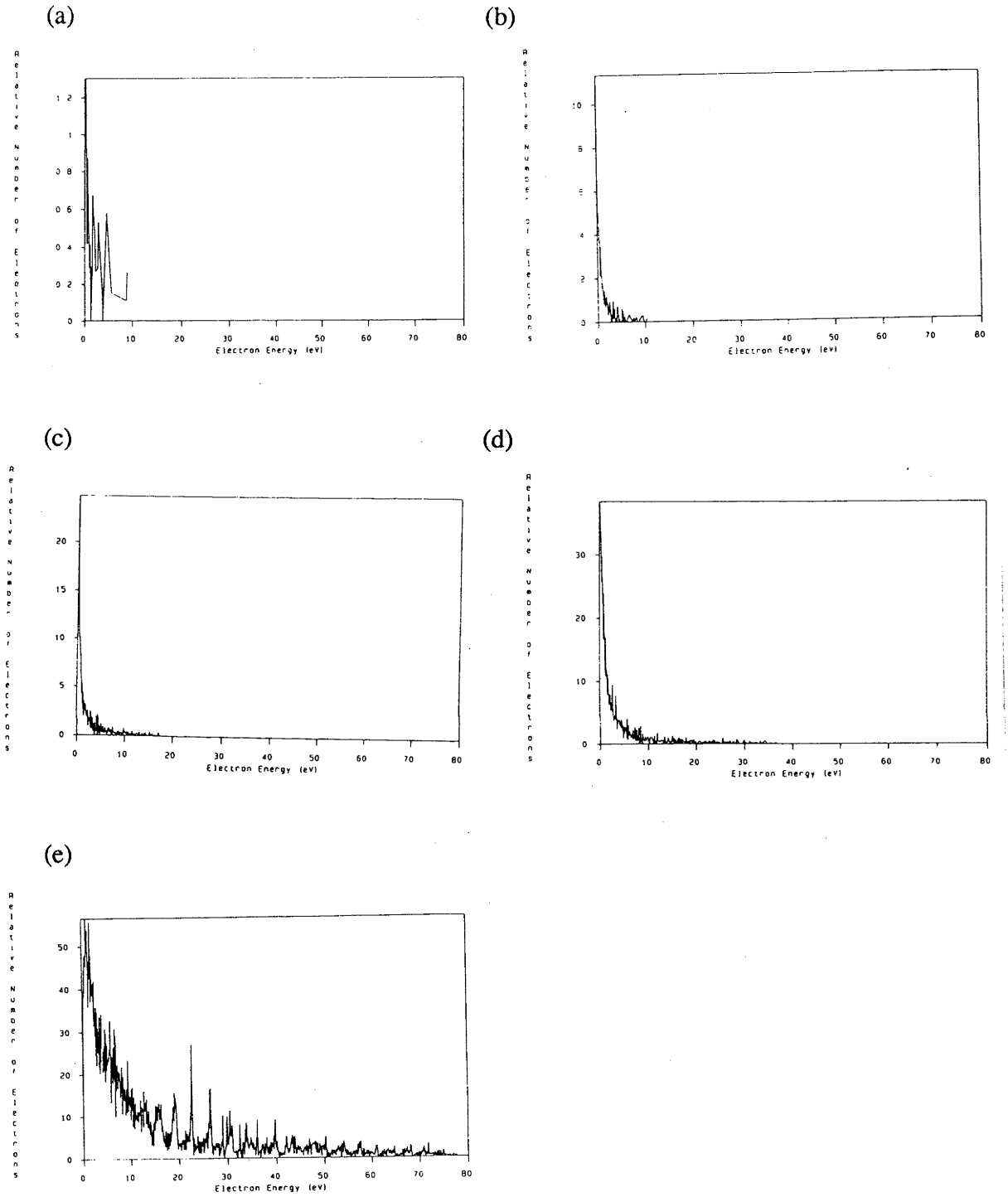

Figure 2.17: Electron energy spectra detected in the ϕ plane ($0°\leq\theta\leq20°$)

(a) $0°\leq\phi\leq10°$; (b) $20°\leq\phi\leq30°$; (c) $40°\leq\phi\leq50°$;

(d) $60°\leq\phi\leq70°$; (e) $80°\leq\phi\leq90°$.

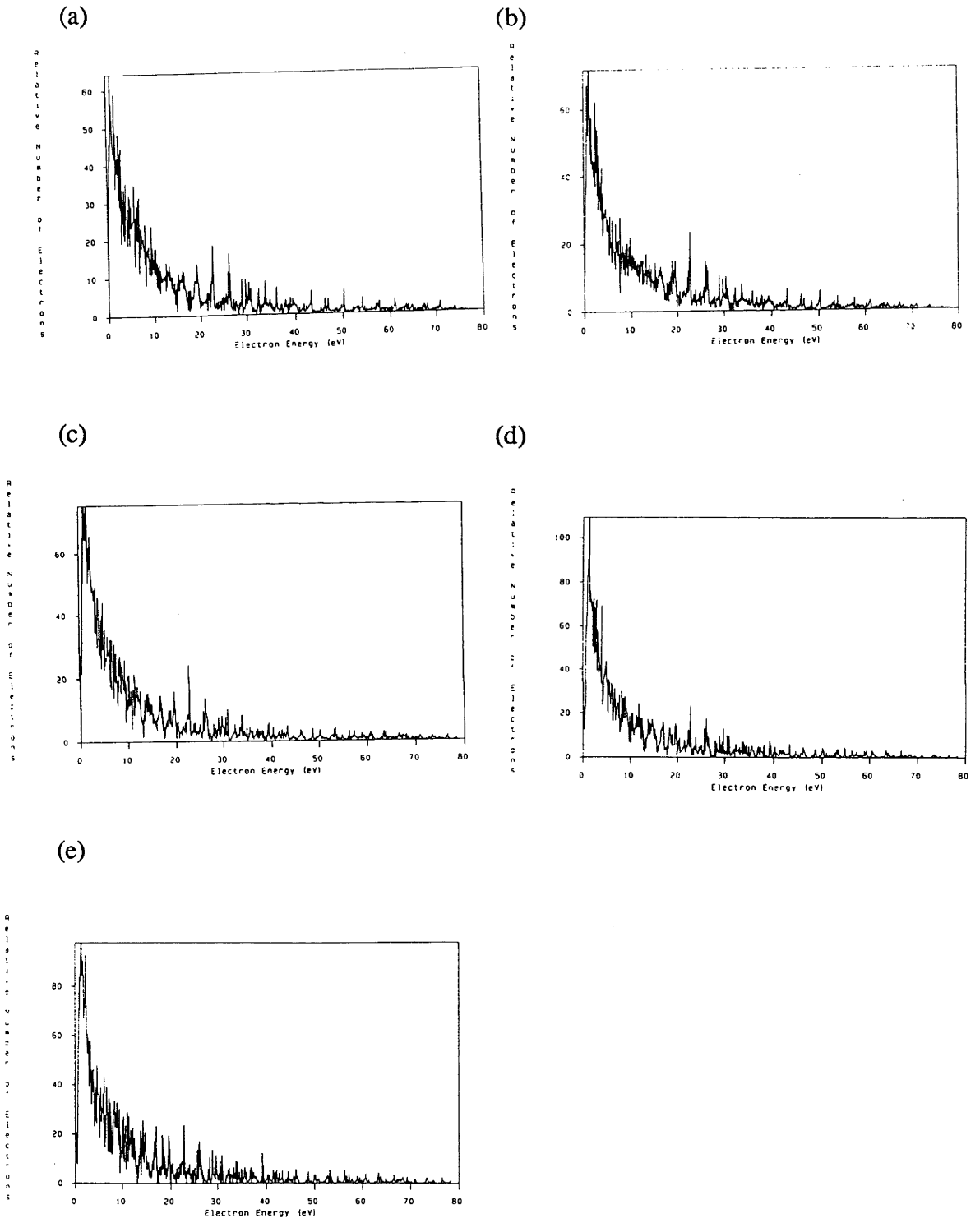

Figure 2.18: Electron energy spectra detected in the θ plane ($90°\leq\phi\leq100°$)

(a) $0°\leq\theta\leq20°$; (b) $20°\leq\theta\leq40°$; (c) $40°\leq\theta\leq60°$;

(d) $60°\leq\theta\leq80°$; (e) $80°\leq\theta\leq100°$.

2.8 CONCLUSION

The ponderomotive calculations were performed in one, two and three dimensions and the following behaviour was observed.

From the one-dimensional studies, it was seen that the amount of energy the electron had at the detector depended primarily on the value of the pulse length to focal spot size ratio. For cases where the peak intensity exceeded the threshold intensity, four regimes were identified:

(i) For a pulse width to spot size ratio <0.1 ps/μm, the electron emerged from the laser beam with $E_{final} = E_{excess}$.

(ii) For a pulse width to spot size ratio >0.1 ps/μm but <0.2 ps/μm, the electron emerged with $E_{excess} < E_{final} < E_{osc} + E_{excess}$.

(iii) For a pulse width to spot size ratio >0.2 ps/μm but <10 ps/μm, the electron emerged with $E_{final} > E_{osc} + E_{excess}$.

(iv) For a pulse width to spot size ratio >10 ps/μm, the electron emerged with $E_{final} = E_{osc} + E_{excess}$.

To a lesser extent, the final energy of the electron was also found to depend on the peak-to-threshold intensity ratio and the relative value of the field intensity compared with the excess energy.

The observations from the 1-D simulations were confirmed with the results from the 2-D and 3-D simulations. Also, individual ATI peaks in the 2-D and 3-D simulations were broadened due to ponderomotive effects experienced by electrons generated throughout the focal region, in contrast to the one electron generated at the origin in the 1-D simulations.

Electrons accelerated from a short pulse were found to have a range of final energies. This was thought to be as a result of the electrons being accelerated from different regions of the laser focus. One explanation is that electrons with energies lower than expected from $E_{osc}+E_{excess}$ may be generated from positions in the focal region where the laser pulse passes over them too quickly for the electrons to convert their oscillation energy to directed kinetic energy. This would cause some of the electrons to emerge from the laser pulse with only the excess energy they had on ionisation. Also, high energy electrons may be formed when the intensity of the laser pulse increases substantially while they are still in the beam. The electrons would experience field intensities much greater than the ionisation intensity and so, their oscillation energy in the field would be increased. If this was later converted to directed kinetic energy, the electrons would then have a final energy which was much greater than expected. Thus, the electrons could gain non-quantal amounts of energy from the laser pulse.

It was also found (Figure 2.13) that if all the electrons were detected after they had been accelerated from the laser beam, the final electron energy spectrum was more or less independent of the electron ejection distribution used, regardless of the pulse length to spot size ratio. However, for short pulses, (Figures 2.17 and 2.18), the electron energy spectrum detected at different positions varied considerably, depending on the angle of detection. In addition to this, it was found that the total number of electrons (of all energies) detected at different angles also varied. However, for small pulse length to spot size ratios (~0.05ps/μm), the distribution of electrons emerging from the laser beam was found to be almost identical to the distribution of electrons ejected from the atom, since they did not move (or moved only slightly) during the pulse. For large pulse to spot size ratios (≥1ps/μm) where $E_{excess} << E_{osc}$, the final distribution of electrons was cylindrically symmetric.

CHAPTER THREE
MULTIPHOTON IONISATION

3.1 INTRODUCTION

There are two distinct stages in the production of electrons from the interaction between an intense laser field and an ensemble of atoms. The first is the above-threshold ionisation process (ATI) and the second is the ponderomotive acceleration of the free electrons down the gradient formed by the laser pulse. The latter of the two phenomena has been examined in detail in Chapter Two. However, in order to simulate experimental results, the two stages must be used together. Postulated ATI spectra give the relative transition probabilities and thereby account for occurrences such as peak suppression, peak switching and also produce the electron ejection distribution. The ponderomotive acceleration modifies the ejected electron energy and velocity distributions and when combined with the detector program, gives the final measured electron energy spectrum.

It is the aim of this chapter to take the results of Chapter Two (based on an assumed ATI process) and combine it with a given detector geometry to simulate the multiphoton ionisation experiments performed by Baldwin and Boreham on argon and by Boreham and Luther-Davies on helium. The simulated spectra will then be compared with those obtained experimentally.

3.2 EXPERIMENTAL CONDITIONS

The experiments on argon and helium used a Nd:YAG glass laser which emitted light with a wavelength of 1.064μm. The laser beam was focussed to a 1/e waist size of 13±2μm. For the experiments using argon the pulse length was 22±2ps, whereas for the experiments using helium the pulse length was 25±2ps. The peak laser intensity for the first argon experiment was $3x10^{15}W/cm^2$, while for the second one it was $2x10^{16}W/cm^2$ and for the helium experiment it was $2.5x10^{16}W/cm^2$.

In simulating the experiments, values for the ionisation potential and ionisation intensity of each of the ionisation states for the two atoms were required. Rather than use the threshold ionisation intensities calculated using the corrected Keldysh formula, (as done in the simulations in Chapter Two), the experimental values obtained by Baldwin and Boreham and Boreham and Luther-Davies were used. More recent values, using different experimental apparatus (L'Huillier et al), were available, but the values obtained by Baldwin and Boreham and Boreham and Luther-Davies were used to attempt to simulate (what was thought to be) the experimental conditions as closely as possible.

In the experiment, the electrons emitted from the focal region of the laser were attenuated by collector grids before being detected by a detector that had a minimum sensitivity of $1.2x10^{-15}C$ or $7.5x10^3$ electrons (Baldwin and Boreham). If all of the electrons were emitted radially, the geometry of the detection system would allow it to detect 56% of the emitted electrons. Allowing for the 10% attenuation by the collector grids, a minimum of $1.5x10^4$ electrons would have to be generated before a signal could be detected. Taking into account the density of the gas, the minimum ionised volume necessary for the detection of the minimum charge was enclosed by iso-intensity contours corresponding to 0.64 times the

laser intensity at the centre of the focal region when electrons were detected. If a further 50% loss of electrons in the axial direction was assumed, the iso-intensity contours enclosing the minimum ionised volume indicated that the threshold ionisation intensity was 0.47 times that of the central laser intensity.

The value for the threshold ionisation intensity used in the present calculations was chosen to lie within the range given by Baldwin and Boreham. The chosen ionisation threshold intensities are listed in Table 3.1, along with the ionisation potential, calculated oscillation energies for the electron in the ionising field and the excess energy for the electrons associated with the first unsuppressed ATI peak for each ionisation state.

ION	Ionisation Potential (eV)	Threshold Ionisation Intensity (W/cm^2)	Oscillation Energy (eV)	Excess Energy (eV)
ArI	15.76	$1.5x10^{14}$	15.86	1.01
ArII	27.63	$5.0x10^{14}$	52.85	1.09
ArIII	40.74	$1.5x10^{15}$	157.50	1.02
ArIV	58.81	$4.1x10^{15}$	433.40	0.71
HeI	24.59	$3.3x10^{14}$	34.78	0.06
HeII	54.42	$3.4x10^{15}$	359.38	1.02

Table 3.1: Parameter values for the ionisation of argon and helium

A schematic of the detection system used is given in Figure 3.1. It consisted of four circular detectors of 3.0cm diameter placed on the $\pm x$ and $\pm y$ axes 3.2cm away from the focus. The resolution of the analyser is not known, although it was tested with an electron gun yielding 20 ± 5eV electrons (see Hollis) and was thought to be around a few eV.

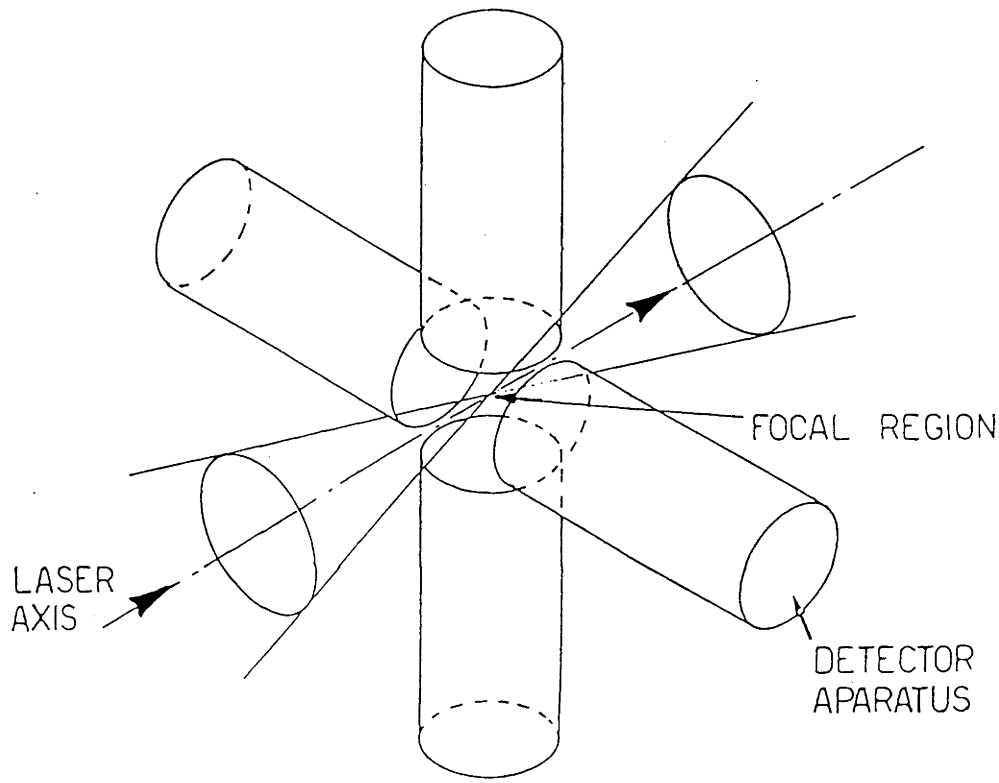

Figure 3.1: Multidirectional detection configuration (Baldwin)

For detectors along the ±x-axis (at x = ±3.2cm), the boundaries of detection are defined by

$$y^2 + z^2 = (d/2)^2$$

where

$$-1.5 \leq y \leq 1.5$$

$$-1.5 \leq z \leq 1.5$$

and

$$d/2 = 1.5\text{cm}.$$

Using the relationships between cartesian and spherical polar co-ordinates given in equation 2.7.8, electrons will be detected in the ±x direction if

$$-A \leq \theta \leq A \text{ (+x direction)}$$

$$(\pi - A) \leq \theta \leq (\pi + A) \text{ (-x direction)}$$

and

$$C \leq \phi \leq (\pi - C)$$

where

$$A = \arctan(1.5/3.2)$$

and

$$C = \arcsin\left[\sqrt{1 - \frac{d^2}{d^2+4x^2}}\ \frac{1}{\cos\theta}\right]$$

Similarly, for detectors along the ±y-axis (at y = ±3.2cm), the boundaries of detection are defined by

$$x^2 + z^2 = (d/2)^2$$

where

$$-1.5 \leq x \leq 1.5$$

$$-1.5 \leq z \leq 1.5$$

and

$$d/2 = 1.5\text{cm}.$$

Again, using the relationships between cartesian and spherical polar co-ordinates given in equation 2.7.8, electrons will be detected in the ±y direction if

$$B \leq \theta \leq (\pi - B) \quad \text{(+y direction)}$$

$$(\pi + B) \leq \theta \leq (2\pi - B) \quad \text{(-y direction)}$$

and

$$D \leq \phi \leq (\pi - D)$$

where

$$B = \arctan(3.2/1.5)$$

and

$$D = \arcsin\left[\sqrt{1 - \frac{d^2}{d^2 + 4y^2}}\ \frac{1}{\sin\theta}\right]$$

The numerical implementation of the detection geometry described above can be found in the program DETECT (Appendix B).

From Figure 2.15, it can be seen that most of the electrons are emitted from the focal region in the x-y plane. The detection system used by Baldwin and Boreham could detect ~56% of the electrons (emitted in the x-y plane), even though it only occupied 22% of the solid angle. This is similar to the 55% detected in the simulations for a 0.05ps pulse with an isotropic distribution of initial electron velocities in the x-y plane. In addition, comparing Figure 3.1A with Figure 2.13(b) shows that approximately one-third of the electrons are detected for a 0.25ps pulse, indicating a preference for ejection in the x-y plane. Further, the shapes of the electron energy spectra in Figure 3.1A and Figure 2.13(b) are identical. Thus, if Baldwin and Boreham had detected all of the electrons from the focal volume, they would have obtained the same distribution of electron energies as they did using only partial detection. As will be seen in Section 3.4, this result can be used to substantially reduce the calculations required for the simulations.

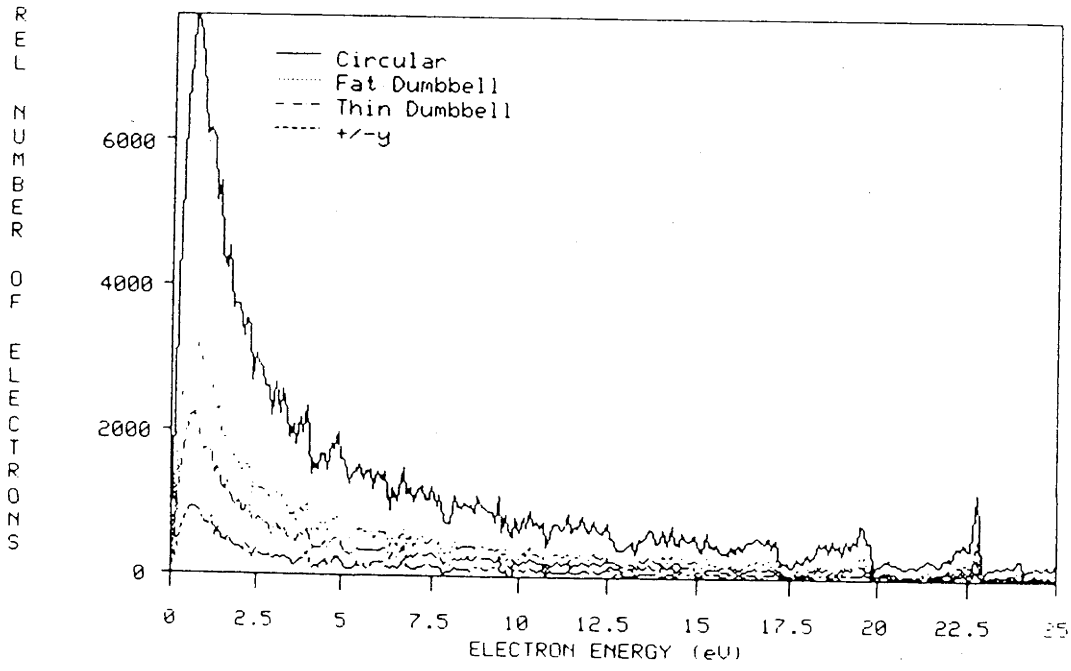

Figure 3.1A Electron energy spectra for ArI ATI peak 10

- detected using experimental geometry

$I_p = 10^{15}W/cm^2$; $I_t = 10^{14}W/cm^2$; $R_0 = 1\mu m$; $E_{excess} = 0.471eV$;

$\tau = 0.25ps$

3.3 ABOVE-THRESHOLD IONISATION

There are two major processes which contribute to the final kinetic energy and direction of an electron produced by multiphoton ionisation in a laser focus: the ejection of the electron in the ionisation process itself and the subsequent ponderomotive acceleration of the electron from the laser beam. In the ionisation process, the atom absorbs photons from the irradiating electromagnetic field, giving the electron sufficient kinetic energy to remove it from the atom. The minimum energy required to overcome the nucleus-electron binding energy in the absence of an external electromagnetic field is commonly known as the ionisation energy. In above-threshold ionisation, however, the atom absorbs more photons than are required to overcome the nucleus-electron binding energy and so, an electron energy spectrum arising from the ATI of an ensemble of atoms will show a number of photoelectron peaks separated by the photon energy (Agostini et al, 1979).

According to Eberly and Javanainen, "...given the experimental data available, it appears that ATI is most easily described with a free electron (Volkov) postulate supplemented by a strong dose of ponderomotive forces."

Since the resolution of the ATI peaks is the primary aim of this work, the relative intensity and number of ATI peaks is of secondary importance. Consequently, the approach used here will be to postulate emission probabilities for the first nine unsuppressed peaks (calculated from Table 3.1) for each of the relevant ionisation states, based on results given in the literature (see, for example, Becker et al (1986, 1987), Javanainen and Eberly and Basile et al). Energy spectra showing the relative heights of the individual ATI peaks for argon and helium can be found in Figures 3.2 and 3.3. In general, the first unsuppressed ATI peak has been chosen to be the strongest, with the signal strength decreasing for higher order

peaks. The position of the first ionisation peak was determined from the ionisation potential and the threshold ionisation intensity of the laser.

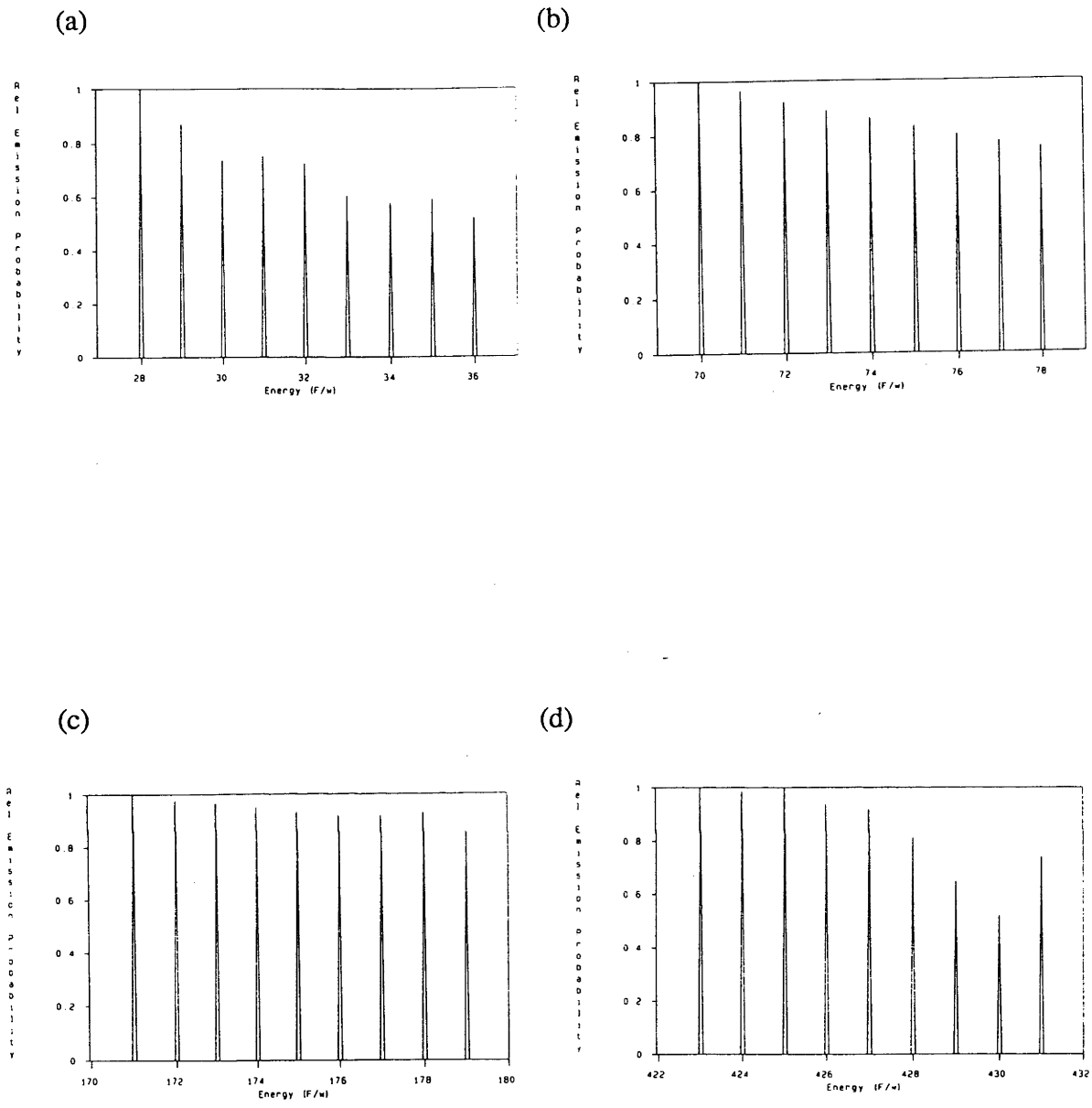

Figure 3.2: Emission probabilities for ATI peaks in argon

(a) ArI; (b) ArII; (c) ArIII; (d) ArIV

(a)

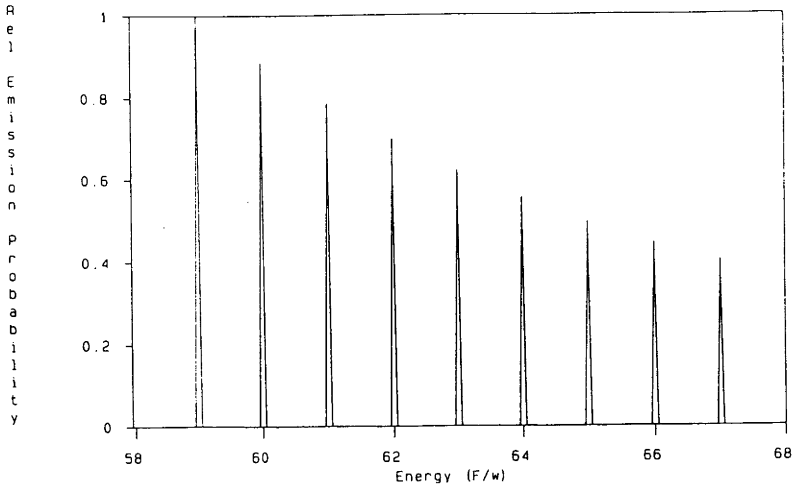

(b)

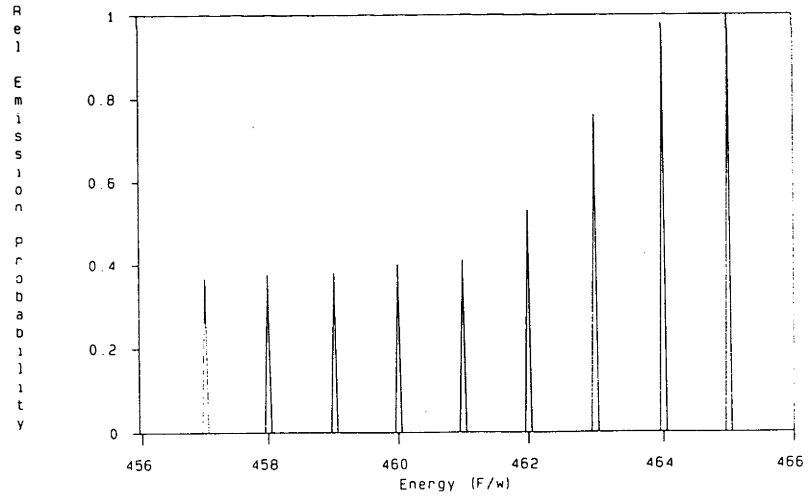

Figure 3.3: Emission probabilities for ATI peaks in helium

(a) HeI; (b) HeII

3.4 PONDEROMOTIVE ACCELERATION CALCULATIONS

From Figure 2.13, it can be seen that, when all electrons are detected, the final electron energy spectrum following ponderomotive acceleration has the same shape, regardless of the electron ejection distribution. That is, the final electron energy spectrum is more or less independent of the angular distribution of ejected electrons, even though the total number of electrons generated in the simulations may vary. Further, when Figures 3.1A and 2.13(b) are compared, it becomes apparent that the experimental detector geometry used in the simulations yields a spectrum which is representative of the total number of electrons, i.e., the experimentally detected electron energy spectrum has the same shape as if all electrons accelerated from the focal volume were detected.

Although this comparison is presented for short pulses (0.25ps), it is valid to assume the same result when simulating experiments which were performed in the long pulse regime (22 and 25ps). In the long pulse regime, changes due to the detection geometry could be expected to be less. This is a result of the fact that for long pulses, the final electron positional distribution becomes cylindrically symmetric around the z-axis (Figure 2.16 and Bucksbaum et al) since the final ponderomotive energy dominates the initial electron energy distribution when $E_{osc} >> E_{excess}$, as is the case considered in the experiments here.

Consequently, when simulating the actual experiments, it was possible to greatly reduce the computational complexity by assuming a simple $\pm y$ initial electron velocity distribution. Electrons were therefore given an inital excess energy in the $\pm y$ directions, the results from which were added together to form the total spectrum. This was significant as it reduced the computation time by a factor of ten, from around 135 hours to 13.5 hours CPU time (on the VP-100), thereby making possible the number of simulations presented here.

The resolution of the detector used in simulation was assumed to be 0.1eV. The simulation used the Runge-Kutta routine for the acceleration of the electrons from the focal region. The time step used was 22fs, after convergence testing showed that accurate results were maintained for time steps up to 500fs.

3.5 MPI RESULTS

For the purposes of the present simulation, it was assumed that the individual ionisation states of argon and helium were completely ionised and so, each state carried an equal weighting. For the first argon experiment (Ip = $3x10^{15}W/cm^2$), corresponding to the top curve in Figure 4,4a of Baldwin and reproduced in Figure 2.10 here, the ionisation states used were ArI, ArII and ArIII. For the second experiment (Ip = $2x10^{16}W/cm^2$), (the top curve in Figure 4,4b of Baldwin), ArIV was also assumed to be completely ionised. The helium experiment (Boreham and Luther-Davies) used the completely ionised states of HeI and HeII, with Ip = $2.5x10^{16}W/cm^2$. The normalised emission probabilities shown in Figures 3.2 and 3.3 were used to give the relative weightings of each of the ATI peaks within each ionisation state.

Ponderomotive acceleration calculations were performed for every ATI peak in every ionisation state in each of the three experiments. The initial (excess) energy was directed in the $\pm y$ directions in order to save computation time. This was an approximation to the dumb-bell patterns since the initial ejection direction could be assumed to have a negligible influence on the final electron energy spectrum at different detector positions as discussed earlier. The resulting electron energy spectra were weighted according to the emission probability associated with the corresponding ATI peak. The final electron energy spectrum for each experiment was then formed by adding together all of the individual spectra for each ATI peak for each ionisation state in the experiment and by detecting only the electrons which would fall on the detectors as defined by the geometry above. The results from the simulation can be seen in Figures 3.4 to 3.6, where experimental points have also been plotted.

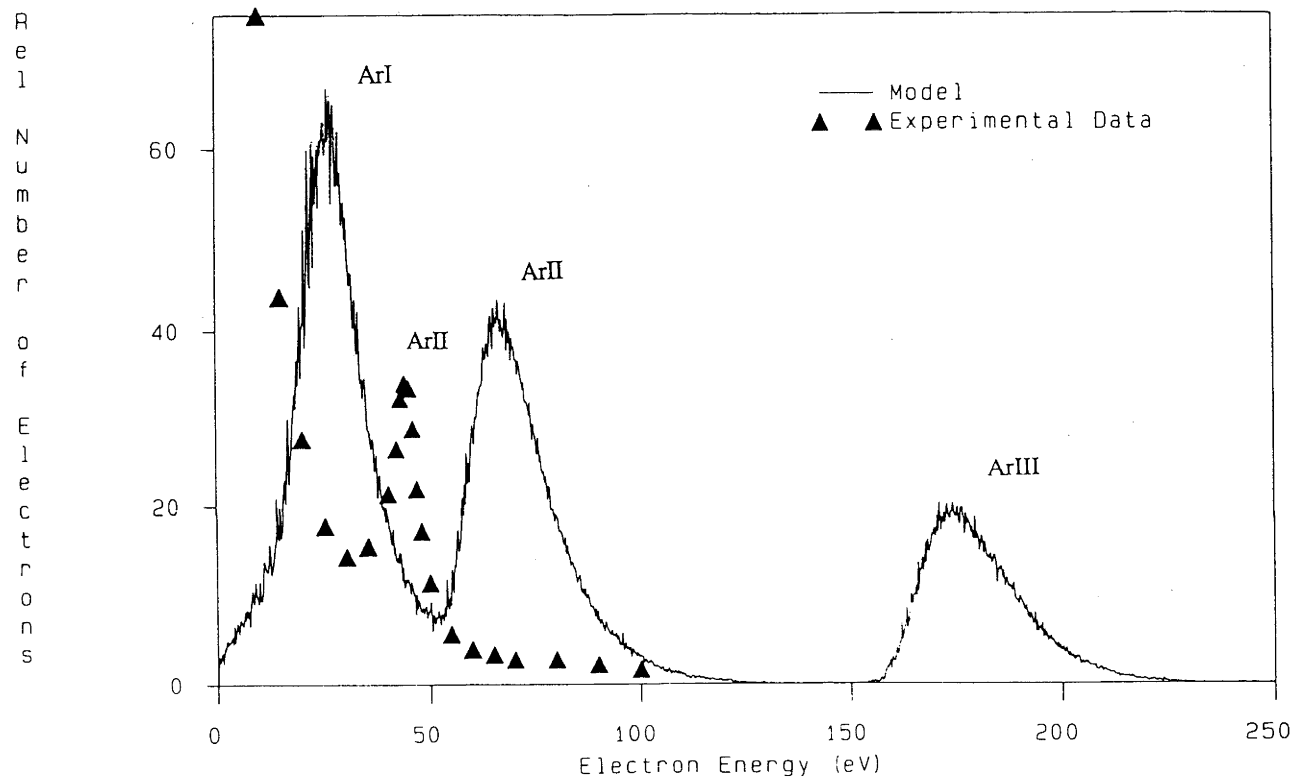

Figure 3.4: Electron energy spectrum for first argon experiment

$Ip = 3x10^{15} W/cm^2$; $R_0 = 6.5\mu m$; $\tau = 22 \pm 2 ps$

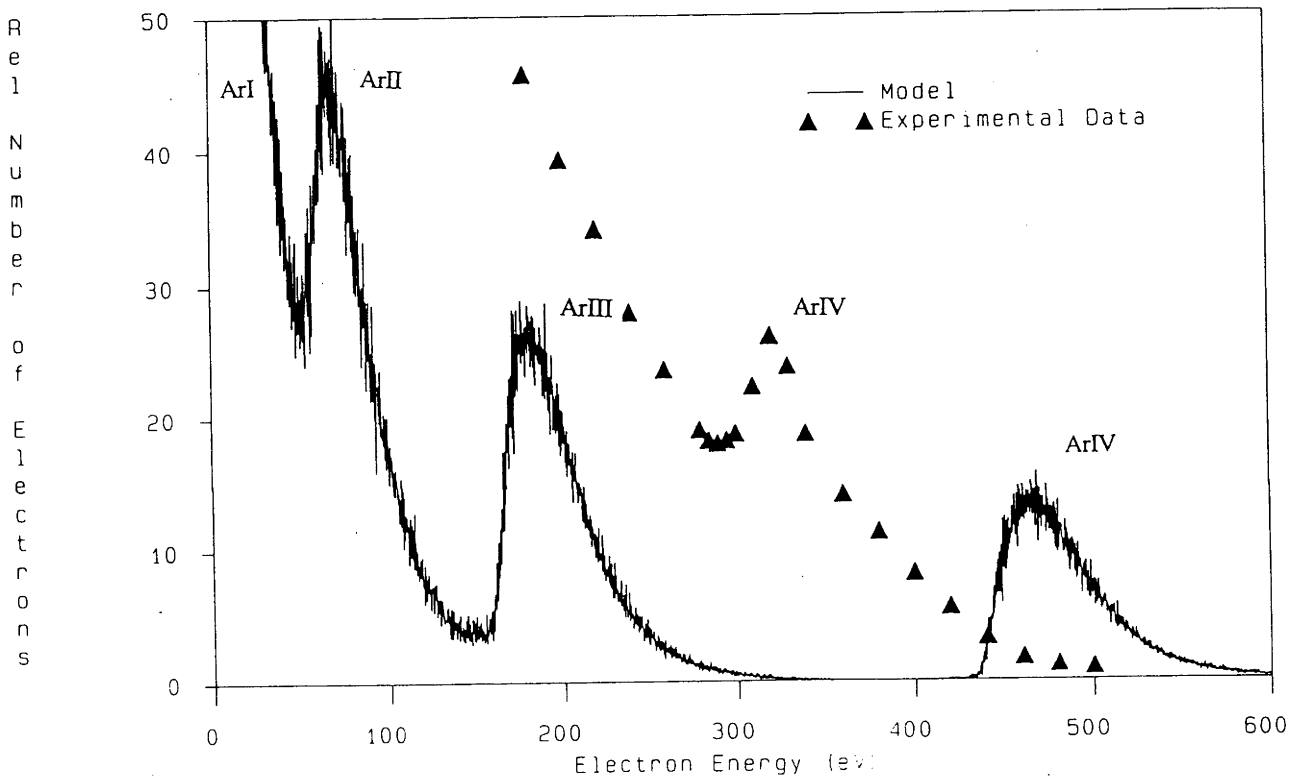

Figure 3.5: Electron energy spectrum for second argon experiment

$I_p = 2 \times 10^{16} W/cm^2$; $R_0 = 6.5 \mu m$; $\tau = 22 \pm 2 ps$

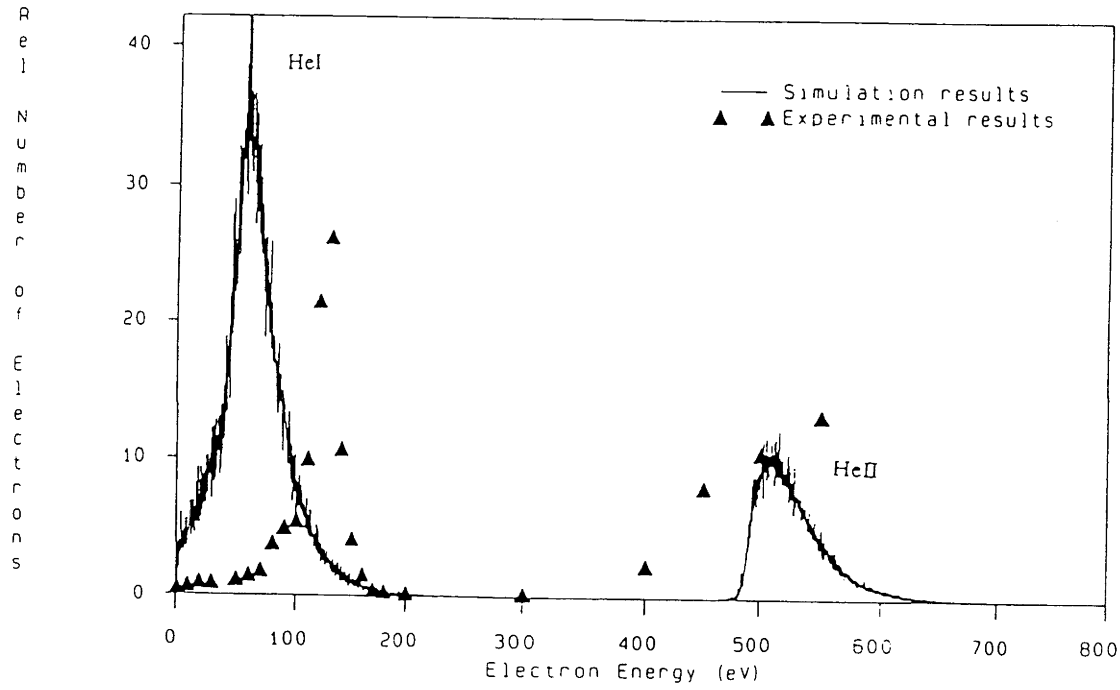

Figure 3.6: Electron energy spectrum for helium experiment

$Ip = 2.5x10^{16} W/cm^2$; $R_0 = 6.5\mu m$; $\tau = 25 \pm 2 ps$

3.6 DISCUSSION

Figures 3.4 to 3.6 show that there are no individual ATI peaks present in either the experimental or the simulated results. This result confirms that the lack of individual ATI peaks in the electron energy spectra detected in the experiments of Baldwin and Boreham was due to the energy gained from the ponderomotive acceleration of electrons down the potential gradient formed by the laser pulse and was independent of instrumental resolution. Further, the experiments were conducted in the "surfing" regime ($\tau/R_0 \sim 4ps/\mu m$) as defined by the earlier simulations presented here. Thus, it would be expected that both higher and lower energies would be detected from a given initial ejection energy, causing the individual ATI peaks to broaden to the extent that they merged with their neighbouring peaks. This behaviour was also shown in the spectra generated by the 2-D calculations (Figure 2.9).

In Figures 3.4 to 3.6, the widths of the simulated peaks are approximately the same as those obtained from the experiments. Since the width of the peaks is influenced by the number and relative intensities of the ATI peaks, the chosen ATI spectra could appear to be correct. However, it is difficult to firmly conclude anything from the widths of the peaks, as it is probable that a number of distributions of ATI peaks would give the same result.

As can be seen from Figures 3.4 and 3.5, the simulated peaks for argon occurred at a higher energy than those in the experiment. In the first argon experiment, there is no apparent maximum in the experimental peak for ArI, perhaps because the electrons are retarded by space charge effects at these low energies. The simulated peak occurred at an energy about 25eV higher than the experimental peak for ArII inferred in Baldwin and the experimental peak for ArIII is not present due to it not being detected at the specified laser intensity. In the second

argon experiment, the simulated peaks also occur at higher energies than the experimental peaks for ArII and ArIII, the latter being a weak feature at ~160eV not shown in Figure 3.4. In addition, the simulated peak for ArIV occurred at an energy about 140eV higher than the experimental peak. Figure 3.6 shows the opposite effect for helium. The simulated peak for HeI is about 60eV lower in energy than the experimental peak and the simulated peak for HeII appears to be at a lower energy than the experimental peak, even though the experimental peak was not fully determined due to the detection limits of the experiment.

There are a number of possible causes for the difference between the experimental and simulated electron energy peak positions. The first obvious source of error is the value of the threshold ionisation intensity. Baldwin and Boreham give the range of values for each of these as follows:

ArI : $(1.2 - 2.0) \times 10^{14}$ W/cm^2

ArII : $(3 - 8) \times 10^{14}$ W/cm^2

ArIII : $(1.0 - 2.5) \times 10^{15}$ W/cm^2

ArIV : $(2.5 - 6) \times 10^{15}$ W/cm^2

HeI : $(2.5 - 8.0) \times 10^{14}$ W/cm^2

HeII : $(0.2 - 1.0) \times 10^{16}$ W/cm^2

These field intensities correspond to oscillation energies of electrons in the laser field of

ArI : 13 - 21 eV

ArII : 32 - 85 eV

ArIII : 106 - 264 eV

ArIV : 264 - 634 eV

HeI : 26 - 85 eV

HeII : 211 - 1057 eV

Comparing these values to the ones in Table 3.1 shows that if a long pulse regime (i.e., no surfing) was assumed and the threshold ionisation intensities for ArII and ArIV were taken at $3x10^{14}W/cm^2$ and $2.8x10^{15}W/cm^2$, respectively, the positions of the simulated ArII and ArIV peaks would roughly correspond to those obtained in the experiment. Similarly, if the threshold intensity for HeI was taken at its upper limit of $8x10^{14}W/cm^2$, the peak in the experimental and simulated spectra would almost coincide. Thus, the large uncertainty in the threshold ionisation intensities can shift the peaks over a large range of energies. This is thought to be the most likely cause of the discrepancies between the experimental and simulated spectra presented here.

Errors in the spot size or pulse length could also lead to a higher or lower gain in energy than expected. This was studied for the 1-D case only, but the results indicated that the effect would be much less. For the pulse length to spot size ratio used here (about 4ps/μm), the plots from the 1-D simulations show that if the pulse length to spot size ratio was actually 20% greater than expected from the experimental measurements, the simulated peaks would appear at an energy about 15% higher than the experimental peaks. Similarly, if the pulse length to spot size ratio was actually 20% smaller than measured, the simulated peaks would appear at an energy roughly 15% lower than the experimental peaks.

The experimental spectra showed a large number of electrons with zero energy, whereas the simulated spectra do not. This could be due to a retardation caused by Debye coupling between the ions and electrons (space charge effects). However, this effect will only be significant for low energy electrons and cannot, therefore, be used here to explain the difference in energies for the higher order peaks. Nevertheless, it is a limitation of the current model that it does not include space charge effects. This is especially so, since the experiments performed by Baldwin and Boreham and Boreham and Luther-Da used gas pressures as high as

10^{-4} torr, whereas Lompré et al (1985) showed that pressures of around $5x10^{-5}$ torr or less were needed before space charge effects could be ignored. Consequently, this deficiency should be taken into account when interpreting results from a model such as the one employed here, since space charge effects could further broaden the ATI peaks.

Discrepancies between the experimental and simulated spectra arising from the chosen electron ejection distributions can also be discounted. It has previously been shown (Section 3.4) that for the cases considered here, the resultant electron energy spectrum is essentially independent of the direction of the initial (excess) energy and detector geometry used.

Another source of error could be the difference between the measured laser beam spatial profile (Figure 3.7) and the gaussian beam (Figure 2.1) used in the simulations. It is not certain what effect the differing beam descriptions may have on the results. Unfortunately, because of the complexity involved with digitising the 3-D intensity profile, computation time constraints prevented the use of the actual beam profile in the simulations.

In summary, short pulse effects are present which significantly broaden the electron energy distribution to eliminate the structure in the ATI spectrum. There is reasonable agreement with the shape and width of the peaks corresponding to each ion stage. However, the peak positions are in poor agreement. This is most probably due to the imprecise determination of the threshold intensities, with possible contributions from space charge effects and the non-Gaussian spatial beam profile. The main feature of these simulations, therefore, is that the studies performed by Baldwin and Boreham in 1979 (under these experimental conditions) could not have measured the ATI structure discovered later, even given the necessary electron spectrometer resolution.

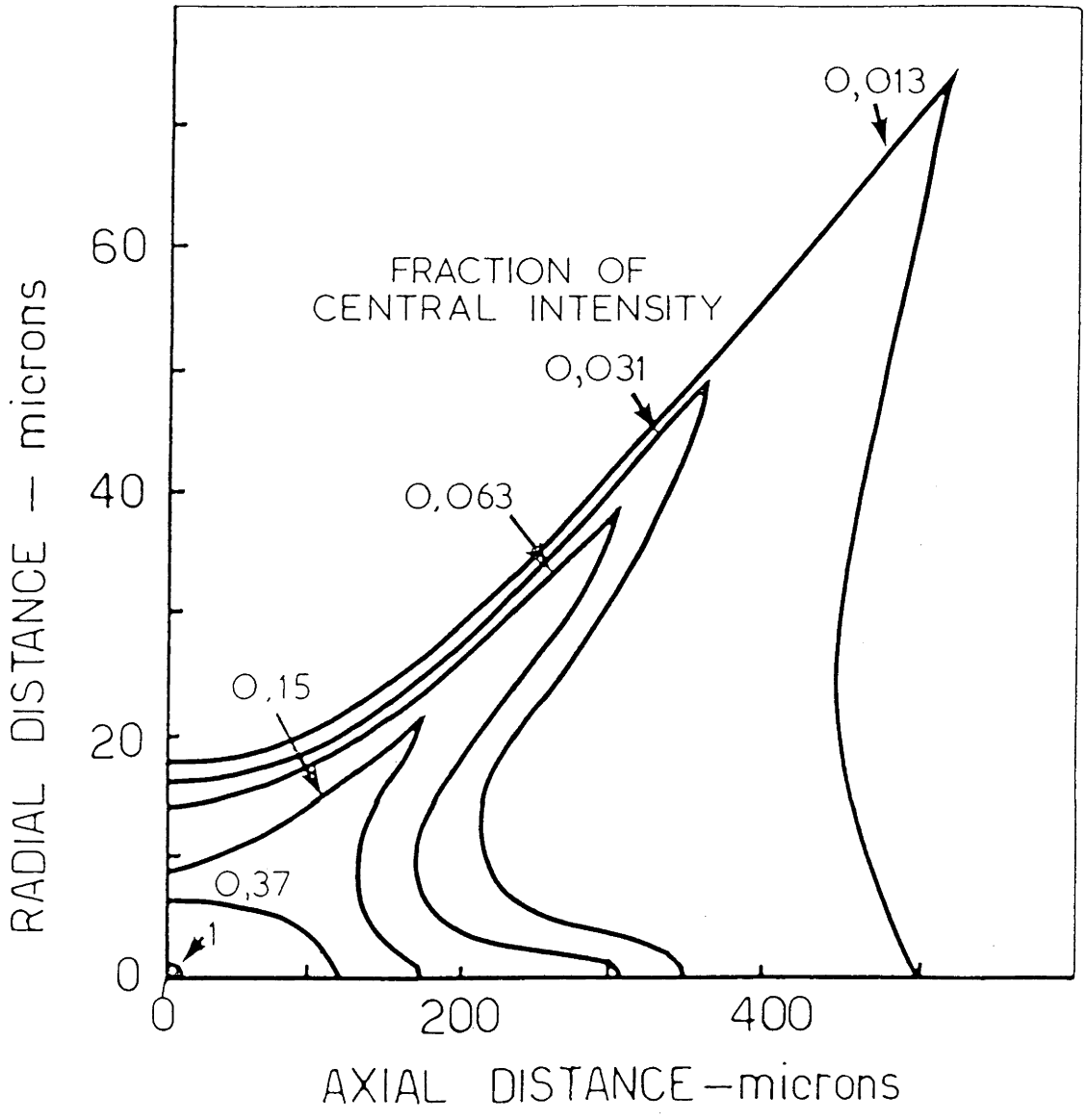

Figure 3.7: Experimental iso-intensity contours for the laser beam (Baldwin)

3.7 CONCLUSION

Postulated above-threshold ionisation peaks and ponderomotive acceleration calculations were used with a detector code to simulate the experimental results of Baldwin and Boreham and Boreham and Luther-Davies. Although the positions of the simulated peaks in the electron energy spectra did not coincide with the positions of the experimental peaks, it was shown that this could easily be due to the errors involved in determining the experimental threshold ionisation intensity which plays a crucial role in accurately modelling the experiments. However, the widths of the simulated and experimental peaks are similar, which is an indication of successful modelling of the effects of surfing and peak suppression on the postulated ATI spectrum generated for each ionisation state.

The most important result of these studies was that both the experimental and the simulated electron energy spectra lacked structure arising from individual ATI peaks. The simulation results showed, therefore, that the lack of individual ATI peaks in the experimental results was not necessarily the result of poor instrumental resolution, but was due to the electrons gaining non-quantal amounts of energy from the laser field.

CHAPTER FOUR
CONCLUSION

A model for the ponderomotive acceleration of electrons during multiphoton ionisation of rare gas atoms was developed. This was then used together with postulated ATI spectra to simulate experiments of the multiphoton ionisation of argon and helium which were performed by Baldwin and Boreham and Boreham and Luther-Davies.

4.1 PONDEROMOTIVE ACCELERATION CALCULATIONS

The ponderomotive acceleration of electrons from the laser field was simulated by performing ponderomotive calculations in one, two and three dimensions. The following observations were made.

From the one-dimensional studies, it was seen that the amount of energy the electron had at the detector depended primarily on the value of the pulse length to focal spot size ratio. For cases where the peak intensity exceeded the threshold intensity, four regimes were identified:

(i) For a pulse width to spot size ratio <0.1 ps/μm, the electron emerged from the laser beam with $E_{final} = E_{excess}$.

(ii) For a pulse width to spot size ratio >0.1 ps/μm but <0.2 ps/μm, the electron emerged with $E_{excess} < E_{final} < E_{osc} + E_{excess}$.

(iii) For a pulse width to spot size ratio >0.2 ps/μm but <10 ps/μm, the electron emerged with $E_{final} > E_{osc} + E_{excess}$.

(iv) For a pulse width to spot size ratio >10 ps/μm, the electron emerged with $E_{final} = E_{osc} + E_{excess}$.

The observations from the 1-D simulations were confirmed by the results from the 2-D and 3-D simulations. Individual ATI peaks in the 2-D and 3-D simulations were broader than those in the 1-D calculations due to electrons being generated from throughout the focal region and experiencing a range of intensity gradients, as opposed to the electron generation at the origin used in the 1-D simulations. Electrons accelerated from a short pulse were found to have a range of final energies. This was thought to be due to the electrons being accelerated from different regions of the laser focus. It was postulated that electrons with energies lower than expected from $E_{osc}+E_{excess}$ were generated from positions in the focal region where the laser pulse passed over them too quickly for the electrons to convert their oscillation energy to directed kinetic energy. High energy electrons were also thought to be formed when the intensity of the laser pulse changed substantially while they were still in the beam, during which time they experienced intensities much greater than that at ionisation. Thus, the electrons were found to gain non-quantal amounts of energy from the laser pulse.

It was also found that if all the electrons were detected after they had been accelerated from the laser beam, the final electron energy spectrum was more or less independent of the electron ejection distribution used. However, the electron energy spectrum detected as a function of position could vary considerably, depending on the pulse duration and the angle of detection. The total number of electrons (of all energies) was also found to vary as a function of detector position. For small pulse length to spot size ratios (~0.05ps/μm), the distribution of electrons emerging from the laser beam was found to be almost identical to the electron ejection distribution. This is to be expected since the electrons did not move (or moved only slightly) during the pulse. For pulse length to spot size ratios larger than ~1ps/μm, the distribution of electrons emerging from the laser beam was found to be cylindrically symmetric and strongly peaked in the x-y plane, with a relatively small z component. Further, the electron energy spectrum

for a 0.25ps pulse (where the distribution was not quite isotropic) was the same shape for both total and partial detection. Consequently, for the longer pulse regime in which the experiments were conducted, it was valid to use a $\pm y$ distribution for the electron ejection pattern.

4.2 MPI CALCULATIONS

Results from the calculations of above-threshold ionisation peaks and ponderomotive acceleration were used with the detection code to simulate the experimental results of Baldwin and Boreham and Boreham and Luther-Davies. Although the positions of the simulated peaks in the electron energy spectra did not coincide with the positions of the experimental peaks, it was shown that this could easily be due to the errors involved in determining the experimental threshold ionisation intensity. Further, the broad electron energy peak produced by the simulation for each ion stage had a simulated width similar to those measured by the experiments, although nothing could be concluded from this as to the correctness of the postulated ATI spectra used.

The main feature of these simulations, however, was that the experiment was conducted in the surfing regime ($\tau/R_0 >\sim 4$ps/μm) and that this yielded a merged energy spectrum in which the individual ATI peaks could not be resolved. The effect of Debye coupling and a non-Gaussian spatial beam profile (not included in this simulation) may have caused a further spread in the electron energies. It was therefore clear that the studies performed by Baldwin and Boreham and Boreham and Luther-Davies (under these experimental conditions) could not have measured the ATI structure discovered later, even given a sufficiently high spectrometer resolution.

4.3 FURTHER WORK

There are a number of different areas of the present work which warrant further investigation. Additional work on the above-threshold ionisation could include generating more realistic ATI spectra (prior to the acceleration of the electrons from the laser pulse) in order to better simulate experimental conditions - for example, using a method similar to that used in the calculations performed by Becker et al (1987).

In the ponderomotive acceleration calculations, it was assumed that ionisation occurred at a fixed laser intensity. Future work could include using an intensity dependent ionisation potential and ionisation probability. The threshold ionisation intensity could be calculated using an extended Keldysh-Faisal-Reiss theory.

More simulations of the Baldwin and Boreham and Boreham and Luther-Davies experiments could then be performed to see if better agreement could be obtained by adjusting ionisation threshold intensities to fit these theoretical predictions as well as measurements made elsewhere (for example, those given in L'Huillier et al and Perry et al, 1988a). This was not done here due to the extensive computer time required for the simulations and the time constraints on the present work. However, it has already been shown that the energy differences between the experimental and simulated peaks arise principally from the errors in determining the threshold ionisation intensities. The principal agreement between the simulations and the experiment still holds: that ATI structure could not have been observed in the electron energy spectra of these early experiments.

As has been discussed earlier, the assumption in the model for ponderomotive acceleration which assumes no space charge effects is not valid for some experimental conditions. It is thought that space charge effects may be

responsible for the low energy electrons present in experimental results. Although Debye coupling could be included in the model, this would lead to a large increase in the computational time required to generate the electron energy spectra as a full plasma hydrodynamic calculation would be required.

The gaussian laser beam description used in the ponderomotive simulation was idealised. In practice, the laser pulse is not quite gaussian and so, the use of the actual beam description (Figure 3.7) may help to better simulate experimental results. The actual intensity profile of the laser beam in the focal region should be measured accurately to allow comparison with the simulations.

During the ponderomotive acceleration simulations, the position and velocity of each electron was updated at each time step. Because of the constraints of computer memory, these values were not kept after the next time step. Another area of further work for the ponderomotive acceleration calculations, therefore, would be to perform a detailed trajectory tracing to see how electrons generated in different regions of the focus are accelerated. In this way, discussions about the origin of low and high energy electrons could be confirmed.

Simulations (and experiments) could then investigate why a single ATI peak shows contributions due to the generation of both high and low energy electrons, (as in Figure 2.13(c)).

Further simulation and experimental studies are needed to determine regimes where the electron energy spectrum does show individual ATI peaks. Results from the one-dimensional studies suggest that this could be achieved by increasing the pulse length to spot size ratio in the Baldwin and Boreham experiments by a factor of about ten or more, although a full 3-D study would be needed to confirm this. This would enable, for example, the prediction of

regimes in which above-threshold ionisation could be measured in higher ion stages to determine whether ion stripping occurred sequentially or via a single multiphoton ionisation event (Baldwin, private communication). If the ionisation process for more than one electron is sequential, (as in the present model), the spectrum (for a long pulse regime with no surfing) should show individual ATI peaks. If the ionisation process for higher ionisation states is simultaneous, however, the spectrum may not show any individual ionisation peaks, (even for a long pulse), because the initial excess energy may be shared by the ionised electrons. Hence, for simultaneous ionisation, the result would be a more or less continuous energy spectrum. The energy spectra resulting from the two processes would therefore yield distinctive signatures which would enable the two processes to be distinguished.

REFERENCES

Agostini P, Barjot G, Bonnal J F, Mainfray G, Manus C and Morellec J, (1968), "Multiphoton ionization of hydrogen and rare gases", IEEE J Quant Electron, Vol 4, No 10, Pp 677-9.

Agostini P, Fabre F, Mainfray G, Petite G and Rahman N K, (1979), "Free-Free Transitions Following Six-Photon Ionization of Xenon Atoms", Phys Rev Lett, Vol 42, No 17, Pp 1127-30.

Agostini P, Kupersztych J, Lompré L A, Petite G and Yergeau F, (1987), "Direct evidence of ponderomotive effects via laser pulse duration in above-threshold ionization", Phys Rev A, Vol 36, No 8, Pp 4111-4.

Agostini P and Petite G, (1988), "Photoelectric effect under strong irradiation", Contemp Phys, Vol 29, No 1, Pp 57-77.

Augst S, Strickland D, Meyerhofer D D, Chin S L and Eberly J H, (1989), "Tunneling Ionization of Noble Gases in a High-Intensity Laser Field", Phys Rev Lett, Vol 63, No 20, Pp 2212-5.

Aymar M and Crance M, (1981), "Multiphoton ionisation probabilities of multiple continua in alkali atoms", J Phys B: At Mol Phys, Vol 14, Pp 2585-601.

Baldwin K G H, (1979), "Laser Induced Ionization of Argon", Masters' Thesis, The Australian National University.

Baldwin K G H, (1987), Private Communication.

Baldwin K G H and Boreham B W, (1981), "Investigation of tunneling processes in laser-induced ionization of argon", J Appl Phys, Vol 52, No 4, Pp 2627-33.

Bardsley J N, Szöke A and Comella M J, (1988), "Multiphoton ionisation from a short-range potential by short-pulse lasers", J Phys B: At Mol Opt Phys, Vol 21, Pp 3899-916.

Bashkansky M, Bucksbaum P H and Schumacher D W, (1988), "Asymmetries in Above-Threshold Ionization", Phys Rev Lett, Vol 60, No 24, Pp 2458-61.

Basile S, Trombetta F, Ferrante G, Burlon R and Leone C, (1988), "Multiphoton ionization of hydrogen by a strong multimode field", Phys Rev A, Vol 37, No 3, Pp 1050-2.

Bebb H B and Gold A, (1966), "Multiphoton Ionization of Hydrogen and Rare-Gas Atoms", Phys Rev, Vol 143, No 1, Pp 1-24.

Becker W, Schlicher R R and Scully M O, (1986), "Final-state effects in above-threshold ionisation", J Phys B: At Mol Phys, Vol 19, L785-92.

Becker W, Schlicher R R, Scully M O and Wodkiewicz, (1987), "Role of final state effects in above-threshold ionisation", J Opt Soc Am B, Vol 4, No 5, Pp 743-50.

Boreham B W, (1979), "Measurement of ionisation threshold intensities in helium using ponderomotive force accelerated electrons", Europhysics conference on multiphoton processes, Benodet, France, June 18-22.

Boreham B W and Hughes J L, (1981), "Measurement of ionization threshold intensities in helium using ponderomotive force accelerated electrons", Sov Phys JETP, Vol 53, No 2, Pp 252-9.

Boreham B W and Luther-Davies B, (1979), "High-energy electron acceleration by ponderomotive forces in tenuous plasmas", J Appl Phys, Vol 50, No 4, Pp 2233-8.

Bucksbaum P H, Bashkansky M and Schumacher D W, (1988), "Above-threshold ionization in helium", Phys Rev A, Vol 37, No 9, Pp 3615-8.

Chen B, Faisal F H M, Jetzke S, Lutz H O and Scanzano P, (1987), "Above-threshold electron ejection spectra", Phys Rev A, Vol 36, No 8, Pp 4091-4.

Cohen-Tannoudji C, Diu B and Laloe F, (1977), "Quantum Mechanics", Vols 1 & 2, John Wiley & Sons, New York, Pp 405-15 and 1343-55.

Collins L A and Merts A L, (1990), "Atoms in strong, oscillating electric fields: momentum-space solutions of the time-dependent, three-dimensional Schrödinger equation", J Opt Soc Am B, Vol 7, No 4, Pp 647-58.

Corkum P B, Burnett N H and Brunel F, (1989), "Above-Threshold Ionization in the Long-Wavelength Limit", Phys Rev Lett, Vol 62, No 11, Pp 1259-62.

Crance M, (1986), "Multiphoton ionisation towards multiple continua: the role of space charge", J Phys B: At Mol Phys, Vol 19, L267-71.

Deng Z and Eberly J H, (1985), "Multiphoton absorption above the ionization threshold by atoms in strong laser fields", J Opt Soc Am B, Vol 2, No 3, Pp 486-93.

Dirac P A M, and Harding J W, (1932), "Photo-electric absorption in hydrogen-like atoms", Proc Camb Philosophical Soc, Vol 28, Pp 209 - 218.

Dutton M E St J and Dalton B J, (1990), "The effect of continuum-continuum transitions on laser-induced continuum structures", J Mod Opt, Vol 37, No 1, Pp 53-73.

Eberly J H, (1965), "Proposed Experiment for Observation of Nonlinear Compton Wavelength Shift", Phys Rev Lett, Vol 15, No 3, Pp 91-3.

Eberly J H and Javanainen J, (1988), "Above-threshold ionisation", Eur J Phys, Vol 9, Pp 265-75.

Eberly J H, Su Q and Javanainen J, (1989), "Nonlinear Light Scattering Accompanying Multiphoton Ionization", Phys Rev A, Vol 62, No 8, Pp 881-4.

Faisal F H M, (1973), "Collision of electrons with laser-photons in a background potential", J Phys B, Vol 6, L312-5.

Freeman R R, McIlrath T J, Bucksbaum P H and Bashkansky M, (1986), "Ponderomotive Effects on Angular Distributions of Photoelectrons", Phys Rev Lett, Vol 57, No 25, Pp 3156-9.

Freeman R R, Bucksbaum P H, Milchberg H, Darack S, Schumacher D and Geusic M E, (1987), "Above-Threshold Ionization with Subpicosecond Laser Pulses", Phys Rev Lett, Vol 59, No 10, Pp 1092-5.

Freeman R R, Bucksbaum P H and McIlrath T J, (1988), "The Ponderomotive Potential of High Intensity Light and Its Role in the Multiphoton Ionization of Atoms", IEEE J Quant Electron, Vol 24, No 7, Pp 1461-9.

Gontier Y and Trahin M, (1980), "Energetic electron generation by multiphoton absorption", J Phys B: At Mol Phys, Vol 13, Pp 4383-90.

Gontier Y, Rahmann N K and Trahin M, (1988), "Resonant multiphoton ionization of atomic hydrogen", Phys Rev A, Vol 37, No 12, Pp 4694-701.

Göppert-Mayer M, (1931), "Two-Quantum Processes", Ann d Physik, Vol 9, No 3, Pp 273-94.

Gradshtein I S and Ryzhik I M, (1980), "Tables of integrals, series and products", Corrected & Enlarged Edition, Academic Press, New York.

Hollis M J, (1978), "Multiphoton Ionization and EM Field Gradient Forces", Opt Comm, Vol 25, No 3, Pp 395-8.

Hora H, (1969), "Nonlinear Confining and Deconfining Forces Associated with the Interaction of Laser Radiation with Plasmas", Phys Fluids, Vol 12, No 1, Pp 182-91.

Javanainen J and Eberly J H, (1989), "Comparison of Keldysh models with numerical experiments on above-threshold ionization", Phys Rev A, Vol 39, No 1, Pp 458-61.

Jönsson L, (1987), "Energy shifts due to the ponderomotive potential", J Opt Soc Am B, Vol 4, No 9, Pp 1422-5.

Keldysh L V, (1965), "Ionization in the Field of a Strong Electromagnetic Wave", Sov Phys JETP, Vol 20, No 5, Pp 1307-14.

Kibble T W B, (1966), "Refraction of Electron Beams by Intense Electromagnetic Waves", Phys Rev Lett, Vol 16, No 23, Pp 1054-6.

Kruit P, Kimman J, Muller H G and van der Wiel M J, (1983), "Electron spectra from multiphoton ionization of xenon at 1064, 532, and 355 nm", Phys Rev A, Vol 28, No 1, Pp 248-55.

Kupersztych J, (1987), "Inverse Half-Bremsstrahlung in Multiphoton Ionization of Atoms in Intense Light Beams", Europhys Lett, Vol 4, No 1, Pp 23-8.

Landau L D and Lifshitz E M, (1960), "Electrodynamics of Continuous Media", Pergamon Press, Oxford, Pp 64-5.

Landen O L, Perry M D and Campbell E M, (1987), "Resonant Multiphoton Ionization of Krypton by Intense uv Laser Radiation", Phys Rev Lett, Vol 59, No 22, Pp 2558-61.

L'Huillier A, Lompré L A, Mainfray G and Manus C, (1983), "Multiply charged ions induced by multiphoton absorption processes in rare-gas atoms at 1.064μm", J Phys B: At Mol Phys, Vol 16, Pp 1363-81.

Lompré L A, L'Huillier A, Mainfray G and Manus C, (1985), "Laser-intensity effects in the energy distributions of electrons produced in multiphoton ionisation of rare gas atoms", J Opt Soc Am B, Vol 2, No 12, Pp 1906-12.

Lompré L A, Mainfray G, Manus C and Kupersztych J, (1987), "The energy distributions of electrons produced in multiphoton ionisation of rare gases", J Phys B: At Mol Phys, Vol 20, Pp 1009-29.

Lorrain P and Corson D, (1970), "Electromagnetic Fields and Waves", 2nd Edition, W H Freeman and Company, New York.

Mainfray G and Manus C, (1991), "Multiphoton ionization of atoms", Rep Prog Phys, Vol 54, Pp 1333-72.

Martin E A Jr and Mandel L, (1976), "Electron energy spectrum in laser-induced multiphoton ionization of atoms", Appl Opt, Vol 15, No 10, Pp 2378-80.

McIlrath T J, Bucksbaum P H, Freeman R R and Bashkansky M, (1987), "Above-threshold ionization processes in xenon and krypton", Phys Rev A, Vol 35, No 11, Pp 4611-23.

McIlrath T J, Freeman R R, Cooke W E and van Woerkom L D, (1989), "Complex spatial structure of ion yield arising from high-intensity multiphoton ionization", Phys Rev A, Vol 40, No 5, Pp 2270-3.

Muller H G, Tip A and van der Wiel M J, (1983), "Ponderomotive force and AC Stark shift in multiphoton ionisation", J Phys B: At Mol Phys, Vol 16, L679-85.

Muller H G, van Linden van den Heuvell H B, Agostini P, Petite G, Antonetti A, Franco M and Migus A, (1988), "Multiphoton Ionization of Xenon with 100-fs Laser Pulses", Phys Rev Lett, Vol 60, No 7, Pp 565-8.

Perry M D, Landen O L, Szöke A and Campbell E M, (1988a), "Multiphoton ionization of the noble gases by an intense 10^{14}-W/cm^2 dye laser", Phys Rev A, Vol 37, No 3, Pp 747-60.

Perry M D, Landen O L, Szöke A and Campbell E M, (1988b), "Nonresonant Multiphoton Ionization of Noble Gases: Theory and Experiment", Phys Rev Lett, Vol 60, No 13, Pp 1270-3.

Perry M D, Landen O L and Szöke A, (1989), "Measurement of the local laser intensity by photoelectron energy shifts in multiphoton ionization", J Opt Soc Am B, Vol 6, No 3, Pp 344-9.

Petite G, Agostini P and Muller H G, (1988), "Intensity dependence of non-perturbative above-threshold ionisation spectra: experimental study", J Phys B: At Mol Opt Phys, Vol 21, Pp 4097-105.

Reiss H R, (1980), "Effect of an intense electromagnetic field on a weakly bound system", Phys Rev A, Vol 22, No 5, Pp 1786-813.

Reiss H R, (1987), "Spectrum of atomic electrons ionised by an intense field", J Phys B: At Mol Phys, Vol 20, L79-83.

Roso-Franco L and Eberly J H, (1990), "Multiphoton and above-threshold detachment computed for a model negative ion and compared with perturbation theory", J Opt Soc Am B, Vol 7, No 4, Pp 407-13.

Shakeshaft R and Potvliege R M, (1987), "Approximate theory for multiphoton ionization of an atom by an intense field", Phys Rev A, Vol 36, No 11, Pp 5478-81.

Shore B W, (1988), Private Communication.

Sundaram B and Armstrong L Jr, (1990), "Modeling strong-field above-threshold ionization", J Opt Soc Am B, Vol 7, No 4, Pp 414-24.

Symons H D, Baldwin K G H, Luther-Davies B and Dragila R, (1988), "Acceleration of Electrons from an Intense Laser Beam", poster presented by author at the Australian Bicentenary Congress of Physicists, Sydney, January 25-29.

Szöke A, (1985), "Interpretation of electron spectra obtained from multiphoton ionisation of atoms in strong fields", J Phys B: At Mol Phys, Vol 18, L427-32.

Volkov D M, (1935), "Uber eine Klasse von Losungen der Diracschen Gleichung", Z Phys, Vol 94, Pp 250-60.

Voronov G S and Delone N B, (1966), "Many-Photon Ionization of the Xenon Atom by Ruby Laser Radiation", Sov Phys JETP, Vol 23, No 1, Pp 54-8.

Yergeau F, Petite G and Agostini P, (1986), "Above-threshold ionisation without space charge", J Phys B: At Mol Phys, Vol 19, L663-9.

APPENDIX A

```
C-----------------------------------------------------------------------
C-----------------------------------------------------------------------
C-----------------------------------------------------------------------
C-----------------------------------------------------------------------
C
      PROGRAM ELECTRON
C
C-----------------------------------------------------------------------
C
C  This program was written in conjunction with Dr Leo Brewin of the
C  Australian National Supercomputer Facility during 1988.
C  All reference or use of this program should therefore acknowledge
C  the joint authorship of Leo Brewin and Heather Symons.
C
C  There are two distinct phases in the execution of this program.
C  In the first phase a list of ionization events is constructed.
C  In the second phase the trajectories of the free electrons are
C  computed by integrating a set of non-coupled second order ode's.
C
C  The list of ionization events is constructed by first constructing
C  a regular cylindrical grid of points within the ionization chamber.
C  Each point in the grid is processed and the ionization condition,
C  that the local intensity exceeds a critical minimum, is used to
C  compute the time of ionization.  This event is represented by
C  seven coordinates -- one time, three space and three velocity
C  variables (see below for a full description).  Notice that for
C  some points in the grid an ionization is not possible.  On average
C  75% of the grid points yield ionizations.
C
C  In the integration phase each of the seven coordinates is updated
C  by integrating seven first order ode's.  This integration is
C  applied to every event until that electron has reached its terminal
C  velocity.  At this point the energy of the electron is determined
C  and the appropriate bin is updated, after which the electron is
C  deleted from the integration list.  The electron is deemed to have
C  reached its terminal velocity when the local intensity has dropped
C  to a very small value (much smaller than any of the local minima of
C  the intensity distribution).  Notice that with this structure a
C  vector containing the active electrons may be easily constructed
C  and passed to the most time consuming part of the programme -- the
C  integration routine.  This leads to an efficient vectorization.
C
C  Memory requirements are proportional to N2*N3*N4.  For N2=N3=N4=21
C  about 1.8Mbytes of extended common and 200kbytes of basic memory
C  was required.  This lead to 6888 ionizations and an execution time
C  of about 18secs.  In scalar mode (but run on the VP) the program
C  completed about 3/4 of the calculations in 5min cpu time.  Most
C  of the memory (3/4 of it) is used as temporary variables in the
C  subroutine RUNGE.  The memory required could be halved by using
C  the subroutine EULER instead of RUNGE but you MUST check that the
C  increase in truncation error does not turn the answers into
C  rubbish.
C
```

```
C ---------------------------------------------------------------------
C
C N1 = the number of runs
C N2 = the number of sub-divisions along the z-axis.
C N3 = the number of sub-divisions along the r-axis.
C N4 = the number of sub-divisions in theta.
C N5 = the max. number of ionization events.
C N6 = the max. number of bins.
C N7 = 7 x N5.
C
C---------------------------------------------------------------------
C
C  The main variables used are
C
C     LST(I  ) = the time associated with electron number I
C     LST(I+1) = the x-coordinate of the electron
C     LST(I+2) = the y-coordinate of the electron
C     LST(I+3) = the z-coordinate of the electron
C     LST(I+4) = the x-velocity of the electron
C     LST(I+5) = the y-velocity of the electron
C     LST(I+6) = the z-velocity of the electron
C
C     LSTFLG(1+I/7) = 1 if the electron is still active.
C                   = 0 if the electron has reached its terminal vel.
C
C     LSTNUM = the number of ionizations.
C     LSTBEG = the first ionization event (not the earliest).
C     LSTEND = the last ionization event (not the latest).
C     LSTADD = position in LST where the next event would be added.
C
C     VOL(1+I/7) = a weight associated with this electron,
C                  proportional to the volume element of the
C                  spatial cell in which the electron was created.
C
C     TMP(...) = an array like LST(...) but containing only the
C                active electrons.
C
C     EPSCUT = the cutoff value for the deletion of an electron.
C
C     DT = the time step used in the integration routines.
C
C---------------------------------------------------------------------
C
C This program uses a LSTFLG integer array, with values 0 or 1,
C indicating whether this item is or is not in the radiation field.
C
      INCLUDE(NEWINC)

         CALL BEGIN
         LSTADD=1
         LSTNUM=0
         LSTBEG=0
         LSTEND=0
         LSTFLG(1)=1
C        IRUN = 0
C
```

```
C  Step along the Z-azis
C
      DO 110 I=1,N2
         ZI=ZMIN+FLOAT(I-1)*DZ
C        ZI=ZMIN+FLOAT((IRUN-1)*N2+(I-1))*DZ
         TEMP0=1.0+(LPIRSQ*ZI)**2
         TEMP1=LOG( I0IP/TEMP0 )
         TEMP2=RAD0SQ*TEMP0
         RRSQ=TEMP1*TEMP2
         RRMAX=ABS( SQRT( RRSQ )-EPS )
         NUM=1.0+RRMAX/DR
C
C  Step along the R-axis.
C  At R=0 cylindrical coordinates are singular.  Thus we must
C  deal with this case separately (otherwise we would obtain
C  multiple ionizations on the R=0 axis).
C
         LSTFLG(1+LSTADD/7)=1
         LST(LSTADD  )=ZI/C - TAU*SQRT( TEMP1 )
         LST(LSTADD+1)=0.0
         LST(LSTADD+2)=0.0
         LST(LSTADD+3)=ZI
         LST(LSTADD+4)=VYINIT*COS(0.5*PI)
         LST(LSTADD+5)=VYINIT*SIN(0.5*PI)
         LST(LSTADD+6)=0.0
         VOL(1+LSTADD/7)=0.5*DR
         LSTADD=LSTADD+7
C
C  Now deal with the non-zero R values.
C
         DO 100 J=2,NUM
            RJ=FLOAT(J-1)*DR
            TIJ=ZI/C - TAU*SQRT( (RRSQ-RJ*RJ)/TEMP2 )
C
C  Step along the THETA-axis.
C
            INIDX=1+LSTADD/7
            DO 90 K=1,N4
               LSTFLG(1+LSTADD/7)=1
               LST(LSTADD  )=TIJ
               LST(LSTADD+1)=RJ*COS( FLOAT(K-1)*DTHETA )
               LST(LSTADD+2)=RJ*SIN( FLOAT(K-1)*DTHETA )
               LST(LSTADD+3)=ZI
               LST(LSTADD+4)=VYINIT*COS(0.5*PI)
               LST(LSTADD+5)=VYINIT*SIN(0.5*PI)
               LST(LSTADD+6)=0.0
C
C  Evaluate the Jacobian at the middle of the cell
C
               VOL(1+LSTADD/7)=RJ + 0.5*DR
               LSTADD=LSTADD+7
 90         CONTINUE
            OUTIDX=LSTADD/7
C
C  Correct Jacobian for edge cells -- only one half of a cell.
C
            VOL( INIDX)=0.5*(RJ + 0.5*DR)
            VOL(OUTIDX)=0.5*(RJ + 0.5*DR)
```

```
 100      CONTINUE
 110   CONTINUE

       LSTBEG=1
       LSTEND=LSTADD-7
       LSTNUM=LSTADD/7

       WRITE(6,1001) LSTNUM
       WRITE(6,1002) RMAX
       WRITE(6,1004) 2*ZMAX

       OPEN(UNIT=10,FILE='HDS111.TEMP.DATA(NEWSAV)',STATUS='SHR')
       CALL SAVE
C
C ----( cut here but retain the INCLUDE and OPEN lines to restart )-----
C
       CALL BEGIN
       CALL START
C
C  In each call to RUNGE, DTNUM time steps are calculated.
C  Before each call to RUNGE the active electrons are gathered
C  into a temporary list.  After the integration the active
C  electrons are scattered back into the main list.
C  Active electrons which have now left the radiation zone
C  are then flagged as being inactive (by setting a flag to zero).
C  Upon completion of the J do loop all relevant data is written
C  to a save data set.
C
       DTNUM=100
       DO 140 I=1,1000
          DO 130 J=1,20
             IF(LSTNUM.LE.0) GOTO 150
             CALL GATHER
             CALL RUNGE
             CALL SCATER
             CALL FILTER
 130      CONTINUE
          CALL SAVE
 140   CONTINUE
 150   CONTINUE

       CALL SAVE
       CLOSE(10)
       CALL BINWRT
       CLOSE(11)
C
C ---------------------------------------------------------------------
 1000 FORMAT(1X,I9,4X,F10.4,2X,F10.4,2X,F10.4,2X,F10.4)
 1001 FORMAT(1X,'There were ',I9,' ionizations.')
 1002 FORMAT(1X,'The pulse radius was ',F10.4,' microns.')
 1004 FORMAT(1X,'The max. pulse length was ',F10.4,' microns.')
C ---------------------------------------------------------------------
C
       OPEN(UNIT=13,FILE='HDS111.ACC337.DATA',STATUS='SHR')
       WRITE(13,*) LSTEND/7
       DO 123 I=1,LSTEND,7
          WRITE(13,1111) VOL(1+I/7),(LST(J),J=I+1,I+6)
 123   CONTINUE
C
```

```
1111  FORMAT(1X,7(1X,F13.7))
C
      STOP
      END
C
C-----------------------------------------------------------------------
C
      SUBROUTINE BEGIN
      INCLUDE(NEWINC)

         EPS=1.0E-10
         EPSCUT=0.001
         C=299.792458
         PI=3.1415926536

         SCALE=0.093372233016
         ACC=0.35176150612
         AMASS=0.59309485424
         AMASSQ=AMASS*AMASS
         ENGEXS= 9.64085
         ENGMIN=0
         ENGDIV=0.3
         ENGBIN=801
         ENGNUM=0
         TAU=25.0
         RAD0=13.0
         LAMBDA=1.064

         EPHOT=(0.0041356948735)*C/LAMBDA
         I0=25000.*SCALE*LAMBDA*LAMBDA
         IP=4520.0*SCALE*LAMBDA*LAMBDA
         VYINIT=AMASS*SQRT(ENGEXS+ENGNUM*EPHOT)
         TAUC=TAU*C
         TAUSQC=TAU*TAU*C

         I0IP=I0/IP
         RAD0SQ=RAD0*RAD0
         LPIR=LAMBDA/(PI*RAD0)
         LPIRSQ=LAMBDA/(PI*RAD0SQ)
         ZMAX=( PI*RAD0SQ/LAMBDA )*SQRT( I0IP-1.0 )-EPS
         ZMIN=-ZMAX
         RMAX=RAD0*( SQRT( EXP( LOG(I0IP)-1.0 ) ) )
         RMIN=0.0
         DZ=(ZMAX-ZMIN)/FLOAT(N2-1)
C        DZ=(ZMAX-ZMIN)/FLOAT((N1*N2)-1)
         DR=(RMAX-RMIN)/FLOAT(N3-1)
         DTHETA=2.D0*PI/FLOAT(N4-1)
         DT=0.25

         DO 20 I=1,N5
            VOL(I)=0.0
            LSTFLG(I)=0
20       CONTINUE
         DO 10 I=1,N6
            BIN(I)=0.0
10       CONTINUE

         RETURN
      END
```

```
C
C-----------------------------------------------------------------------
C
      SUBROUTINE GATHER
      INCLUDE(NEWINC)

         J=1
*VOCL LOOP,NOVREC(TMP)
         DO 100 I=1,LSTEND,7
            IF(LSTFLG(1+I/7).NE.0) THEN
               TMP(J )=LST(I )
               TMP(J+1)=LST(I+1)
               TMP(J+2)=LST(I+2)
               TMP(J+3)=LST(I+3)
               TMP(J+4)=LST(I+4)
               TMP(J+5)=LST(I+5)
               TMP(J+6)=LST(I+6)
               J=J+7
            ENDIF
 100     CONTINUE
         RETURN
      END
C
C-----------------------------------------------------------------------
C
      SUBROUTINE SCATER
      INCLUDE(NEWINC)

         J=1
         DO 100 I=1,LSTEND,7
            IF(LSTFLG(1+I/7).NE.0) THEN
               LST(I )=TMP(J )
               LST(I+1)=TMP(J+1)
               LST(I+2)=TMP(J+2)
               LST(I+3)=TMP(J+3)
               LST(I+4)=TMP(J+4)
               LST(I+5)=TMP(J+5)
               LST(I+6)=TMP(J+6)
               J=J+7
            ENDIF
 100     CONTINUE
         RETURN
      END
C
C-----------------------------------------------------------------------
```

```
C
      SUBROUTINE FILTER
      INCLUDE(NEWINC)

         KILL=0
         DO 100 I=1,LSTEND,7
            IF(LSTFLG(1+I/7).NE.0) THEN
               RSQ=LST(I+1)**2 + LST(I+2)**2
               R2SQ=RAD0SQ+(LPIR*LST(I+3))**2
               PHASE=(RSQ/R2SQ)+((LST(I)/TAU)-(LST(I+3)/TAUC))**2
               E=I0*EXP(-PHASE)*RAD0SQ/R2SQ
               IF(ABS(E).LT.EPSCUT) THEN
                  KILL=KILL+1
                  CALL BINTOT(I)
                  CALL DELETE(I)
               ENDIF
            ENDIF
 100     CONTINUE
         PRINT*, '--  Killed ',KILL,' events;  ',LSTNUM,' left.'
         RETURN
C110     CONTINUE
C        RETURN
      END
C
C-----------------------------------------------------------------------
C
      SUBROUTINE BINTOT(KEY)
      INCLUDE(NEWINC)
      INTEGER BINNUM

         ENG=( LST(KEY+4)**2+LST(KEY+5)**2+LST(KEY+6)**2 )/AMASSQ
         BINNUM=INT( (ENG-ENGMIN)/ENGDIV )+1
         IF(BINNUM.LE.N6) THEN
            BIN( BINNUM )= BIN( BINNUM ) + VOL(1+KEY/7)
         ELSE
            PRINT*, '-- Whoops, bin too big.  ',BINNUM
         ENDIF
         RETURN
      END
C
C-----------------------------------------------------------------------
C
      SUBROUTINE BINWRT
      INCLUDE(NEWINC)

         OPEN(UNIT=11,FILE='HDS111.TEMP.DATA(NEWOUT)',STATUS='SHR')
         REWIND(11)
         DO 10 I=1,N6
            IF(BIN(I).GE.0.125*DR) THEN
               ENG=ENGMIN+FLOAT(I)*ENGDIV
               WRITE(11,100) I,ENG,BIN(I)
            ENDIF
  10     CONTINUE
         RETURN
 100     FORMAT(1X,I9,4X,',',4X,F12.7,4X,',',4X,E20.12)
      END
C
C-----------------------------------------------------------------------
C
```

```
      SUBROUTINE START
      INCLUDE(NEWINC)

         REWIND(10)
         READ(10,*) LSTBEG,LSTEND,LSTNUM,LSTADD
         DO 10 I=1,LSTNUM
            LSTFLG(I)=0
            VOL(I)=0.0
   10    CONTINUE
         DO 20 I=1,LSTEND,7
            READ(10,*) K,(LST(J),J=K,K+6),VOL(1+K/7)
            LSTFLG(1+K/7)=1
   20    CONTINUE
         DO 40 J=1,N6
            READ(10,*,END=50) K,BK
            BIN(K)=BK
   40    CONTINUE
   50    CONTINUE
         RETURN
      END
C
C-----------------------------------------------------------------------
C
      SUBROUTINE SAVE
      INCLUDE(NEWINC)

         REWIND(10)
         WRITE(6,1011) LSTBEG,LSTEND,LSTNUM,LSTADD
         WRITE(10,1011) LSTBEG,LSTEND,LSTNUM,LSTADD
         DO 10 J=1,LSTEND,7
            IF(LSTFLG(1+J/7).EQ.1) THEN
               WRITE(10,1000) J,(LST(I),I=J,J+6),VOL(1+J/7)
            ENDIF
   10    CONTINUE
         DO 40 J=1,N6
            IF(BIN(J).GE.0.125*DR) THEN
               WRITE(10,1012) J,BIN(J)
            ENDIF
   40    CONTINUE
         RETURN
C1000    FORMAT(1X,I9,',',E20.13,7(',',E20.13))
 1000    FORMAT(1X,I9,',',F13.7,7(',',F13.7))
 1011    FORMAT(1X,I9,3(',',I9))
C1012    FORMAT(1X,I9,',',E20.13)
 1012    FORMAT(1X,I9,',',F13.7)
      END
C
C-----------------------------------------------------------------------
```

```
C
      SUBROUTINE RUNGE
      INCLUDE(NEWINC)

      INTEGER STEP
      REAL*8 CT(4),CW(4)

         CT(1)=0.5*DT
         CT(2)=0.5*DT
         CT(3)=DT
         CT(4)=0.0
         CW(1)=0.16666666666666*DT
         CW(2)=0.33333333333333*DT
         CW(3)=0.33333333333333*DT
         CW(4)=0.16666666666666*DT

         DO 130 STEP=1,DTNUM
            DO 90 J=1,7*LSTNUM
               XX(J)=TMP(J)
               XY(J)=0.0
 90         CONTINUE
            DO 110 I=1,4
               DO 95 J=1,7*LSTNUM,7
                  RSQ=XX(J+1)**2 + XX(J+2)**2
                  R2SQ=RAD0SQ+(LPIR*XX(J+3))**2
                  PHASE=(RSQ/R2SQ)+((XX(J)/TAU)-(XX(J+3)/TAUC))**2
                  E=I0*EXP(-PHASE)*RAD0SQ/R2SQ
                  DXX(J  )=1.0
                  DXX(J+1)=XX(J+4)
                  DXX(J+2)=XX(J+5)
                  DXX(J+3)=XX(J+6)
                  DXX(J+4)=ACC*E*XX(J+1)/R2SQ
                  DXX(J+5)=ACC*E*XX(J+2)/R2SQ
                  DXX(J+6)=ACC*E*((XX(J+3)/C)-XX(J))/TAUSQC
     +                     -ACC*E*(RSQ-R2SQ)*XX(J+3)*((LPIR/R2SQ)**2)
 95            CONTINUE
               DO 100 J=1,7*LSTNUM
                  XX(J)=TMP(J)+CT(I)*DXX(J)
                  XY(J)= XY(J)+CW(I)*DXX(J)
100            CONTINUE
110         CONTINUE
            DO 120 I=1,7*LSTNUM
               TMP(I)=TMP(I)+XY(I)
120         CONTINUE
130      CONTINUE
         RETURN
      END
C
C-----------------------------------------------------------------------
```

```
C
      SUBROUTINE EULER
C
C  Use this routine in place of RUNGE only when you can be sure that
C  the increase in truncation errors does not effect the solutions,
C
      INCLUDE(NEWINC)

      INTEGER STEP

      DO 110 STEP=1,DTNUM
         DO 100 J=1,7*LSTNUM,7
            RSQ=TMP(J+1)**2 + TMP(J+2)**2
            R2SQ=RAD0SQ+(LPIR*TMP(J+3))**2
            PHASE=(RSQ/R2SQ)+((TMP(J)/TAU)-(TMP(J+3)/TAUC))**2
            E=I0*EXP(-PHASE)*RAD0SQ/R2SQ
            DXX(J  )=1.0
            DXX(J+1)=TMP(J+4)
            DXX(J+2)=TMP(J+5)
            DXX(J+3)=TMP(J+6)
            DXX(J+4)=ACC*E*TMP(J+1)/R2SQ
            DXX(J+5)=ACC*E*TMP(J+2)/R2SQ
            DXX(J+6)=ACC*E*((TMP(J+3)/C)-TMP(J))/TAUSQC
     +              -ACC*E*(RSQ-R2SQ)*TMP(J+3)*((LPIR/R2SQ)**2)
  100    CONTINUE
         DO 105 J=1,7*LSTNUM,7
            TMP(J  )=TMP(J  )+DXX(J  )*DT
            TMP(J+1)=TMP(J+1)+(DXX(J+1)+0.5*DXX(J+4)*DT)*DT
            TMP(J+2)=TMP(J+2)+(DXX(J+2)+0.5*DXX(J+5)*DT)*DT
            TMP(J+3)=TMP(J+3)+(DXX(J+3)+0.5*DXX(J+6)*DT)*DT
            TMP(J+4)=TMP(J+4)+DXX(J+4)*DT
            TMP(J+5)=TMP(J+5)+DXX(J+5)*DT
            TMP(J+6)=TMP(J+6)+DXX(J+6)*DT
  105    CONTINUE
  110 CONTINUE
      RETURN
      END
C
C-------------------------------------------------------------------------
C
      SUBROUTINE DELETE(DELKEY)
      INCLUDE(NEWINC)

         LSTNUM=LSTNUM-1
         LSTFLG(1+DELKEY/7)=0

         RETURN
      END

C-------------------------------------------------------------------------
C-------------------------------------------------------------------------
C-------------------------------------------------------------------------
C-------------------------------------------------------------------------
```

```
C
            NEWINC
C
C     PARAMETER (N1=24,N2=19,N3=51,N4=61,N5=59109,N6=3000,N7=413763)
      PARAMETER (N2=61,N3=31,N4=31,N5=58621,N6=3000,N7=410347)
C     PARAMETER (N2=5,N3=5,N4=5,N5=100,N6=2000,N7=700)

      IMPLICIT REAL*8(A-H,O-Z)
      REAL*8 I0,IP,I0IP,LAMBDA,LPIR,LPIRSQ
      REAL*8 LST(N7),TMP(N7),VOL(N5),BIN(N6),XX(N7),XY(N7),DXX(N7)
      INTEGER LSTFLG(N7)
      INTEGER LSTBEG,LSTEND,INSKEY,DELKEY,PRVKEY,
     +        LSTADD,LSTNUM,DTNUM,INIDX,OUTIDX

      COMMON /LINKED/ LST,LSTFLG,LSTBEG,LSTEND,LSTADD,LSTNUM
      COMMON /WORK/   TMP,VOL,BIN,XX,XY,DXX,DZ,DR,DTHETA,DT
      COMMON /CONST/  EPS,EPSCUT,C,PI,SCALE,ACC,AMASS,AMASSQ,
     +                ENGEXS,ENGMIN,ENGDIV,ENGBIN,ENGNUM,
     +                TAU,TAUC,TAUSQC,RAD0,RAD0SQ,LAMBDA,EPHOT,
     +                I0,IP,I0IP,VYINIT,LPIR,LPIRSQ,ZMAX,ZMIN,
     +                RMAX,RMIN,DTNUM
C
C-------------------------------------------------------------------------
C-------------------------------------------------------------------------
C-------------------------------------------------------------------------
C-------------------------------------------------------------------------
```

APPENDIX B

```
C-----------------------------------------------------------------------
C-----------------------------------------------------------------------
C-----------------------------------------------------------------------
C-----------------------------------------------------------------------
C
      PROGRAM DETECT
C
C     This program is designed to read the final co-ordinates and
C     velocities from the file accend*.data and by using a specified
C     detection geometry, generate electron energy spectra.
C
C-----------------------------------------------------------------------
C
      PARAMETER N=18, N1=18, N2=1100
C
      REAL*8 A,AMASSQ,B,C,ENERGY,PHFIN,PI
      REAL*8 RHO,SUMPHI,SUMTHETA,THFIN,T1,T2,TIME,TOTWAY
      REAL*8 VX,VY,VZ,WEIGHT,X,XF,Y,YF,Z,ZF
      REAL*8 WFAC(20),ESPEC(0:N2),ENGDIV,ENGMIN
      REAL*8 ANGLE,ANGLEA,ANGLEB,CONST,PARTWAY
      INTEGER BINNUM,I,J,K,M,NFILE,NFILE1,NUM,PHBIN,THBIN
      CHARACTER*15 F(20)
C
C-----------------------------------------------------------------------
C
      OPEN(UNIT=12,FILE='TESTX2',STATUS='NEW')
      OPEN(UNIT=21,FILE='TESTY2',STATUS='NEW')
C
C     Put in constants
C
      PI = 3.1415926536
      AMASSQ = 0.35176150584
      RHO = 20000.0
      ENGDIV = 0.25D0
      ENGMIN = 0.D0
      ANGLEA = ATAN(1.5D0/3.2D0)
      ANGLEB = ATAN(3.2D0/1.5D0)
      CONST = DSQRT(40.96D0/49.96D0)

C
      DO 15 I = 0,N2
          ESPEC(I) = 0.D0
15    CONTINUE
C
```

```
C     Initialise variable for weighted sum
C
      TOTWAY = 0.D0
C
      WFAC(1) =  0.005D0
      WFAC(2) =  0.03D0
      WFAC(3) =  0.685D0
      WFAC(4) =  0.93D0
      WFAC(5) =  1.D0
      WFAC(6) =  0.93D0
      WFAC(7) =  0.685D0
      WFAC(8) =  0.03D0
      WFAC(9) =  0.005D0
      WFAC(10) = 0.D0
      WFAC(11) = 0.005D0
      WFAC(12) = 0.03D0
      WFAC(13) = 0.685D0
      WFAC(14) = 0.93D0
      WFAC(15) = 1.D0
      WFAC(16) = 0.93D0
      WFAC(17) = 0.685D0
      WFAC(18) = 0.03D0
      WFAC(19) = 0.005D0
      WFAC(20) = 0.D0
C
      F(1) = 'ACCEND5.DATA'
      F(2) = 'ACCEND36.DATA'
      F(3) = 'ACCEND37.DATA'
      F(4) = 'ACCEND38.DATA'
      F(5) = 'ACCEND6.DATA'
      F(6) = 'ACCEND39.DATA'
      F(7) = 'ACCEND40.DATA'
      F(8) = 'ACCEND41.DATA'
      F(9) = 'ACCEND42.DATA'
      F(10) = 'ACCEND43.DATA'
      F(11) = 'ACCEND44.DATA'
      F(12) = 'ACCEND45.DATA'
      F(13) = 'ACCEND46.DATA'
      F(14) = 'ACCEND47.DATA'
      F(15) = 'ACCEND48.DATA'
      F(16) = 'ACCEND49.DATA'
      F(17) = 'ACCEND50.DATA'
      F(18) = 'ACCEND51.DATA'
      F(19) = 'ACCEND52.DATA'
      F(20) = 'ACCEND53.DATA'
C
```

```
      DO 45 I = 1,20
C
          IF (WFAC(I).EQ.0.D0) GO TO 45
C
          OPEN(UNIT=10,FILE=F(I),STATUS='OLD')
          REWIND(10)
C
C     Read in number of electrons
C
          READ(10,*) NUM

C
          DO 40 M = 1,NUM

C
C     Read in electron weight,co-ordinates and velocities
C
              READ(10,*) WEIGHT,X,Y,Z,VX,VY,VZ
C
C     Add weight to sum for weighted total
C
              WEIGHT = WEIGHT*WFAC(I)
              TOTWAY = TOTWAY + WEIGHT

C
C     Calculate time to reach outside of sphere
C
              A = VX**2 + VY**2 + VZ**2
              B = 2.D0*(X*VX + Y*VY + Z*VZ)
              C = X**2 + Y**2 + Z**2 - RHO**2
              T1 = (-B + DSQRT(B**2 - 4.D0*A*C))/(2.D0*A)
              T2 = (-B - DSQRT(B**2 - 4.D0*A*C))/(2.D0*A)
              IF ((T1.LE.0.D0).AND.(T2.LE.0.D0)) THEN
                  WRITE(11,*) 'T1 & T2 both -ve for electron at:',X,Y,Z
                  WRITE(11,*) 'It has a weight of:',WEIGHT
                  WRITE(11,*) ' '
                  GO TO 40
              END IF
              IF ((T1.LE.0.D0).AND.(T2.GT.0.D0)) TIME = T2
              IF ((T1.GT.0.D0).AND.(T2.LE.0.D0)) TIME = T1
              IF ((T1.GT.0.D0).AND.(T2.GT.0.D0)) THEN
                  IF (T1.LT.T2) TIME = T1
                  IF (T2.LT.T1) TIME = T2
              END IF
C
C     Find final position in Cartesian co-ordinates
C
              XF = X + VX*TIME
              YF = Y + VY*TIME
              ZF = Z + VZ*TIME
```

```
C
C     Find final position in spherical co-ordinates
C
              IF (XF.EQ.0.D0) THEN
                  IF (YF.GT.0.D0) THFIN = PI/2.D0
                  IF (YF.LT.0.D0) THFIN = 1.5D0*PI
              ELSE
                  THFIN = ATAN(YF/XF)
              END IF
              IF (ZF.EQ.0.D0) THEN
                  PHFIN = PI/2.D0
              ELSE
                  PHFIN = ATAN((DSQRT(XF**2+YF**2))/ZF)
              END IF
C
              IF ((THFIN.EQ.0.D0).AND.(XF.LT.0.D0)) THFIN = PI
              IF ((THFIN.GT.0.D0).AND.(XF.LT.0.D0)) THFIN = THFIN + PI
              IF ((THFIN.LT.0.D0).AND.(XF.GT.0.D0)) THFIN = THFIN +
     1                                                      2.D0*PI
              IF ((THFIN.LT.0.D0).AND.(XF.LT.0.D0)) THFIN = PI -
     1                                                ABS(THFIN)
              IF (PHFIN.LT.0.D0) PHFIN = PI - ABS(PHFIN)
C
              IF ((THFIN.GE.0.D0).AND.(THFIN.LE.ANGLEA)) THEN
                  ANGLE = DABS(ASIN(CONST/COS(THFIN)))
                  IF ((PHFIN.GE.ANGLE).AND.(PHFIN.LE.(PI-ANGLE))) THEN
                      ENERGY = (VX**2 + VY**2 + VZ**2)/AMASSQ
                      BINNUM = INT((ENERGY-ENGMIN)/ENGDIV)
                      ESPEC(BINNUM) = ESPEC(BINNUM) + WEIGHT
                  END IF
              END IF
C
              IF((THFIN.GE.(PI-ANGLEA)).AND.(THFIN.LE.(PI+ANGLEA))) THEN
                  ANGLE = DABS(ASIN(CONST/COS(THFIN)))
                  IF ((PHFIN.GE.ANGLE).AND.(PHFIN.LE.(PI-ANGLE))) THEN
                      ENERGY = (VX**2 + VY**2 + VZ**2)/AMASSQ
                      BINNUM = INT((ENERGY-ENGMIN)/ENGDIV)
                      ESPEC(BINNUM) = ESPEC(BINNUM) + WEIGHT
                  END IF
              END IF
C
              IF ((THFIN.GE.(2.D0*PI-ANGLEA)).AND.(THFIN.LE.(2.D0*PI)))
     1        THEN
                  ANGLE = DABS(ASIN(CONST/COS(THFIN)))
                  IF ((PHFIN.GE.ANGLE).AND.(PHFIN.LE.(PI-ANGLE))) THEN
                      ENERGY = (VX**2 + VY**2 + VZ**2)/AMASSQ
                      BINNUM = INT((ENERGY-ENGMIN)/ENGDIV)
                      ESPEC(BINNUM) = ESPEC(BINNUM) + WEIGHT
                  END IF
              END IF
```

```
C
              IF ((THFIN.GE.ANGLEB).AND.(THFIN.LE.(PI-ANGLEB))) THEN
                  ANGLE = DABS(ASIN(CONST/SIN(THFIN)))
                  IF ((PHFIN.GE.ANGLE).AND.(PHFIN.LE.(PI-ANGLE))) THEN
                      ENERGY = (VX**2 + VY**2 + VZ**2)/AMASSQ
                      BINNUM = INT((ENERGY-ENGMIN)/ENGDIV)
                      ESPEC(BINNUM) = ESPEC(BINNUM) + WEIGHT
                  END IF
              END IF
C
              IF((THFIN.GE.(PI+ANGLEB)).AND.(THFIN.LE.(2.D0*PI-ANGLEB))
     1        THEN
                  ANGLE = DABS(ASIN(CONST/SIN(THFIN)))
                  IF ((PHFIN.GE.ANGLE).AND.(PHFIN.LE.(PI-ANGLE))) THEN
                      ENERGY = (VX**2 + VY**2 + VZ**2)/AMASSQ
                      BINNUM = INT((ENERGY-ENGMIN)/ENGDIV)
                      ESPEC(BINNUM) = ESPEC(BINNUM) + WEIGHT
                  END IF
              END IF
C
40        CONTINUE
C
          CLOSE(10)
C
45    CONTINUE
C
C     Write out bins to files
C
      DO 60 I = 0,N2
          PARTWAY = PARTWAY + ESPEC(I)
          WRITE(12,*) ENGMIN + DFLOAT(I)*ENGDIV
          WRITE(21,*) ESPEC(I)
60    CONTINUE
C
      WRITE(6,*) 'TOTAL WEIGHT:',TOTWAY,'WEIGHT DETECTED:',PARTWAY
C
      CLOSE(12)
      CLOSE(21)
C
      STOP
      END
C
C-------------------------------------------------------------------------
C-------------------------------------------------------------------------
C-------------------------------------------------------------------------
C-------------------------------------------------------------------------
```